

**Subject Areas:**

Astrophysics, Computer Science

Keywords:neural networks, astrophysics,
machine learning**Authors for correspondence:**

M. J. Smith

e-mail: mike@mjjsmith.com

J. E. Geach

e-mail: j.geach@herts.ac.ukAstronomia ex machina: a
history, primer, and outlook on
neural networks in astronomy

Michael J. Smith and James E. Geach

Department of Physics, Astronomy & Mathematics,
School of Physics, Engineering and Computer Science,
University of Hertfordshire, Hatfield, AL10 9AB

In recent years, deep learning has infiltrated every field it has touched, reducing the need for specialist knowledge and automating the process of knowledge discovery from data. This review argues that astronomy is no different, and that we are currently in the midst of a deep learning revolution that is transforming the way we do astronomy. We trace the history of astronomical connectionism from the early days of multilayer perceptrons, through the second wave of convolutional and recurrent neural networks, to the current third wave of self-supervised and unsupervised deep learning. We then predict that we will soon enter a fourth wave of astronomical connectionism, in which finetuned versions of an all-encompassing 'foundation' model will replace expertly crafted deep learning models. We argue that such a model can only be brought about through a symbiotic relationship between astronomy and connectionism, whereby astronomy provides high quality multimodal data to train the foundation model, and in turn the foundation model is used to advance astronomical research.

1. Introduction

The concept of artificial intelligence (AI) can be traced back at least 350 years to Leibniz's *Dissertation on the Art of Combinations* [1]. Inspired by Descartes and Lull, Leibniz posited that, through the development of a 'universal language,' all ideas could be represented by the combination of a small set of fundamental concepts, and that *new* concepts could be generated in a logical fashion, potentially by some computing machine. Leibniz's ambitious vision ('*let us calculate*') has not yet been realised, but the quest to emulate human reasoning, or at least to build a machine to mimic the computational and data processing capabilities of the human brain, has persisted to this day.

© 2022 The Authors. Published by the Royal Society under the terms of the Creative Commons Attribution License <http://creativecommons.org/licenses/by/4.0/>, which permits unrestricted use, provided the original author and source are credited.

It might be fair to say that the roots of AI stretch even as far back as Lull's medieval philosophy that inspired Leibniz [2,3]. However, if we now consider AI to be a *bona fide* scientific discipline, then that discipline clearly emerged in the post-war years of the twentieth century, following Turing's simple enquiry 'can machines think?' [4]. Somewhat philosophical in nature, Turing's 1950 question succinctly articulates the ambition of AI, but from a nuts and bolts standpoint it took a further five years from Turing's query for what one might call the first AI program – the so-called 'Logic Theorist' – to be developed by Allen Newell, Cliff Shaw, and Herbert Simon. Funded by the Research and Development (RAND) Corporation, the Logic Theorist was designed, in part, to emulate the role of a human mathematician, in that it could automate the proof of mathematical theorems. This was a breakthrough in computer science and the Logic Theorist was presented at the seminal Dartmouth Summer Research Project on Artificial Intelligence (DSRPAI) conference in 1956, now regarded as the true birth of AI as a field. Indeed, it was DSRPAI organiser John McCarthy who is credited with coining the term 'artificial intelligence' [5].

Natural intrigue – and clearly a good deal of fear – of the idea of AI has inspired popular culture no end, from Dick's *Do Androids Dream Of Electric Sheep?* to Crichton's *Westworld*, *Terminator's 'Skynet'* and beyond. Iain M. Banks's Galactic civilisation known as 'The Culture' imagines a society run by powerful 'Minds' whose intelligence and wisdom far exceeds that of humans, and where biological beings and machines of equivalent sentience generally co-exist peacefully, cooperatively, and equitably. Science fiction notwithstanding, if these dreams are even possible, we are still many years away from a machine that can genuinely think for itself [6,7]. Nevertheless, the question of how one mathematically (and algorithmically) models the workings and inter-relationships of biological neurons – neural networks – and the subsequent exploration of how they can find utility as tools in the data analyst's workshop is really what is being referred to when most people use the term 'AI' today¹. While we must always be wary of hype and buzzwordism, it is the *application* of neural networks – and the possibility of tackling hitherto intractable problems – that offers genuine reason for excitement across many disparate fields of enquiry, including astronomy.

Astronomers have made use of artificial neural networks (ANNs) for over three decades. In 1994, Ofer Lahav, an early trailblazer, wryly identified the '*neuro-skeptics*' – those resistant to the use of such techniques in serious astrophysics research – and argued that ANNs '*should be viewed as a general statistical framework, rather than as an estoteric approach*' [8]. Unfortunately, this skepticism has persisted, despite the recent upsurge in the use of neural networks (and machine learning in general) in the field, as illustrated in Fig. 1. Most of the criticism of machine learning techniques, and deep learning² in particular, is levelled at the perceived 'black box' nature of the methodology. In this review we provide a primer on how deep neural networks are constructed, and the mathematical rules governing their learning, which we hope will serve as a useful resource for neuro-skeptics. Nevertheless, we must recognise that a unified theoretical picture of how deep neural networks work does not yet exist. This remains a point of debate even within the deep learning community. For example, Yann LeCun responding to Ali Rahimi's 'Test of Time' award talk at the 31st Conference on Neural Information Processing Systems (NIPS) remarked:

Ali gave an entertaining and well-delivered talk. But I fundamentally disagree with the message. The main message was, in essence, that the current practice in machine learning is akin to 'alchemy' (his word). It's insulting, yes. But never mind that: It's wrong! Ali complained about the lack of (theoretical) understanding of many methods that are currently used in ML, particularly in deep learning ... Sticking to a set of methods just because you can do theory about it, while ignoring a set of methods that empirically work better just because you don't (yet) understand them theoretically is akin to looking for your lost car keys under the street light knowing you lost them someplace else. Yes, we need better understanding of our methods. But the correct attitude is to attempt to fix the situation, not to insult a whole community for not having succeeded in fixing it yet. This is like criticizing James Watt for not being Carnot or Helmholtz. [9]

¹And the term is regularly misused, not only erroneously, but often cynically.

²Deep learning referring to the use of a network constructed of many layers of artificial neurons.

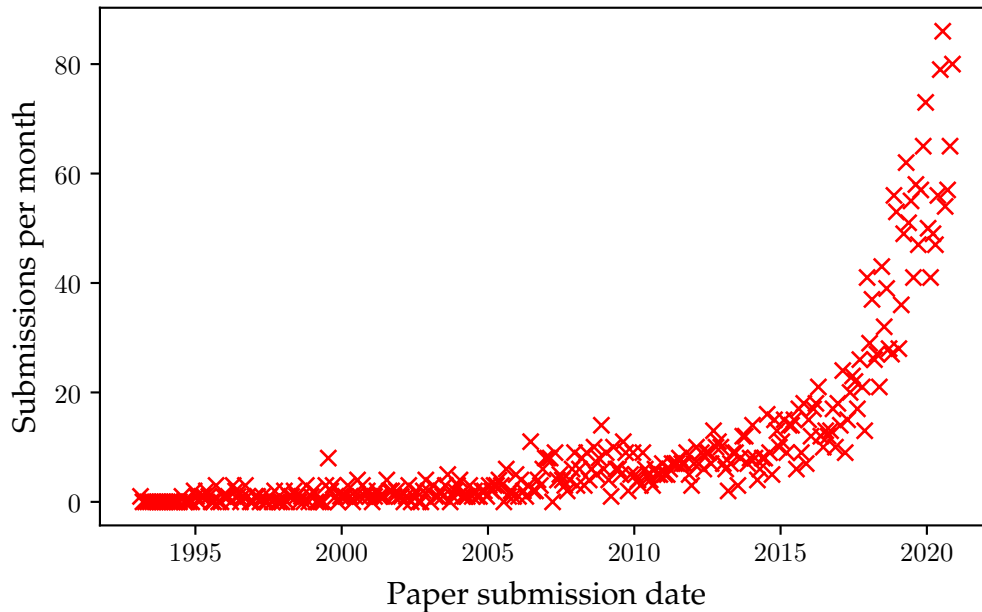


Figure 1: Here we see the number of arXiv:astro-ph submissions per month that have abstracts or titles containing one or more of the strings: ‘machine learning’, ‘ML’, ‘artificial intelligence’, ‘AI’, ‘deep learning’, or ‘neural network’. The raw data is in the public domain and is available at <https://www.kaggle.com/Cornell-University/arxiv>.

Philosophical concerns aside, LeCun’s fundamental point is that deep learning ‘works’ and therefore we should use it, even if we do not fully understand it. If one were being uncharitable, we could make similar arguments about the Λ CDM paradigm.

It is clear that in every field that deep learning has infiltrated we have seen a reduction in the use of specialist knowledge, to be replaced with knowledge automatically derived from data. We have already seen this process play out in many ‘applied deep learning’ fields such as computer Go [10], protein folding [11], natural language processing [12], and computer vision [13]. We argue that astronomy’s data abundance corrals it onto a path no different to that trodden by other applied deep learning fields. This abundance is not a passing phase; the total astronomical data volume is already large and will increase exponentially in the coming years. We illustrate this in Fig. 2, where we present a selection of astronomical surveys and their estimated data volume output over their lifetimes [14]. And this is not even considering data associated with ever larger and more detailed numerical simulations [15]. The current scale of the data volume already poses an issue for astronomy as many classical methods rely on human supervision and specialist expertise, and the increasing data volume will make exploring and exploiting these surveys through traditional human supervised and semi-supervised means an intractable problem. Of serious concern is the possibility that we will miss – or substantially delay – interesting and important discoveries simply due to our inability to accurately and consistently interrogate astronomical data at scale. Deep learning has shown great promise in automating information extraction in various data intensive fields, and so is ideally poised as a solution to the challenge of processing ultra-large scale astronomical data. But we do not need to stop there. This review’s outlook ventures a step further, and argues that astronomy’s wealth of data should be considered a unique opportunity, and not merely an albatross.

Since astronomical connectionism's³ humble beginnings in the late 1980s, there have been numerous excellent reviews on the application of artificial neural networks to astronomy [e.g. 16–18]. We take an alternative approach to previous literature reviews and survey the field holistically, in an attempt to paint astronomical connectionism's 'Big Picture' with broad strokes. While we cannot possibly include all works within astronomical connectionism⁴, we hope that this review serves as a historical background on astronomy's 'three waves' of increasingly automated connectionism, as well as presenting a general primer on neural networks that may assist those seeking to explore this fascinating topic for the first time.

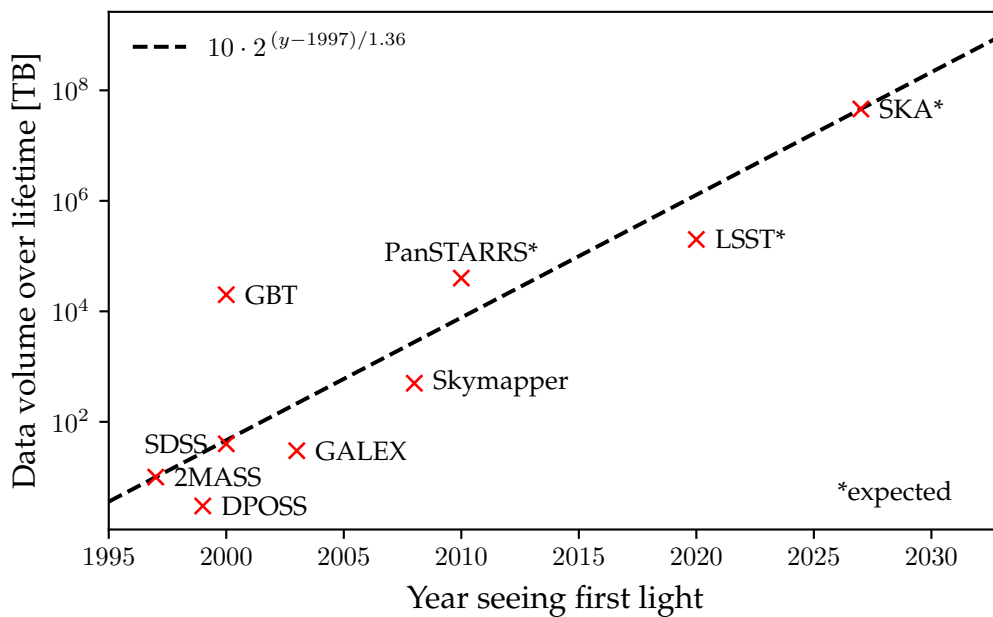


Figure 2: The data volume output of a selection of astronomical surveys over their lifetimes. We can see the astronomical survey data volume doubles every 16 months. Data is taken from Zhang and Zhao [14].

In §2 and §3 we explore initial work on multilayer perceptrons within astronomy, where models required manually selected emergent properties as input. In §4 and §5 we explore the second wave, which coincided with the dissemination of convolutional neural networks and recurrent neural networks – models where the multilayer perceptron's manually selected inputs are replaced with raw data ingestion. In the third wave that is happening now we are seeing the removal of human supervision altogether with deep learning methods inferring labels and knowledge directly from the data, and we explore this wave in §6–§8. Finally, in §9, we look to the future and predict that we will soon enter a fourth wave of astronomical connectionism. We argue that if astronomy follows the pattern of other applied deep learning fields we will see the removal of expertly crafted deep learning models, to be replaced with fine-tuned versions of an all-encompassing 'foundation' model. As part of this fourth wave we argue for a symbiosis between astronomy and connectionism, a symbiosis predicated on astronomy's relative data wealth and deep learning's insatiable data appetite. Many ultra-large datasets in machine learning are proprietary or of poor quality, and so there is an opportunity for astronomers as a community to develop and provide a high quality multimodal public dataset. In turn, this dataset could be

³As a shorthand, in this review we will refer to 'parallel distributed processing' – the dominant connectionist paradigm – as simply 'connectionism'.

⁴We refer the reader to Fig. 1!

used to train an astronomical foundation model to serve state-of-the-art downstream tasks. Due to foundation models' hunger for data and compute, a single astronomical research group could not bring about such a model alone. Therefore, we conclude that astronomy as a discipline has slim chance of keeping up with a research pace set by the Big Tech goliaths – that is, unless we follow the examples of EleutherAI and HuggingFace and pool our resources in a grassroots open source fashion.

Before moving on, we must first admit to our readers that we have not been entirely honest with them. The abstract of this review has not been written by us. It has actually been generated by prompting OpenAI's 'GPT-3' neural network based foundation model [12] with the abstract from MJS's PhD thesis [19]! We explore these models in more detail in §9.

2. A primer on artificial neurons

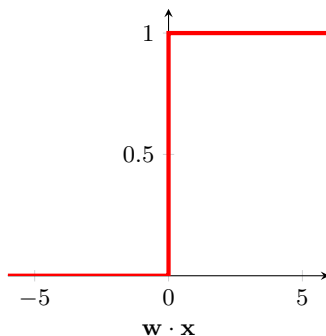
In 1943, McCulloch and Pitts proposed the first computational model of a biological neuron [MP neuron; 20]. Their model consisted of a set of binary inputs $x_i \in \{0, 1\}$ and a single binary output $y \in \{0, 1\}$. Their model also defines a single 'inhibitory' input $\mathcal{I} \in \{0, 1\}$ that blocks output if $\mathcal{I} = 1$. If the sum of the inputs exceeds a threshold value Θ , the MP neuron 'fires' and outputs $y = 1$. Mathematically we can write the MP neuron function as

$$\text{MP}(\mathbf{x}) = \begin{cases} 1 & \text{if } \sum_{i=1}^n x_i > \Theta \text{ and } \mathcal{I} = 0, \\ 0 & \text{otherwise.} \end{cases}$$

The MP neuron is quite a powerful abstraction. Single MP neurons can calculate simple boolean functions, and more complicated functions can be calculated when many MP neurons are chained together. However, there is one show-stopping issue: the MP neuron is missing the capacity to learn. Rosenblatt [21] addressed this by combining the MP neuron with Hebb's neuronal wiring theory⁵ [22], and we will explore Rosenblatt's formulation in the next subsection.

2(a) The perceptron

Like the MP neuron, Rosenblatt's perceptron takes a number of numeric inputs (x_i). However, unlike the MP neuron each one of these inputs is multiplied by a corresponding weight (w_i) signifying the importance the perceptron assigns to a given input. As shown in Fig. 3, Rosenblatt then sums this list of products and passes it into an 'activation function'. Rosenblatt used the Heaviside step function in his original formulation:



$$\text{prediction} = H(\mathbf{w} \cdot \mathbf{x}) = \begin{cases} 0 & \text{if } \mathbf{w} \cdot \mathbf{x} < 0, \\ 1 & \text{if } \mathbf{w} \cdot \mathbf{x} \geq 0. \end{cases} \quad (2.1)$$

To concretise exactly how Rosenblatt's perceptron learns we will use an example. Let us say that we want to automatically label a set of galaxy images as either 'spiral' or 'elliptical'. To do this we first need to compile a training dataset of galaxy images. This training set would consist of spiral and elliptical galaxies, and each image would have a ground truth label y – say '0' for a spiral galaxy and '1' for an elliptical. To train our perceptron we randomly choose

⁵Also known by the mantra 'cells that fire together wire together'.

one image from the training set, and feed it to the perceptron, with the numerical value of each pixel corresponding to an input $\{x_1, \dots, x_N\}$. These inputs are multiplied by their corresponding weight $\{w_1, \dots, w_N\}$. A bias term ($b = w_0 x_0$, where $x_0 = 1$) is also added to the inputs, which allows the neuron to shift its activation function linearly. Since we do not want our perceptron to have any prior knowledge of the task, we initialise the weights at random. The resulting products are then summed. Finally, our activation function H transforms $\mathbf{w} \cdot \mathbf{x}$ and produces a prediction p . We then compare p to y via a ‘loss function,’ which is a function that measures the difference between p and y . The loss can be any differentiable function, so for illustration purposes we will define it here as the L1 loss: $\mathcal{L}(y, p) = |y - p|$. Now that we can compare to the ground truth, we need to work out how a change in one of our weights affects the loss (that is, we want to find $\partial\mathcal{L}/\partial\mathbf{w}$). We can calculate this change with the chain rule

$$\frac{\partial\mathcal{L}}{\partial\mathbf{w}} = \frac{\partial\mathcal{L}}{\partial p} \frac{\partial p}{\partial\mathbf{w}}, \quad (2.2)$$

and since $p = H(\mathbf{w} \cdot \mathbf{x})$ and $\partial p/\partial\mathbf{w} = H' \mathbf{x}^T$ we get

$$\frac{\partial\mathcal{L}}{\partial\mathbf{w}} = \frac{\partial\mathcal{L}}{\partial p} \odot (H' \mathbf{x}^T)$$

where \odot is the distributive Hadamard product. Thus we can update the weights to decrease the loss function:

$$\begin{aligned} \mathbf{w}_{\text{next}} &= \mathbf{w} - \eta \frac{\partial\mathcal{L}}{\partial\mathbf{w}} \\ &= \mathbf{w} - \eta \frac{\partial\mathcal{L}}{\partial p} \odot (H' \mathbf{x}^T), \end{aligned}$$

where η is the learning rate⁶. If we repeat this process our perceptron will get better and better at classifying our galaxies!

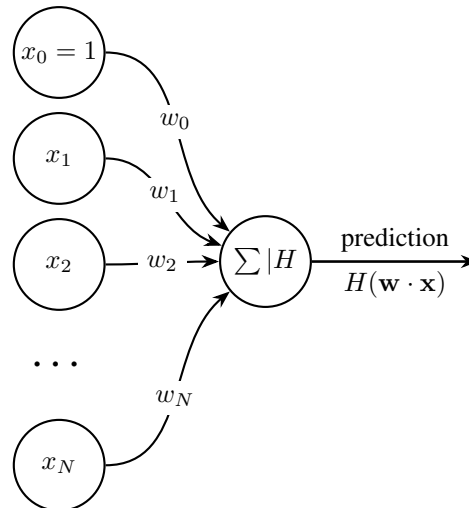


Figure 3: A single neuron (or perceptron) with a bias w_0 , inputs x_1, x_2, \dots, x_N , and weights w_1, w_2, \dots, w_N .

⁶The eagle-eyed reader may have noticed that since the derivative of the Heaviside step function is the Dirac delta function, we will only update the perceptron’s weights on an incorrect prediction. If we want to also learn from positive examples, we need to use a smoothly differentiable activation function. This is explored in the next subsection.

We must go further than training a single layer perceptron; in *Perceptrons: An Introduction to Computational Geometry*, Minsky and Papert [e.g. §13.0; 23] show that the single layer perceptron is only able to calculate linearly separable functions, among other limitations. Their book (alongside a consensus that AI had failed to deliver on its early grandiose promises) delivered a big blow to the connectionist school of artificial intelligence⁷. In the years following Minsky and Papert [23] governmental and industry funding was pulled from connectionist research laboratories, ushering in the first ‘AI winter’⁸.

Yet, as exemplified in Rosenblatt [§5.2, theorem 1; 27] it was known at the time that multilayer perceptrons could calculate non-linearly separable functions (such as the ‘exclusive or’). We can prove intuitively that a set of neurons can calculate *any* function: a perceptron can perfectly emulate a NAND gate (Fig. 4), and the singleton set {NAND} is functionally complete. Since we can combine a set of NAND gates to calculate any function, *we must also be able to combine a set of neurons to calculate any function*⁹. Such a group of neurons is known as the multilayer perceptron (MLP). Unfortunately, we cannot simply stack perceptrons together as we are missing one vital ingredient: a way to train the network! At the time of Minsky and Papert’s treatise on perceptrons there was no widely known algorithm [in the West; see 25] that could train such a multilayer network. In Minsky and Papert’s own words:

Nevertheless, we consider it to be an important research problem to elucidate (or reject) our intuitive judgment that the extension [from one layer to many] is sterile. Perhaps some powerful convergence theorem will be discovered, or some profound reason for the failure to produce an interesting ‘learning theorem’ for the multilayered machine will be found. (§13.2; Minsky and Papert [23], on MLPs)

The field had to wait almost two decades for such an algorithm to become widespread. In the next subsection we will explore backpropagation, the algorithm that ultimately proved Minsky and Papert’s intuition wrong.

2(b) The multilayer perceptron

Grouping many artificial neurons together may result in something resembling Fig. 5. This network consists of an input layer, two intermediate ‘hidden’ layers, and an output layer. As in the previous section, let us say that we want a classifier that can classify a set of galaxy images into elliptical and spiral types. In an MLP similar to Fig. 5 a neuron would be assigned to each pixel in a galaxy image. Each neuron would take the numeric value of that pixel, and propagate that signal forward into the network. The next layer of neurons does the same, with the input being the previous layer’s output. This process continues until we reach the output layer. In a binary classification task like our galaxy classifier this layer outputs a value between zero and one. Thus, if we define a spiral galaxy as zero, and an elliptical galaxy as one, we would want the network output to be near zero for a spiral galaxy input (and vice versa).

In §2(a) we found the change we needed to apply to a single neuron’s weights to make it learn from a training example. We can train an MLP in a similar way by employing the reverse mode of automatic differentiation (or backpropagation) to learn from our galaxy training data set [36–38]¹⁰. We want our network to learn when it makes both a correct and incorrect prediction, so we define our activation function as a smoothed version of Rosenblatt’s perceptron activation. This ensures that a signal is present in the derivative no matter which values are input. This activation

⁷See Metz [24] for a closer look at the conflicts and personalities that shaped AI.

⁸At least, in the Western world. Connectionism continued in earnest in the Soviet Union [25,26].

⁹More formally, Cybenko [28] and Hornik et al. [29] prove that an infinitely wide neural network can calculate any function, and Lu et al. [30] prove that an infinitely deep neural network is a universal approximator.

¹⁰Some controversy surrounds backpropagation’s discovery. The Finnish computer scientist Linnainmaa proposed the reverse mode of automatic differentiation and adapted the algorithm to run on computers in their 1970 (Finnish language) thesis [39]. They first published their findings in English in 1976. Werbos then proposed applying an adaptation of Linnainmaa’s method to artificial neural networks. Rumelhart et al. [38] showed experimentally that backpropagation can generate meaningful internal representations within a neural network, and popularised the method. Here we will err on the side of caution and cite all three manuscripts. For further reading we recommend Schmidhuber [40] and Baydin et al. [41].

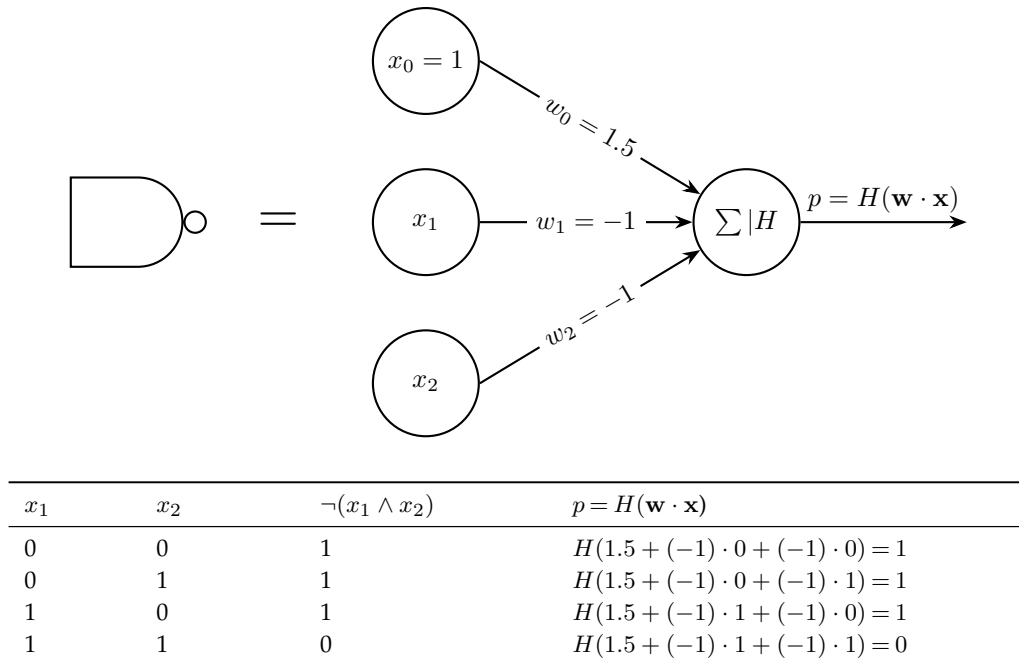


Figure 4: If we define $H(\mathbf{w} \cdot \mathbf{x})$ as in Eq. 2.1 we can set a perceptron's weights so that it is equivalent to the NAND gate.

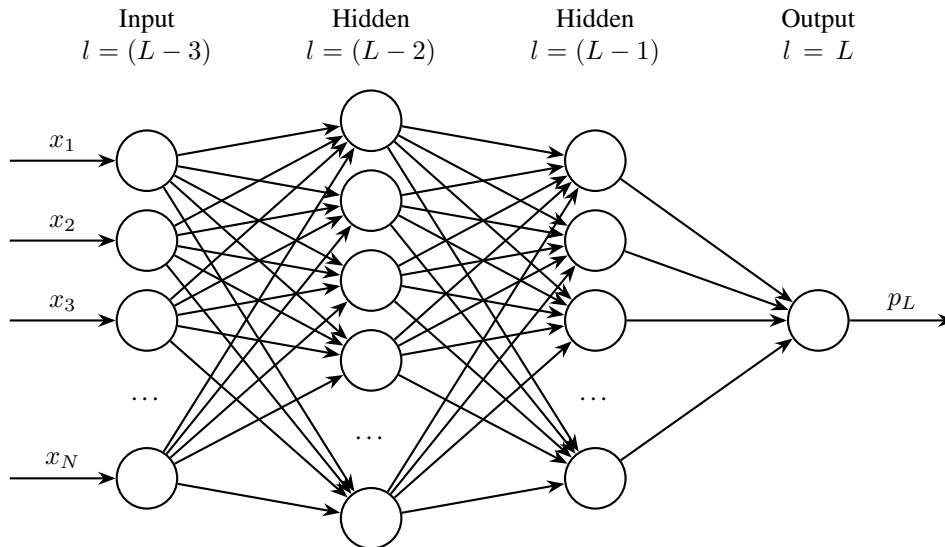


Figure 5: The multilayer perceptron, or artificial neural network. The depicted network has two hidden layers. It takes N inputs x_1, x_2, \dots, x_N , and outputs a prediction p_L . Note that here we omit the explicit bias terms (i.e. w_0).

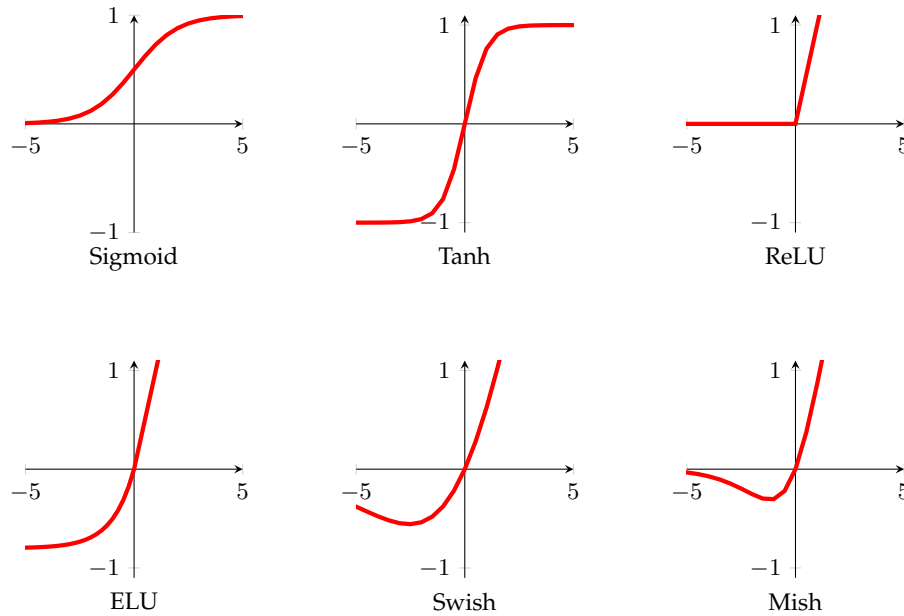


Figure 6: A curated selection of activation functions. In all plots, the x axis is the input, and the y axis is the output. The rectified linear unit (ReLU) activation function was first introduced in the context of neural networks in Fukushima [31] and later rediscovered, named, and popularised in Nair and Hinton [32]. The exponential linear unit (ELU), Swish and Mish activations were respectively introduced in Clevert et al. [33], Ramachandran et al. [34], and Misra [35].

function is known as the ‘sigmoid’ function, and is shown in Fig. 6. As in §2(a) we define a loss function $\mathcal{L}(y, p)$ that describes the similarity between a ground truth (y) and a prediction (p). We also define a neuron’s activation function as $\varphi(\mathbf{w} \cdot \mathbf{x})$ where $\mathbf{w} \cdot \mathbf{x}$ is the weighted sum of a neuron’s inputs. Following from Eq. 2.2:

$$\frac{\partial \mathcal{L}}{\partial \mathbf{w}_l} = \frac{\partial \mathcal{L}}{\partial \mathbf{p}_l} \frac{\partial \mathbf{p}_l}{\partial \mathbf{w}_l}$$

where l is a layer in the MLP. In the same way as in §2(a) we can calculate an MLP’s final layer’s ($l = L$) weight updates in terms of known values:

$$\frac{\partial \mathcal{L}}{\partial \mathbf{w}_L} = \frac{\partial \mathcal{L}}{\partial p_L} \odot (\varphi'_L \mathbf{p}_{L-1}^T), \quad (2.3)$$

where \mathbf{p}_{L-1} are the outputs from the previous layer. To calculate the $(L - 1)$ th layer’s weight updates we use the chain rule:

$$\frac{\partial \mathcal{L}}{\partial \mathbf{w}_{L-1}} = \frac{\partial \mathcal{L}}{\partial p_L} \frac{\partial p_L}{\partial \mathbf{p}_{L-1}} \frac{\partial \mathbf{p}_{L-1}}{\partial \mathbf{w}_{L-1}}.$$

Likewise for the $(L - n)$ th layer:

$$\frac{\partial \mathcal{L}}{\partial \mathbf{w}_{L-n}} = \frac{\partial \mathcal{L}}{\partial p_L} \left(\prod_{i=1}^n \frac{\partial \mathbf{p}_{L+1-i}}{\partial \mathbf{p}_{L-i}} \right) \frac{\partial \mathbf{p}_{L-n}}{\partial \mathbf{w}_{L-n}}.$$

Now we can start plugging in some known values. Since $\mathbf{p}_l = \varphi_l(\mathbf{w}_l \cdot \mathbf{p}_{l-1})$, it follows that $\partial \mathbf{p}_l / \partial \mathbf{p}_{l-1} = \varphi'_l \mathbf{w}_l^T$, and $\partial \mathbf{p}_l / \partial \mathbf{w}_l = \varphi'_l \mathbf{p}_{l-1}^T$. So:

$$\frac{\partial \mathcal{L}}{\partial \mathbf{w}_{L-n}} = \frac{\partial \mathcal{L}}{\partial p_L} \odot \left(\prod_{i=1}^n \varphi'_{L-i} \mathbf{w}_{L-i}^T \right) (\varphi'_{L-n} \mathbf{p}_{L-n-1}^T). \quad (2.4)$$

Combining Eq. 2.3 with Eq. 2.4 we get the weight update algorithm for the $(L - n)$ th layer of the MLP:

$$\mathbf{w}_{\text{next}} = \mathbf{w} - \eta \begin{cases} \frac{\partial \mathcal{L}}{\partial p_L} \odot \left(\varphi'_L \mathbf{P}_{L-1}^T \right), & \text{for } n = 0, \\ \frac{\partial \mathcal{L}}{\partial p_L} \odot \left(\prod_{i=1}^n \varphi'_{L-i} \mathbf{w}_{L-i}^T \right) \left(\varphi'_{L-n} \mathbf{P}_{L-n-1}^T \right), & \text{for } n > 0. \end{cases} \quad (2.5)$$

With this equation¹¹ in hand we can use the same technique described earlier in this section and in §2(a) to update the network's weights with each galaxy image to decrease the loss function \mathcal{L} . Again, as \mathcal{L} is minimised, our MLP will classify our elliptical and spiral galaxy images with increasing accuracy.

3. Astronomy's first wave of connectionism

Connectionism was first discussed within astronomy in the late 1980s, after the popularisation of backpropagation (see footnote 10) and the consequent passing of the first 'AI winter'. Two radical studies emerged in 1988 that recognised areas where astronomy could benefit from the use of ANNs [42,43]. Together, they identified that astronomical object classification¹² and telescope scheduling could be solved through the use of an ANN. These studies were followed by a rapid broadening of the field, and the application of connectionism to many disparate astronomical use cases [16, and references therein]. In this section, we will outline areas where MLPs found an early use in astronomy.

3(a) Classification problems

Odehahn et al. [44] classified astronomical objects into star and galaxy types. These were taken from the Palomar Sky Survey Automated Plate Scanner catalogue [45]. To compile their dataset, they first extracted a set of emergent image parameters from the scanned observations. These parameters included the diameter, ellipticity, area, and plate transmission. The parameters were then used to train both a linear perceptron and a feedforward MLP to classify the objects into stars or galaxies. Odehahn et al. [44] found that their best performing model could classify galaxies with a completeness of 95% for objects down to a magnitude < 19.5 . This work was followed by many more studies on the star/galaxy classification problem [e.g. 46–49]. Galaxy morphological type classification was explored in the early 1990s. Storrie-Lombardi et al. [50] describe an MLP that takes an input a selected set of thirteen galaxy summary statistics, and uses this information to classify a galaxy into one of five morphological types. Storrie-Lombardi et al. [50] report a top one accuracy of 64%, and a top two accuracy of 90%. This pilot study was followed by several studies from the same group that confirmed that MLPs are effective automatic galaxy morphological classifiers [51–56, see §5 for a continuation of this line of research].

MLPs were also used in other classification tasks; here we highlight a few further areas where MLPs were applied. von Hippel et al. [57] classified stellar spectra into temperature types, and Klusch and Napiwotzki [58] did the same for Morgan-Keenan System types. Chon [59] described the use of an MLP to search for and classify muon events (and therefore neutrino observations) in the Sudbury Neutrino Observatory. Quasar classification has been explored in several studies [60–62]. Seminaly, Carballo et al. [60] used an MLP to select quasar candidates given their radio flux, integrated-to-peak flux ratio, photometry and point spread function in the red and blue bands, and their radio-optical position separation. They found good agreement between their model and that of the decision tree described in White et al. [63], confirming MLPs as a competitive alternative to more traditional machine learning. As part of the Supernova photometric Classification Challenge [SPCC; 64], Karpenka et al. [65] proposed the use of a neural network to classify supernovae into Type-1a/non-Type-1a classes. To classify their light curves,

¹¹If we examine Eq. 2.5 carefully, we can see why we add nonlinearities between the MLP layers; without activation functions Eq. 2.5 collapses to the equivalent of a single layer MLP!

¹²Specifically, galaxies were discussed in Rappaport and Anderson [42] and point sources observed with the Infra-Red Astronomical Satellite (IRAS) were discussed in Adorf and Johnston [43].

they first used a hand-crafted fitting function, and then trained their MLP on the fitted coefficients. They found that their model was competitive with other, more complex models trained on the SPCC dataset. From the studies discussed in this section we can safely conclude that MLPs are effective classifiers of astronomical data, when given important parameters extracted by an expert guide.

3(b) Regression problems

MLPs have also been used in regression problems. Angel et al. [66] applied them first to adaptive telescope optics. They trained their MLP on 250 000 simulated in focus and out of focus observations of stars as seen by the Multiple Mirror Telescope (MMT). From the flattened 13×13 pixel observations, their network predicted the piston position and tilt required for each of the MMT's mirrors to bring the stars into focus. After the application of these corrections, the authors were able to recover the original profile. In follow up studies, Sandler et al. [67] and Lloyd-Hart et al. [68] proved that Angel et al.'s MLP worked on the real MMT.

Photometric redshift estimation was explored in many concurrent studies [e.g. 56,69–72]. Firth et al. [69] train a neural network to predict the redshift of galaxies contained in the Sloan Digital Sky Survey (SDSS) early data release [73]. The galaxies were input to the neural network as a set of summary parameters, and the output was a single float representing the galaxy redshift. They found their network attained a performance comparable to classical techniques. Extending and confirming the work by Firth et al. [69], Ball et al. [56] used an MLP to predict the redshift of galaxies contained in the SDSS's first data release [74]. They also showed that MLPs were capable of predicting the galaxies' spectral types and morphological classifications.

Of course, MLPs have been used more widely in astronomical regression tasks. Here we will cherry pick a few studies to show the MLP's early breadth of use. Sunspot maxima prediction was carried out by Koons and Gorney [75]. They found their MLP based method was capable of predicting the number of sunspots when trained on previous cycles. Bailer-Jones et al. [76] predicted the effective temperature of a star from its spectrum. Auld et al. [77] and Auld et al. [78] applied MLPs to cosmology, demonstrating that MLPs are capable of predicting the cosmic microwave background, given a set of cosmological parameters. Nørgaard-Nielsen and Jørgensen [79] used an MLP to remove the foreground from microwave temperature maps. From the studies discussed in this section we can see that MLPs are effective regressors of astronomical data, when given significant parameters extracted by an expert guide.

4. Contemporary supervised deep learning

There are some issues with MLPs. Primarily they do not scale well to high dimensional datasets. For example, if our dataset consists of images with a 128×128 pixels, we will need 16 384 neurons in the MLP's input layer alone! As we move into the hidden layers, this scaling issue only gets worse. Also, since MLPs must take an unrolled image as an input, they disregard any spatial properties of their training images, and so either need a substantial amount of training data to classify or generate large images¹³, or an expert to extract descriptive features from the data in a preprocessing step. We can see this issue writ large in the previous section—most of the MLP applications described in §3 require an expert to extract features from the data for the network to then train on! This drawback is not ideal; what if there are features within the raw data that are not present in these cherry picked statistics? In that case, it would be preferable to let the neural network take in the raw data as input, and then learn which features are the most descriptive. We will discuss neural network architectures that solve both the MLP scaling problem and the expert

¹³At the height of the convolutional neural network architecture's popularity in the mid 2010s these were real problems. However, with the growth of computing power and data in recent years we are seeing a resurgence of the more general MLP model [e.g. 80–83]. This follows the prevailing trend in AI where the removal of human-crafted features and biases ultimately results in more expressive models that learn such features and biases directly from data [84,85].

reliance problem in this section. After we have explored these architectures in general, we will discuss their application to astronomical problems in §5.

4(a) Convolutional neural networks

Unlike the MLP described in the previous section, convolutional neural networks (CNNs; introduced in Fukushima [31] and first combined with backpropagation in LeCun et al. [86]) do not entirely consist of fully connected layers, where each neuron is connected to every neuron in the previous and subsequent layers. Instead, the CNN (such as the one depicted in Fig. 7) uses convolutional layers in place of the majority (or all) of the dense layers.

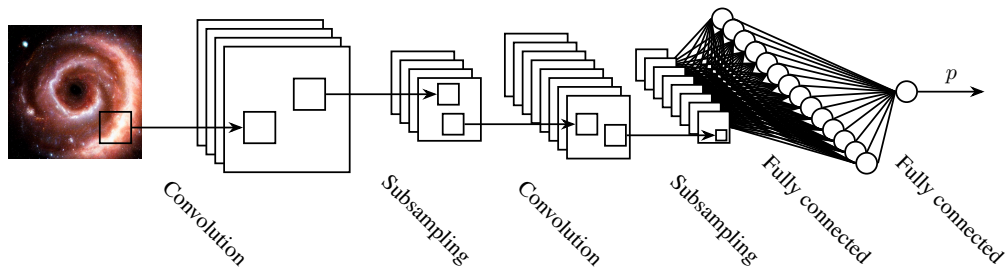


Figure 7: A convolutional neural network classifying a spiral galaxy image¹⁴.

We can think of a convolutional layer as a set of learnt ‘feature filters’. These feature filters perform a local transform on input imagery. In classical computer vision, these filters are hand crafted, and perform a predetermined function, such as edge detection or blurring. In contrast, a CNN learns the optimal set of filters for its task (say, galaxy classification). Eq. 4.1 shows two different convolution¹⁵ operators being performed on an array.

$$\begin{bmatrix} 39 & 57 & 86 & 9 & 26 \\ 90 & 74 & 63 & 87 & 98 \\ 79 & 34 & 26 & 16 & 46 \\ 67 & 61 & 96 & 1 & 79 \\ 33 & 47 & 15 & 49 & 29 \end{bmatrix} * \begin{bmatrix} 0 & 0 & 0 \\ 0 & 0 & 0 \\ 0 & 0 & 1 \end{bmatrix} = \begin{bmatrix} 26 & 16 & 46 \\ 96 & 1 & 79 \\ 15 & 49 & 29 \end{bmatrix} \quad (4.1)$$

$$\begin{bmatrix} 39 & 57 & 86 & 9 & 26 \\ 90 & 74 & 63 & 87 & 98 \\ 79 & 34 & 26 & 16 & 46 \\ 67 & 61 & 96 & 1 & 79 \\ 33 & 47 & 15 & 49 & 29 \end{bmatrix} * \begin{bmatrix} 1 & 0 & 0 \\ 0 & 1 & 0 \\ 0 & 0 & 1 \end{bmatrix} = \begin{bmatrix} 139 & 136 & 219 \\ 220 & 101 & 158 \\ 155 & 179 & 56 \end{bmatrix}$$

In the above equation the operation is represented as a matrix. In a CNN the matrix is a set of neuronal weights. As seen in Fig. 7 there are multiple feature maps in a convolutional layer, each containing a set of weights independent to the other feature maps, and learning to extract a different feature. As in the MLP described in the previous section, the weights are updated using backpropagation to minimise a loss function. We will discuss astronomical applications of CNNs in §5, after we introduce modern CNN architectures.

¹⁴All astronomical objects shown in the neural network diagrams within this manuscript are generated via text prompts fed into a latent diffusion neural network model [87].

¹⁵We must note that in Eq. 4.1 we follow most deep learning libraries and perform a cross-correlation and *not* a convolution. However, since the weights are learnt, this does not matter; the neural network will simply learn a flipped representation of the cross-correlation.

4(b) Recurrent neural networks

Standard feedforward neural networks like the MLP (§2(b)) and CNN (§4(a)) generate a fixed size vector given a fixed size input¹⁶. But, what if we want to classify or generate a variably sized vector? For example, we might want to classify a galaxy's morphology given its rotation curve. A rotation curve describes the velocity of a galaxy's visible stars versus their distance from the galaxy's centre. Fig. 8 shows a possible rotation curve for Messier 81. A rotation curve's length depends on the size of its galaxy, and due to this variable length, and the fact that MLPs take a fixed size input, we cannot easily use an MLP for classification. Recurrent neural networks (RNNs), however, can take a variable length input and produce a variable length output. An

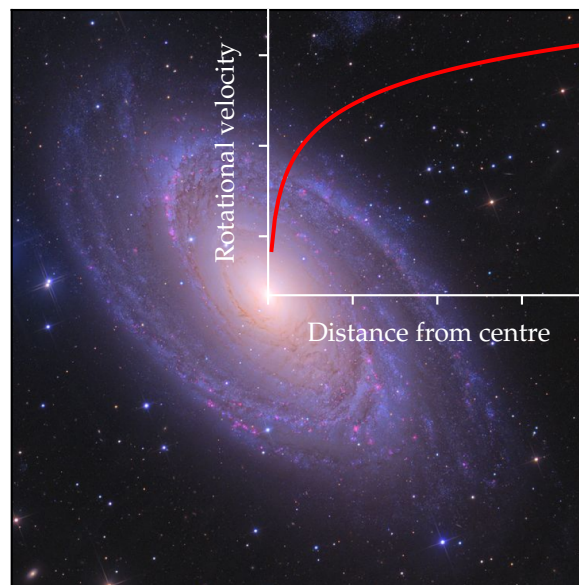


Figure 8: An example of a galaxy rotation curve, plotted over an image of Messier 81 [89].

RNN differs from a feed forward MLP by having a hidden state that acts as a 'memory' store of previously seen information. As the RNN encounters new data, its weights are altered through the backpropagation through time algorithm [BPTT; 90, and references therein. Also see footnote 10].

We can use an RNN similar to Fig. 9 to classify our rotation curves. We express the rotation curve as a list $\{x_1, x_2, \dots, x_N\}$, with each x being a measurement of the rotational velocity at a certain radius. Then we feed this list into the RNN sequentially in the same way as shown in Fig. 9. The RNN will produce an output for each x fed to it, but we ignore those until we feed in x_N , the rotational velocity furthest from the galaxy's centre. When we feed in x_N , the RNN produces a prediction p_N , which we can then compare to a ground truth y_N via a loss function \mathcal{L}_N . In our case, y is an integer label representing the galaxy's morphological class. The comparison $\mathcal{L}_N(y_N, p_N)$ is a function that represents the distance between the RNN prediction and the ground truth. We can then reduce $\mathcal{L}_N(y_N, p_N)$ by updating the RNN's weights through BPTT so that the weights $\{\mathbf{w}_x, \mathbf{w}_p, \mathbf{w}_h\}$ follow $\nabla \mathcal{L}_N$ downwards. As we do this, our RNN will improve its galaxy classifications.

¹⁶As with any rule there are exceptions, such as CNNs containing a global average pooling layer [88].

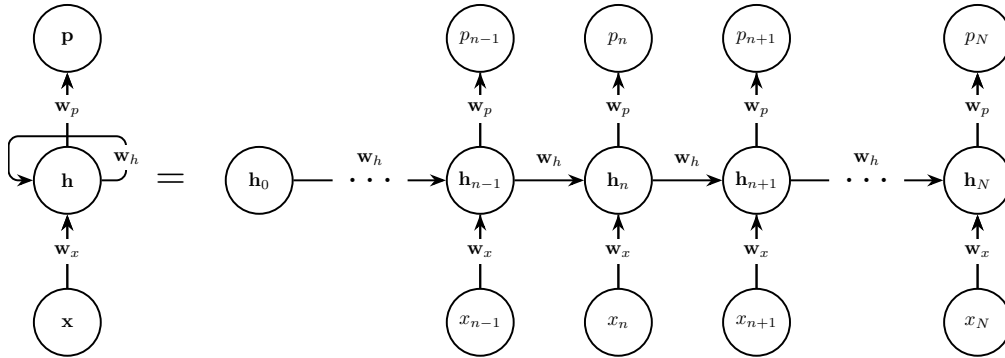


Figure 9: A recurrent neural network with weights $\{\mathbf{w}_x, \mathbf{w}_p, \mathbf{w}_h\}$, a hidden state \mathbf{h}_n , inputs \mathbf{x} , and a prediction $p_{n=N}$ is unrolled into its constituent processes.

BPTT's mathematical derivation is akin to the one we explored in §2(b), and we will quickly derive it here for posterity. Let us first look at the forward propagation equations:

$$\begin{aligned}\mathcal{L}_n &= |y_n - p_n|, \\ p_n &= \varphi(\mathbf{w}_p \cdot \mathbf{h}_n), \text{ and} \\ \mathbf{h}_n &= \phi(\mathbf{w}_h \cdot \mathbf{h}_{n-1} + \mathbf{w}_x \cdot \mathbf{x}_n).\end{aligned}$$

From these we see that we need to express $\partial \mathcal{L}_n / \partial \mathbf{w}_p$, $\partial \mathcal{L}_n / \partial \mathbf{w}_h$, and $\partial \mathcal{L}_n / \partial \mathbf{w}_x$ as known values to train the network. $\partial \mathcal{L}_n / \partial \mathbf{w}_p$ is relatively easy; via the chain rule, and the fact that $\partial p_n / \partial \mathbf{w}_p = \varphi' \mathbf{h}_n^T$:

$$\begin{aligned}\frac{\partial \mathcal{L}_n}{\partial \mathbf{w}_p} &= \frac{\partial \mathcal{L}_n}{\partial p_n} \frac{\partial p_n}{\partial \mathbf{w}_p}, \\ &= \frac{\partial \mathcal{L}_n}{\partial p_n} \odot \varphi' \mathbf{h}_n^T.\end{aligned}\quad (4.2)$$

$\partial \mathcal{L}_n / \partial \mathbf{w}_h$ is more tricky, so we will go step by step. We already know that

$$\frac{\partial \mathcal{L}_n}{\partial \mathbf{w}_h} = \frac{\partial \mathcal{L}_n}{\partial p_n} \frac{\partial p_n}{\partial \mathbf{h}_n} \frac{\partial \mathbf{h}_n}{\partial \mathbf{w}_h}.\quad (4.3)$$

However, we see in Fig. 9 that \mathbf{h}_n depends on \mathbf{h}_{n-1} , which depends on \mathbf{h}_{n-2} (and so on). We also notice that all the hidden states depend on \mathbf{w}_h . We therefore rewrite Eq. 4.3 to make this explicit:

$$\begin{aligned}\frac{\partial \mathcal{L}_n}{\partial \mathbf{w}_h} &= \frac{\partial \mathcal{L}_n}{\partial p_n} \frac{\partial p_n}{\partial \mathbf{h}_n} \sum_{j=1}^n \frac{\partial \mathbf{h}_n}{\partial \mathbf{h}_j} \frac{\partial \mathbf{h}_j}{\partial \mathbf{w}_h}, \\ &= \frac{\partial \mathcal{L}_n}{\partial p_n} \frac{\partial p_n}{\partial \mathbf{h}_n} \sum_{j=1}^n \left(\prod_{i=j+1}^n \frac{\partial \mathbf{h}_i}{\partial \mathbf{h}_{i-1}} \right) \frac{\partial \mathbf{h}_j}{\partial \mathbf{w}_h}.\end{aligned}$$

We can now substitute in some known values:

$$\frac{\partial \mathcal{L}_n}{\partial \mathbf{w}_h} = \frac{\partial \mathcal{L}_n}{\partial p_n} \odot \varphi' \mathbf{h}_n^T \sum_{j=1}^n \left(\prod_{i=j+1}^n \phi' \mathbf{w}_{h,i}^T \right) \phi' \mathbf{h}_{j-1}^T.\quad (4.4)$$

Finally, $\partial\mathcal{L}_n/\partial\mathbf{w}_x$ is derived in the same way as $\partial\mathcal{L}_n/\partial\mathbf{w}_h$:

$$\begin{aligned}\frac{\partial\mathcal{L}_n}{\partial\mathbf{w}_x} &= \frac{\partial\mathcal{L}_n}{\partial p_n} \frac{\partial p_n}{\partial\mathbf{h}_n} \sum_{j=1}^n \left(\prod_{i=j+1}^n \frac{\partial\mathbf{h}_i}{\partial\mathbf{h}_{i-1}} \right) \frac{\partial\mathbf{h}_j}{\partial\mathbf{w}_x}, \\ &= \frac{\partial\mathcal{L}_n}{\partial p_n} \odot \phi' \mathbf{h}_n^T \sum_{j=1}^n \left(\prod_{i=j+1}^n \phi' \mathbf{w}_{h,i}^T \right) \phi' \mathbf{x}_j^T.\end{aligned}\quad (4.5)$$

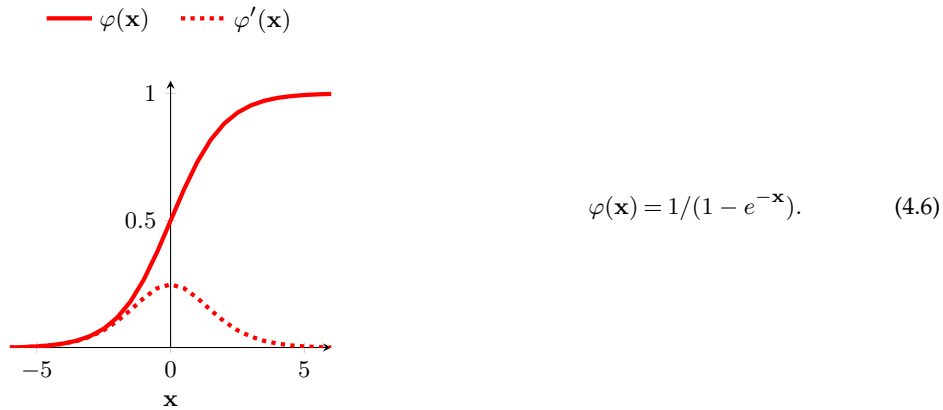
With $\partial\mathcal{L}_n/\partial\mathbf{w}_p$, $\partial\mathcal{L}_n/\partial\mathbf{w}_{h,i}$, and $\partial\mathcal{L}_n/\partial\mathbf{w}_x$ in hand we can apply the same update rule shown in Eq. 2.5.

Aside from many-to-one encoding, RNNs can produce many predictions given many inputs, or act similarly to an MLP and produce one or many outputs given a single input. We will discuss the application of recurrent neural networks to astronomical data in §5, after we introduce gated recurrent neural networks.

4(c) Sidestepping the vanishing gradient problem

In the early 1990s, researchers identified a major issue with the training of deep neural networks through backpropagation. Hochreiter first formally examined the ‘vanishing gradient’ problem in their diploma thesis (Hochreiter [91], see also later work by Bengio et al. [92]). Due to the vanishing gradient problem, it was widely believed that training very deep artificial neural networks from scratch via backpropagation was impossible. In this section we will explore what the vanishing gradient problem is, and how contemporary end-to-end trained neural networks sidestep this issue.

First let us remind ourselves of the sigmoid activation function introduced in Fig. 6:



Eq. 4.6 and its accompanying plot shows the output of a sigmoid function φ and its derivative φ' , when given an input \mathbf{x} .

Now, let us revisit the weight update rule for the $(L-n)$ th layer of a feedforward MLP (Eq. 2.4):

$$\frac{\partial\mathcal{L}}{\partial\mathbf{w}_{L-n}} = \frac{\partial\mathcal{L}}{\partial p_L} \odot \underbrace{\left(\prod_{i=1}^n \varphi'_{L-i} \mathbf{w}_{L-i}^T \right)}_{\lim_{n \rightarrow \infty} \prod_{i=1}^n \varphi'_{L-i} \mathbf{w}_{L-i}^T = 0} \left(\varphi'_{L-n} \mathbf{p}_{L-n-1}^T \right).\quad (4.7)$$

If φ' is typically less than one (as in Eq. 4.6 and most other saturating nonlinearities) the product term in the above equation becomes an issue. In that case, we can see that the product rapidly goes to zero as n (the number of layers) becomes large¹⁷. If we study Eq. 4.4, we can see the same

¹⁷Likewise, if φ' is typically greater than one, the product term rapidly ‘explodes’ to infinity. This is known as the ‘exploding gradient’ problem, also first identified in Hochreiter [91].

problem also plagues RNNs as we backpropagate through hidden states:

$$\frac{\partial \mathcal{L}_n}{\partial \mathbf{w}_h} = \frac{\partial \mathcal{L}_n}{\partial p_n} \odot \varphi' \mathbf{h}_n^T \sum_{j=1}^n \underbrace{\left(\prod_{i=j+1}^n \phi' \mathbf{w}_{h,i}^T \right)}_{\lim_{n \rightarrow \infty} \prod_{i=j+1}^n \phi' \mathbf{w}_{h,i}^T = 0} \phi' \mathbf{h}_{j-1}^T. \tag{4.8}$$

Let us solidify this issue by reminding ourselves of Eq. 2.5—the weight update rule for a network trained through backpropagation:

$$\mathbf{w}_{\text{next}} = \mathbf{w} - \eta \frac{\partial \mathcal{L}}{\partial \mathbf{w}}. \tag{4.9}$$

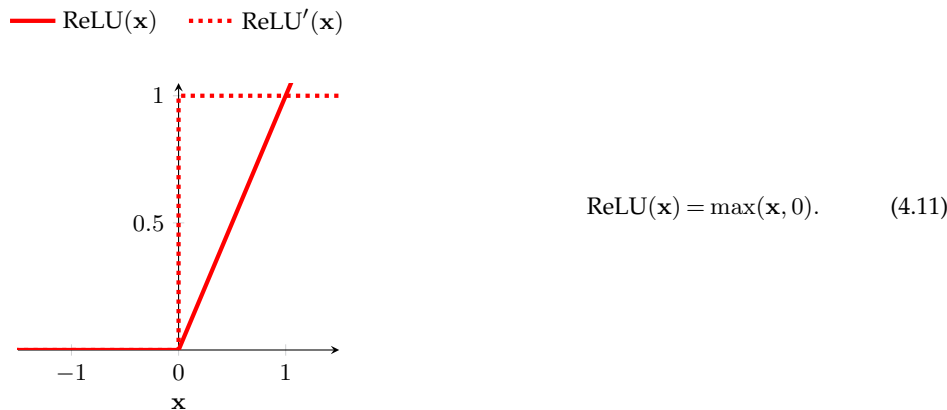
Combining Eq. 4.9 and the limits defined in Eq. 4.7 and Eq. 4.8 results in the below weight update rule in the limit $n \rightarrow \infty$.

$$\lim_{n \rightarrow \infty} \mathbf{w}_{\text{next}} = \mathbf{w}. \tag{4.10}$$

Eq. 4.10 shows that learning via backpropagation slows as we move deeper into the network. This problem once again caused a loss of faith in the connectionist model, ushering in the second AI winter. It took until 2012 for a new boom to begin. In the following three subsections we will explore some of the proposed partial solutions to the vanishing gradient problem and show how they came together to contribute to the current deep learning boom.

4(c.i) Non-saturating activation functions

We can see in Eq. 4.8 and Eq. 4.7 that if $\varphi' = 1$ then the product term does not automatically go to zero or infinity. If this is the case, why not simply design our activation function around this property? The rectified linear unit [ReLU; 31,32] is an activation function that does precisely this¹⁸:



The gradient of ReLU is unity if the inputs are above zero, exactly the property we needed to mitigate the vanishing gradient problem. Similar non-saturating activation functions also share the ReLU gradient’s useful property, see for example the Exponential Linear Unit, Swish, and Mish functions in Fig. 6.

4(c.ii) Graphics processing unit acceleration

If we can speed up training, we can run an inefficient algorithm (such as backpropagation through saturating activations) to completion in less time. One way to speed up training is by ¹⁸ReLU’ is always zero if its inputs are < 0, removing any signal for further training. This is known as the ‘dying ReLU’ problem, but is not as big of an issue as it first seems. Since contemporary deep neural networks are greatly overparameterised (see for example Frankle and Carbin [93] and other work on the ‘lottery ticket hypothesis’) backpropagation through the ReLU activation function can act as a pruning mechanism, creating sparse representations within the neural network and thus reducing training time even further [94].

using hardware that is specifically suited to the training of neural networks. Graphics processing units (GPUs) were originally developed to render video games and other intensive graphical processing tasks. These rendering tasks require a processor capable of massive parallelism. We have seen in the previous sections that neural networks trained through backpropagation also require many small weight update calculations. With this in mind, it is natural to try to accelerate deep neural networks using GPUs.

In 2004, Oh and Jung [95] were the first to use GPUs to accelerate an MLP model, reporting a $20\times$ performance increase on inference with a ATI RADEON 9700 PRO GPU accelerated neural network. Shortly after, Steinkrau et al. [96] showed that backpropagation can also benefit from GPU acceleration, reporting a three-fold performance increase in both training and inference. These two breakthroughs were followed by a flurry of activity in the area [e.g. 97–100], culminating in a milestone victory for GPU accelerated neural networks at ImageNet 2012. AlexNet [101] won the ImageNet classification and localisation challenges [102], scoring an unprecedented top-5 classification error of 16.4%, and a single object localisation error of 34.2%. In both challenges AlexNet scored over 10% better than the models in second place. Krizhevsky et al.’s winning network was a CNN [31] trained through backpropagation [36,86], with ReLU activation [32], and dropout [103] as a regulariser¹⁹. The performance increase afforded by GPU accelerated training enabled the network to be trained from scratch via backpropagation in a reasonable amount of time. The discovery that it is possible to train a neural network from scratch by using readily available hardware ultimately resulted in the end of connectionism’s second winter, and ushered in the Cambrianesque deep learning explosion of the mid-to-late 2010s and the 2020s (Fig. 10).

4(c.iii) Gated recurrent neural networks and residual networks

The long short-term memory unit [LSTM; 105,106]²⁰ mitigates the vanishing gradient problem by introducing a new hidden state, the ‘cell state’ (\mathbf{c}_n), to the standard RNN architecture. This cell state allows the network to learn long range dependencies, and we will show why this is the case via a brief derivation²¹. First, as always, let us study Fig. 11 and write down the forward pass equation for updating the cell state:

$$\mathbf{c}_n = f(\mathbf{c}_{n-1}, \mathbf{h}_{n-1}, \mathbf{x}_n) + g(\mathbf{h}_{n-1}, \mathbf{x}_n)$$

where $f(\mathbf{c}_{n-1}, \mathbf{h}_{n-1}, \mathbf{x}_n) = \mathbf{c}_{n-1} \odot \varphi(\mathbf{h}_{n-1}, \mathbf{x}_n)$. For brevity we define $\varphi_n = \varphi(\mathbf{h}_{n-1}, \mathbf{x}_n)$.

Like the RNN case (Eq. 4.4 and Eq. 4.5), we will need to find $\partial \mathbf{c}_n / \partial \mathbf{c}_{n-1}$ to calculate $\nabla \mathcal{L}$. Therefore,

$$\begin{aligned} \frac{\partial \mathbf{c}_n}{\partial \mathbf{c}_{n-1}} &= \frac{\partial f(\mathbf{c}_{n-1}, \mathbf{h}_{n-1}, \mathbf{x}_n)}{\partial \mathbf{c}_{n-1}} + \frac{\partial g(\mathbf{h}_{n-1}, \mathbf{x}_n)}{\partial \mathbf{c}_{n-1}}, \\ &= \frac{\partial \mathbf{c}_{n-1} \odot \varphi_n}{\partial \mathbf{c}_{n-1}}, \\ &= \mathbf{c}_{n-1} \frac{\partial \varphi_n}{\partial \mathbf{c}_{n-1}} + \frac{\partial \mathbf{c}_{n-1}}{\partial \mathbf{c}_{n-1}} \varphi_n, \\ &= \varphi_n. \end{aligned}$$

¹⁹Dropout reduces the amount of neural network overfitting – where a network performs well on the training set at the expense of performance on data it has not yet seen. One performs dropout by randomly removing a set of neurons at each training step, and using all neurons at test time. This set up essentially trains a large ensemble of sub-models, whose average prediction outperforms that inferred by a single model.

²⁰Compare also the gated recurrent unit [GRU; 107].

²¹Here we loosely follow Bayer [108, §1.3.4].

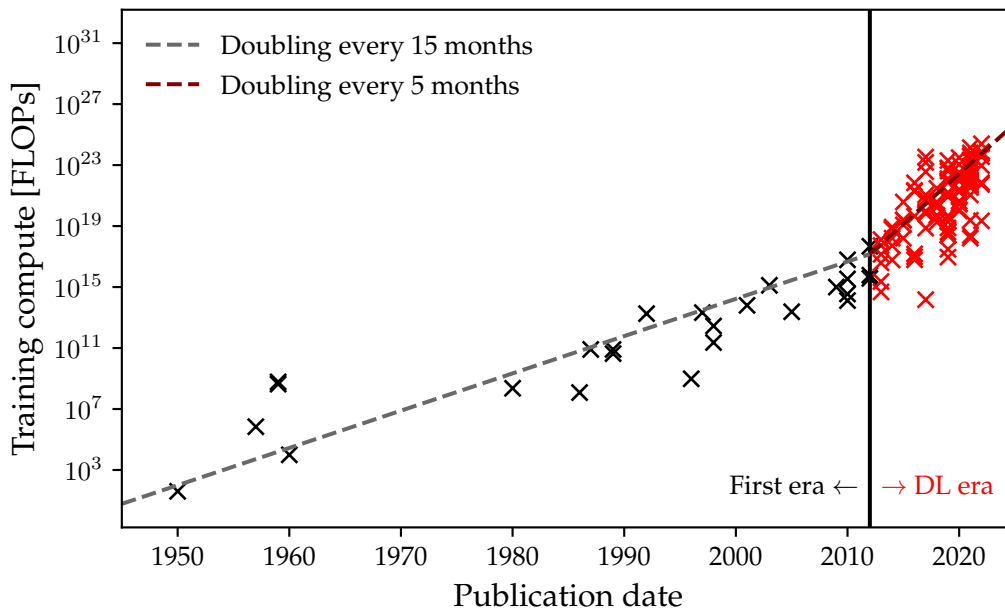


Figure 10: If we plot the total number of floating point operations (FLOPs) required to train a neural network model, and compare it to the model’s publication date, we can see a change in trend at around 2012. This corresponds to the popularisation of GPU accelerated training of very deep neural networks, with 2012 demarcating AI’s ‘Deep Learning Era’ and the beginning of astronomy’s second wave of connectionism (S5). Data is taken from Sevilla et al. [104].

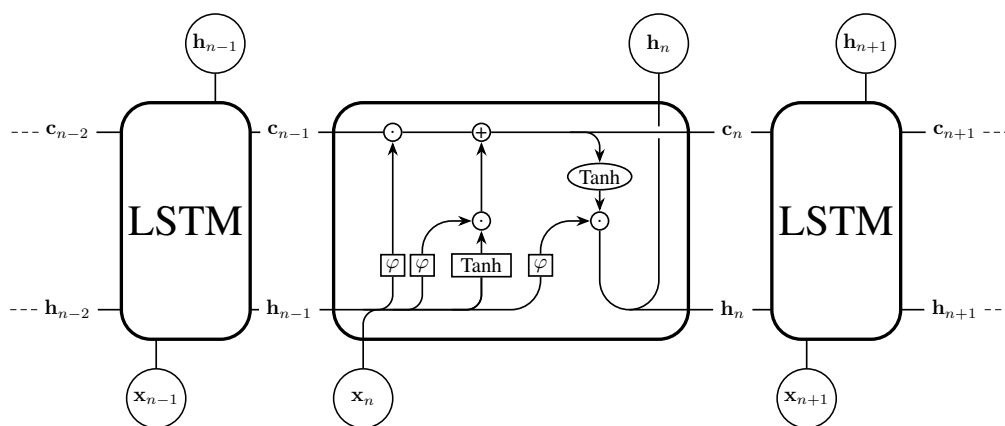


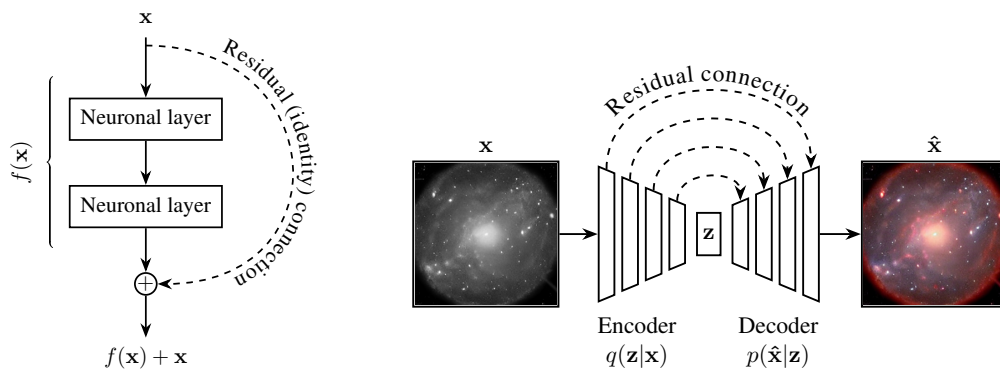
Figure 11: A set of sequential data \mathbf{x}_n is input into an LSTM network. Inside the cell \circ denotes elementwise operations and \square denotes neuronal layers. φ is the sigmoid activation function, and Tanh is the hyperbolic tangent activation function. \oplus is an elementwise addition, \odot is the Hadamard product, and line mergers are concatenations. \mathbf{c}_n is the cell state, and \mathbf{h}_n is the hidden state.

Thus, if we want to backpropagate to a cell state deep in the network we must calculate

$$\frac{\partial \mathbf{c}_n}{\partial \mathbf{c}_N} = \prod_{i=1}^{n-N} \varphi_i, \quad n > N. \tag{4.12}$$

The product term above does not depend on the derivative of a saturating activation function, and so does not automatically vanish as N goes to ∞ . This means that a gradient signal can be carried through the LSTM cell state without losing amplitude and vanishing²².

We can use a technique derived from the LSTM to solve our vanishing gradient problem for deep feedforward neural networks (as studied in §2(b)). Srivastava et al. [111] do this by applying the concept of the LSTM’s cell state to their deep convolutional ‘highway network’. The highway network uses gated connections to modulate the gradient flow back through neuronal layers. Later work by He et al. [112] introduces the residual network (ResNet) by taking a highway network and simplifying its connections. They apply an elementwise addition (or ‘residual connection’) in place of the highway network’s gated connection (Fig. 12a). One can go even further with residual connections, as Ronneberger et al. [113] demonstrate with their U-Net model. The U-Net combines residual connections with an autoencoder-like architecture (Fig. 12b). The U-Net has gone on to become the *de facto* network for many tasks that require an input and output of the same size (such as segmentation, colourisation, and style transfer).



(a) A single residual connection is applied within a neural network. (b) The U-Net, a network that was originally developed to segment biological imagery uses the residual connection.

Figure 12: The left subfigure shows the residual connection as originally introduced in He et al. [112]. The right subfigure shows an application of the residual connection to an autoencoder like architecture [113], in this case colourising an astronomical object.

4(d) Translation, attention, and transformers

Theoretically, gated RNNs (GRNNs) such as the LSTM can learn very long range dependencies (see Eq. 4.12 and its accompanying text). In practice, GRNNs tend to forget information about distant inputs. This is because the GRNN lacks unmediated access to inputs beyond the immediate antecedent as a consequence of its recurrent architecture. The problem is especially apparent in neural machine translation tasks that require knowledge of an entire sequence to produce an output, such as language to language translation. Fig. 13 shows such a sequence to

²²Which is great in theory. In practice, LSTMs still have trouble learning very long range dependencies due to their reliance on recurrent processing [109]. Transformer networks [110] are an architecture that uses the concept of attention to address this issue. We will discuss transformer networks in §4(d).

sequence [Seq2Seq; 109] model. Seq2Seq translates between two sets of sequential data by sharing a hidden state between two GRNN units. In Fig. 13 we can see that the shared information is bottlenecked by the hidden state. Therefore, to resolve the GRNN ‘forgetting problem’ we must find a way to avoid any recursion, or serial processing of input and output. We can do this by providing the neural network access to all input while it is calculating an output. This was the primary motivation behind the transformer architecture [110,114].

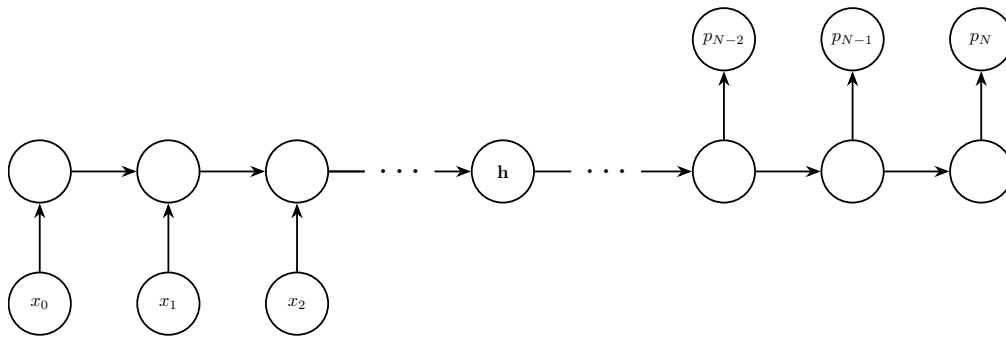


Figure 13: A sequence to sequence [Seq2Seq; 109] model. A sequence \mathbf{x} is input into a GRNN. The final hidden state (\mathbf{h}) of the input network is then passed into a second GRNN. The second GRNN then unrolls to predict an output sequence \mathbf{p} . Due to the hidden state acting as an intermediary, \mathbf{x} and \mathbf{p} need not be of equal length.

Modern transformer architectures consist of a series of self-attention layers, often interspersed with other layer types²³. Self-attention as described in Vaswani et al. [110] is shown in Fig. 14. Intuitively, it captures the relationships between quanta within a data input. To perform self-attention we first take an input sequence

$$\mathbf{x} = [x_1 \quad x_2 \quad \cdots \quad x_n],$$

where \mathbf{x} can be any sequence, such as a sentence, a variable star’s time series, or an unravelled galaxy image²⁴. Here we will follow the literature and refer to $[x_1, \dots, x_n]$ as tokens. As we can see in Fig. 14 the input is passed through a trainable pair of weight matrices \mathbf{Q} and \mathbf{K} . The output matrices \mathbf{q} and \mathbf{k}^\dagger are then multiplied together to yield

$$(\mathbf{Q} \cdot \mathbf{x})(\mathbf{K} \cdot \mathbf{x})^\dagger = \mathbf{q}\mathbf{k}^\dagger = \begin{bmatrix} Q_1x_1K_1x_1 & Q_1x_1K_2x_2 & \cdots & Q_1x_1K_nx_n \\ Q_2x_2K_1x_1 & Q_2x_2K_2x_2 & \cdots & Q_2x_2K_nx_n \\ \vdots & \vdots & \ddots & \vdots \\ Q_nx_nK_1x_1 & Q_nx_nK_2x_2 & \cdots & Q_nx_nK_nx_n \end{bmatrix}. \quad (4.13)$$

We can see that Eq. 4.13 describes the relationships between tokens within \mathbf{x} . For example, if x_1 is similar semantically to x_2 , we would expect $Q_1x_1K_2x_2$ and $Q_2x_2K_1x_1$ to have a high value. We then normalise $\mathbf{q}\mathbf{k}^\dagger$ to mitigate vanishing gradients²⁵, and apply a softmax nonlinearity so that the maximum weighting (or similarity) is one.

²³In the original transformer formulation described in Vaswani et al. [110], the network consisted of a connected ‘encoder’ and ‘decoder’ section much like a Seq2Seq model (Fig. 13). Later work has found this to be an unnecessary complication. For example, the generative pretrained transformer (GPT) 2 and 3 models [12,115] consist of only decoder layers, and the bidirectional encoder representations from transformers (BERT) model consists of only encoder layers [116].

²⁴One can go very general with this, as DeepMind demonstrated with their ‘Gato’ transformer model [117]. Gato can predict sequences for myriad tasks, from operating a physical robotic arm, to completing natural language sentences, to playing Atari games.

²⁵See Footnote 17.

Meanwhile, the input sequence \mathbf{x} is passed through the neuronal layer \mathbf{V} , resulting in a weighted representation \mathbf{v} :

$$\mathbf{V} \cdot \mathbf{x} = \mathbf{v} = [V_1x_1 \quad V_2x_2 \quad \dots \quad V_nx_n].$$

\mathbf{v} is multiplied with the similarity matrix $\varsigma(\mathbf{q}\mathbf{k}^\dagger/\sqrt{n})$. This process weighs similar tokens within the sequence higher, increasing their relative importance in later neuronal layers.

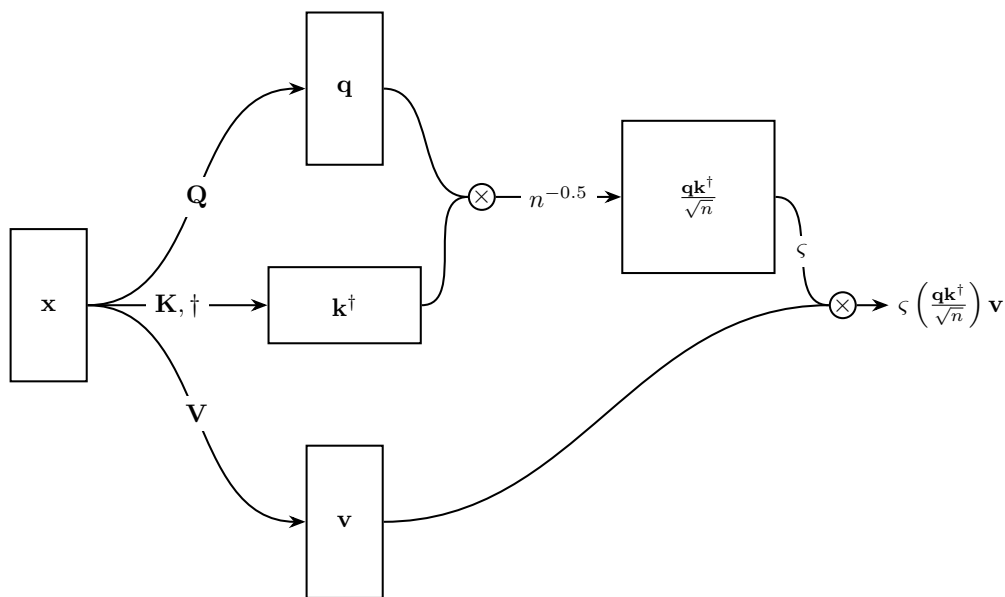


Figure 14: An input (\mathbf{x}) is fed into a self-attention mechanism. The weights used to produce the query (\mathbf{q}), key (\mathbf{k}), and value (\mathbf{v}) matrices are learnt via backpropagation. Here the learnt weights are denoted as the capitalised versions of their child matrices. \mathbf{q} and \mathbf{k} are normalised and multiplied together, and a softmax nonlinearity (ς) is applied. Finally, \mathbf{v} is multiplied with output of the upper path and the final output is fed forward to the next neuronal layer. \otimes denotes a matrix multiplication.

5. Astronomy’s second wave of connectionism

Compared to classical machine learning techniques²⁶ deep learning as outlined in §4 does not require an extraction of emergent parameters to train its models. RNNs in particular are well suited to observing the full raw information within a time series. Likewise, CNNs are well suited to observing raw information within image-based data. Astronomy is rich with both types of data, and in this section we will review the history of the application of RNN, CNN, and transformer models to astronomical data.

5(a) Recurrent neural network applications

RNNs were first applied in astronomy very close to home; Aussem et al. [118] predicted atmospheric seeing for observations from ESO’s Very Large Telescope, and the prediction of geomagnetic storms given data on the solar wind was also explored in the mid-to-late 1990s and early 2000s ([119], [120], and other work from the same group; [121]).

²⁶This includes most MLP applications in astronomy, see §3.

The first use of RNNs for classification in astronomy was carried out in a prescient study by Brodrick et al. [122]. They describe the use of an RNN-like Elman network [123]. Their RNN was tasked with the search for artificially generated narrowband radio signals that resemble those that may be produced by an extraterrestrial civilisation. They found that their model had a test set accuracy of 92%, suggesting that RNNs could be a useful tool in the search for extraterrestrial intelligence. More than a decade after Brodrick et al. [122], Charnock and Moss [124] used an LSTM (Fig. 11) to classify simulated supernovae. They describe two classification problems. One, a binary classification between type-Ia and non type-Ia supernovae, and the other a classification between supernovae types I, II, and III. For their best performing model they report an accuracy of more than 95% for their binary classification problem, and an accuracy of over 90% for their trinary classification. This study cemented the usefulness of RNNs for classification problems in astronomy. Charnock and Moss [124] was followed by numerous projects studying the use of RNNs for classification of time series astronomical data. A non-exhaustive list of modern RNN use in astronomy includes: stochastically sampled variable star classification [125]; exoplanet instance segmentation [126]; variable star/galaxy sequential imagery classification [127]; and gamma ray source classification [128]. We must conclude from these studies that RNNs are effective classifiers of astronomical time series, provided that sufficient data is available.

Of course, recurrent networks are not limited to classification; they can also be used for regression problems. First, Weddell and Webb [129] successfully used an echo state network [130] to predict the point spread function of a target object in a wide field of view. Capizzi et al. [131] used an RNN to inpaint missing NASA Kepler time series data for stellar objects. They found that their model could recreate the missing time series to an excellent accuracy, suggesting that the RNN could internalise information about the star it was trained on. As in the classification case, research into the use of RNNs for regression problems picked up massively in the late 2010s, and here we will highlight a selection of these studies that represent the range of RNN use cases. Shen et al. [132] used both an LSTM and an autoencoder based RNN to denoise gravitational wave data, and Morningstar et al. [133] used a recurrent inference machine to reconstruct gravitationally lensed galaxies. Liu et al. [134] used an LSTM to predict solar flare activity. From these studies, similarly to the classification case above, we can once again conclude that RNNs are effective regressors of astronomical time series.

RNNs have also been used in cases that are a little more unconventional. For example, Kügler et al. [135] used an autoencoding RNN (specifically an echo state network) to extract representation embeddings of variable main sequence stars. They find that these embeddings capture some emergent properties of these variable stars, such as temperature, and surface gravity, suggesting that clustering within the embedding space could result in semantically meaningful variable star classification. We will revisit this line of research when we explore representation learning within astronomy in detail in §8. An example of more drastic cross-pollination between ideas within deep learning and those within astronomy is Smith et al. [136]. They use an encoder-decoder network comprising of a CNN encoder and RNN decoder to predict surface brightness (SB) profiles of galaxies. This class of neural network was previously used extensively within natural language image captioning, and by treating SB profiles as ‘captions’ their model was capable of prediction over $100\times$ faster than the previous classical, human-agent based method.

5(b) Convolutional neural network applications

It did not take long after Krizhevsky et al. [101] established CNNs as the *de facto* image classification network for astronomers to take notice: in 2014 they were applied in the search for pulsars [137] as part of an ensemble of methods. Zhu et al. [137] found that their ensemble was highly effective, with 100% of their test set pulsar candidates being ranked within the top 961 of the 90 008 test candidates. Shortly after, Hála [138] described the use of one dimensional CNNs for a ternary classification problem. They find that their model is capable of classifying 1D spectra into quasars, galaxies, and stars to an impressive accuracy. CNNs have been also been

extensively used in galaxy morphological classification. First on the scene was Dieleman et al. [139]. They used CNNs to classify galaxy morphology parameters as defined in the Galaxy Zoo dataset [140] from galaxy imagery. They observed their galaxies via the SDSS, and found a 99% consensus between the Galaxy Zoo labels, and the CNN classifications. Huertas-Company et al. [141] showed that Dieleman et al.'s CNN is equally applicable to morphological classification of galaxies in the CANDELS fields [142]. Likewise, Aniyan and Thorat [143] showed that CNNs are capable of classifying radio galaxies. The combined work of Dieleman et al. [139], Huertas-Company et al. [141], and Aniyan and Thorat [143] confirms that CNNs are equally applicable to visually dissimilar surveys, with little-to-no modification. Looking a little further afield, Wilde et al. [144] used a deep CNN model to classify simulated lensing events. They also applied some interpretability techniques to their data, using occlusion mapping [145], gradient class activation mapping [146], and Google's DeepDream to prove that the CNN was indeed classifying via observing the gravitational lenses. Alternative CNN models have also been used, such as the U-Net (Fig. 12b). The U-Net was initially developed to segment biological imagery [113]. Its first use in astronomy was related: Akeret et al. [147] use a U-Net [113] CNN to isolate via segmentation, and ultimately remove, radio frequency interference from radio telescope data. Likewise, Berger and Stein [148] used a three dimensional U-Net [V-Net; 149] to predict and segment out galaxy dark matter haloes in simulations, and Aragon-Calvo [150] used a V-Net to segment out the cosmological filaments and walls that make up the large scale structure of the Universe. Hausen and Robertson [151] demonstrate that a U-Net is capable of performing pixelwise semantic classification of objects in *HST*/CANDELS imagery, thus proving that U-Nets are capable of useful work directly within large imaging surveys, particularly in the deblending of overlapping objects, which is a perennial challenge in deep imaging. The U-Net in Lauritsen et al. [152] is used to superresolve simulated submillimetre observations. They found that the U-Net could successfully do this when using a loss comprising of the L1 loss, and a custom loss that measures the distance between predicted and ground truth point sources. We must conclude from the studies described in this subsection that CNNs are effective classifiers and regressors of image-based astronomical data.

5(c) Transformer applications

Although initially used for natural language, transformers have also been adapted for use in imagery, first by Parmar et al. [153], and also in Dosovitskiy et al. [13]. To our knowledge, transformers have not yet been applied to astronomical imagery, but they have started to find use in time-series astronomy. Donoso-Oliva et al. [154] used BERT [116] to generate a representation space for light curves in a self-supervised manner. Morvan et al. [155] use an encoding transformer to denoise light curves from the Transiting Exoplanet Survey Satellite [TESS; 156], and show that the denoising surrogate task results in an expressive embedding space. Pan et al. [157] also use a transformer model to analyse light curves for exoplanets. Transformers have taken the fields of natural language processing and computer vision by storm (§9), and so if we extrapolate from trends in other fields we expect to see many more examples of transformers applied to astronomical use cases in the near future. We will revisit the transformer architecture in the context of foundation models [158, and references therein], and their possible future astronomical applications in §9.

5(d) A problem with supervised learning

Supervised learning requires a high quality labelled dataset to train a neural network. In turn, these datasets require labourious human intervention to create, and so supervised data is in short supply. One can avoid this issue by letting the deep learning model infer the data labels itself, and project these labels onto a hidden descriptive 'latent space'. Indeed, all of the networks described previously in this review can be repurposed for non-supervised tasks, and in §6 and §7 we will explore some deep learning frameworks that do not require supervision.

6. Deep generative modelling

In this section we discuss generative modelling within the context of astronomy. Unlike discriminative models, generative models explicitly learn the distribution of classes in a dataset (Fig. 15). Once we learn the distribution of data, we can use that knowledge to generate new synthetic data that resembles that found in the training dataset. In the following subsections we will explore in detail three popular forms of deep generative model: the variational autoencoder (§6(a)); the generative adversarial network (§6(b)); and the family of score-based (or diffusion) models (§6(c)). Finally, in §8 we discuss applications of deep generative modelling in astronomy.

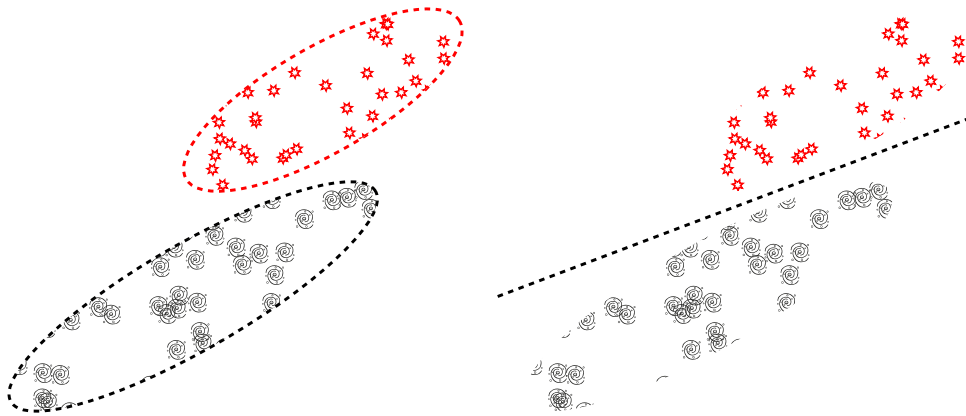


Figure 15: On the left we see a generative model attempting to learn the probability distributions of a dataset that contains a set of galaxies, and a set of stars. On the right is a discriminative model, which is attempting to learn the boundary that separates the star and galaxy types.

6(a) (Variational) autoencoders

Autoencoders have long been a neural network architectural staple. In a sister paper to backpropagation's populariser, Rumelhart et al. [159] demonstrate backpropagation within an autoencoder. Fig. 16 demonstrates the basic neural network autoencoder architecture. An autoencoder is tasked with recreating some input data, squeezing the input information (\mathbf{x}) into a bottleneck latent vector (\mathbf{z}) via a neural network $q(\mathbf{z}|\mathbf{x})$. \mathbf{z} is then expanded to an imitation of the input data ($\hat{\mathbf{x}}$) by a second neural network $p(\hat{\mathbf{x}}|\mathbf{z})$. The standard autoencoder is trained via a reconstruction loss; $\mathcal{L}_R(\mathbf{x}, \hat{\mathbf{x}})$, where $\mathcal{L}_R(\mathbf{x}, \hat{\mathbf{x}})$ measures the difference in pixelspace between \mathbf{x} and $\hat{\mathbf{x}}$.

Naïvely, one would think that once trained, one could 'just' sample a new latent vector, and produce novel imagery via the decoding neural network $p(\hat{\mathbf{x}}|\mathbf{z})$. We cannot do this, as autoencoders trained purely via a reconstruction loss have no incentive to produce a smoothly interpolatable latent space. This means we can use a standard autoencoder to embed and retrieve data contained in the training set, but cannot use one to generate new data. To generate new data we require a smooth latent space, which variational autoencoders (VAEs; Fig 17) produce by design [160].

A VAE differs from the standard autoencoder by enforcing a spread in each training set samples' latent vector. We can see in Fig. 17 how this is done; instead of directly predicting \mathbf{z} the encoder q predicts two vectors, $\boldsymbol{\mu}$ and $\boldsymbol{\sigma}$. \mathbf{z} is then sampled stochastically via the equation

$$\mathbf{z} = \boldsymbol{\mu} + \boldsymbol{\sigma} \odot \boldsymbol{\epsilon}, \quad (6.1)$$

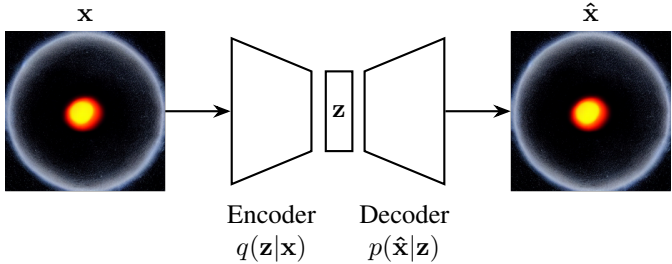


Figure 16: An autoencoder [159] attends to an image of a black hole. \mathbf{z} is a latent vector and \mathbf{x} is a sample from a training set. The encoder, q learns to encode the incoming data into a latent vector while the decoder p takes as input \mathbf{z} and attempts to recreate \mathbf{x} .

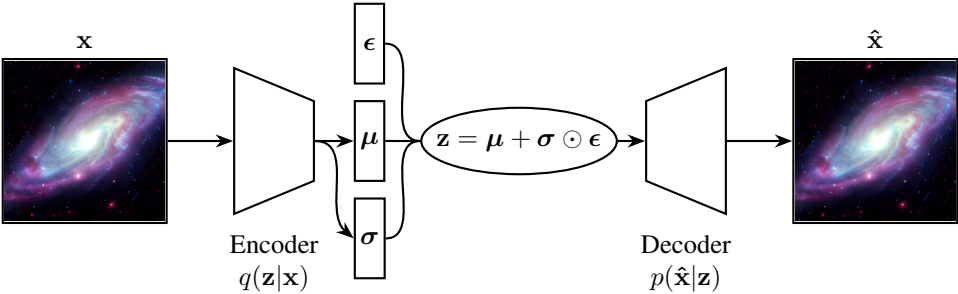


Figure 17: A variational autoencoder [160] operates on a spiral galaxy. \mathbf{z} is a latent vector and \mathbf{x} is a sample from the training set. The encoder, q learns to compress the incoming data into a latent vector that encodes the normal distribution. The decoder p takes as input \mathbf{z} and attempts to recreate \mathbf{x} .

where \odot is the Hadamard product, and ϵ is noise generated externally to the neural network graph²⁷. This spread results in similar samples overlapping within the latent space, and therefore we end up with a smooth latent space that we can interpolate through. However, currently there is no incentive for the neural network to provide a coherent, compact global structure in the latent space. For that we require a regularisation term in the loss. This regularisation is provided via the Kullback-Leibler (KL) divergence, which is a measure of the difference between two probability distributions. A standard VAE uses the KL divergence to push the latent distribution towards the standard normal distribution, incentivising a compact, continuous latent space. Hence, the final VAE loss is a combination of the reconstruction loss and KL divergence:

$$\mathcal{L}_{\text{VAE}} = \mathcal{L}_R(\mathbf{x}, \hat{\mathbf{x}}) + \text{KL}(q(\mathbf{x}|\mathbf{z})||p), \tag{6.2}$$

where p is some prior. In a standard VAE $p = \mathcal{N}(\mathbf{0}, \mathbf{1})$.

6(b) Generative adversarial networks

Generative adversarial networks [GAN; 161] can be thought of as a minimax game between two competing neural networks. If we anthropomorphise we can gain an intuition for how a GAN learns: let us imagine an art forger, and an art critic. The forger wants to paint paintings that are similar to famous expensive works, and needs to fool the critic when selling these

²⁷To avoid breaking the backpropagation chain the VAE injects noise via an external parameter, ϵ . This is described in Kingma and Welling [160] as the ‘reparameterisation trick’.

paintings. Meanwhile, the critic wants to ensure that no reproductions are sold and so they need to accurately determine whether any painting is an original or a reproduction. At first, our forger is a poor painter, and so the critic can easily identify our forger's works. However, the forger learns from the critic's choices and produces more realistic paintings. As the forger's paintings improve, the critic also learns better methods for detecting forgeries. This minimax game incentivises the critic to keep improving their classifications, and the forger to keep improving their painting. If this continues, we get to a point where the forger's works are indiscernible from the real thing—the forger has learnt to perfectly mimic the dataset! In a GAN, we name the critic the discriminator (D), and we name the forger the generator (G).

In Goodfellow et al.'s original GAN formulation (Fig. 18a), G and D compete during training in a minimax game where G aims to maximise the probability of D mispredicting that a generated datapoint is sampled from the real dataset. G takes as input a randomly sampled latent vector \mathbf{z} , and outputs a synthetic datapoint $G(\mathbf{z})$. D takes either this synthetic datapoint, or a real datapoint \mathbf{x} , and outputs $D(G(\mathbf{z}))$ or $D(\mathbf{x})$. This output is the probability that the datapoint is drawn from the real dataset. We compare this probability to a binary label indicating whether the datapoint is real or not, and backpropagate the error through both D and G . The network's weights are updated with each training datapoint to follow $\nabla_{\mathbf{w}} \mathcal{L}$ downwards until the distribution of $G(\mathbf{z})$ closely resembles that of the real dataset. Once trained, G can be used to generate entirely novel synthetic data that closely resembles (but is not identical to) the training set data.

In Fig. 18b we see that the GAN adversarial loss can be used to translate between image domains [162]. In Isola et al.'s Pix2Pix model, the generator takes as input an image \mathbf{x} , and attempts to produce a related image \mathbf{y} . Meanwhile, the discriminator attempts to discern whether the (\mathbf{x}, \mathbf{y}) pair that it is given is sampled from the training set, or the generator. Otherwise, Pix2Pix is trained in the same way as the standard GAN.

6(c) Score-based generative modelling and diffusion models

Diffusion models were introduced by Sohl-Dickstein et al. [163] and were first shown to be capable of producing high quality synthetic samples by Ho et al. [164]. Diffusion models are part of a family of generative deep learning models that employ denoising score matching via annealed Langevin dynamic sampling (first explored by Hyvärinen [165], Vincent [166]. More recent work can be found in Ho et al. [164], Song and Ermon [167], Jolicœur-Martineau et al. [168, 169], Song et al. [170]). This family of score-based generative models (SBGMs) can generate imagery of a quality and diversity surpassing state of the art GAN models [161], a startling result considering the historic disparity in interest and development between the two techniques [170–173]. SBGMs can super-resolve images [174,175], translate between image domains [176], separate superimposed images [177], and in-paint information [170,174].

Diffusion models define a diffusion process that projects a complex image domain space onto a simple domain space. In the original formulation, this diffusion process is fixed to a predefined Markov chain $q(\mathbf{x}_t | \mathbf{x}_{t-1})$ that adds a small amount of Gaussian noise with each step. As Fig. 19 shows, this 'simple domain space' can be noise sampled from a Gaussian distribution $\mathbf{x}_T \sim \mathcal{N}(\mathbf{0}, \mathbf{1})$.

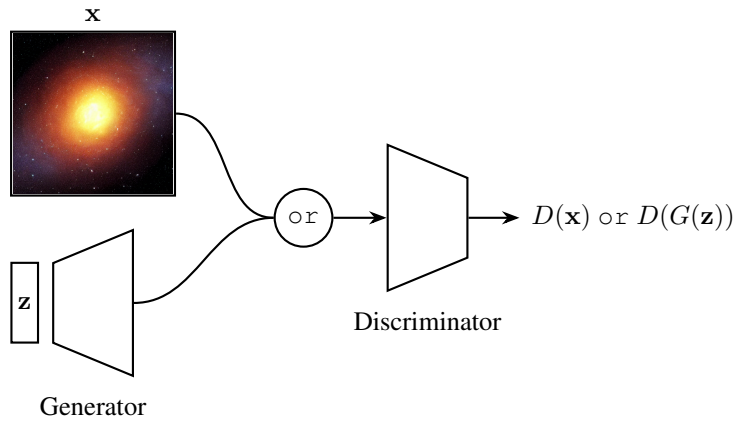
6(c.i) Forward process

To slowly add Gaussian noise to our data we define a Markov chain

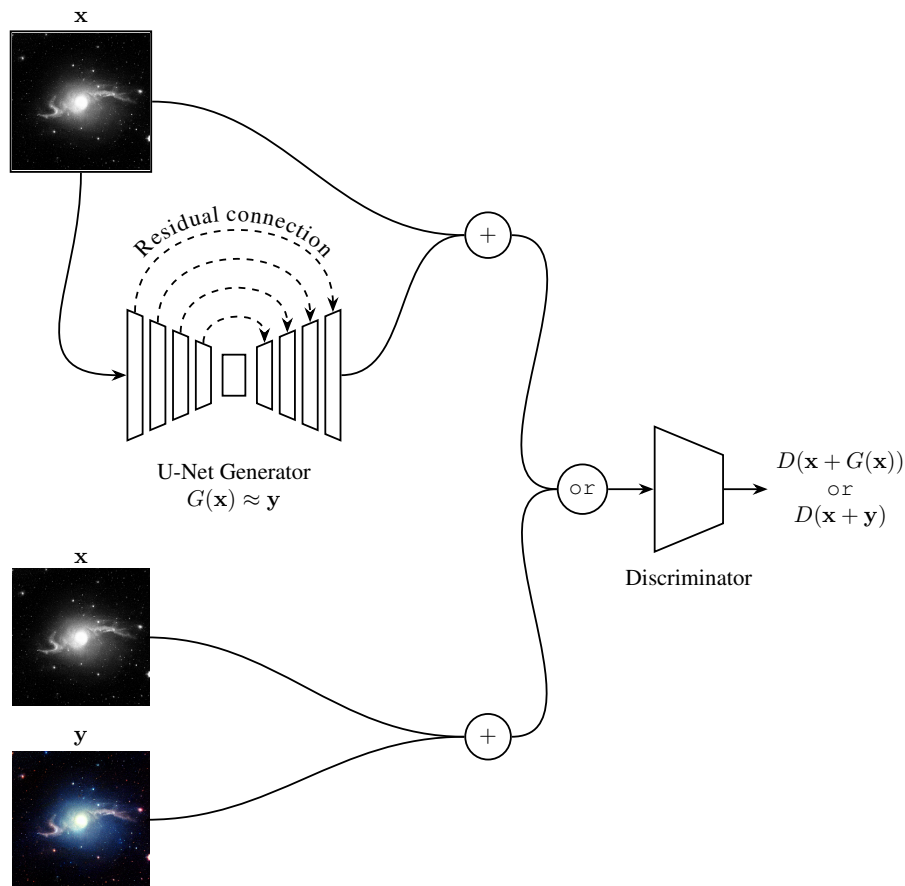
$$q(\mathbf{x}_{0..T}) = q(\mathbf{x}_0) \prod_{t=1}^T q(\mathbf{x}_t | \mathbf{x}_{t-1}).$$

The amount of noise added per step is controlled with a variance schedule $\{\beta_t \in (0, 1)\}_{t=1}^T$:

$$q(\mathbf{x}_t | \mathbf{x}_{t-1}) = \mathcal{N}(\mathbf{x}_t; \sqrt{1 - \beta_t} \mathbf{x}_{t-1}, \beta_t \mathbf{1}). \quad (6.3)$$



(a) A typical GAN according to Goodfellow et al. [161]. z is a noise vector, x is a sample from the training set. The discriminator learns to classify the incoming images as either fake or real, and the generator learns to fool the discriminator by producing realistic fakes.



(b) A Pix2Pix-like model with a U-Net generator [113,162]. The discriminator learns to classify the incoming image tuples as either fake or real. Meanwhile, the generator learns to fool the discriminator by approximating the colourisation function mapping $x \rightarrow y$.

Figure 18: The GAN and Pix2Pix models.

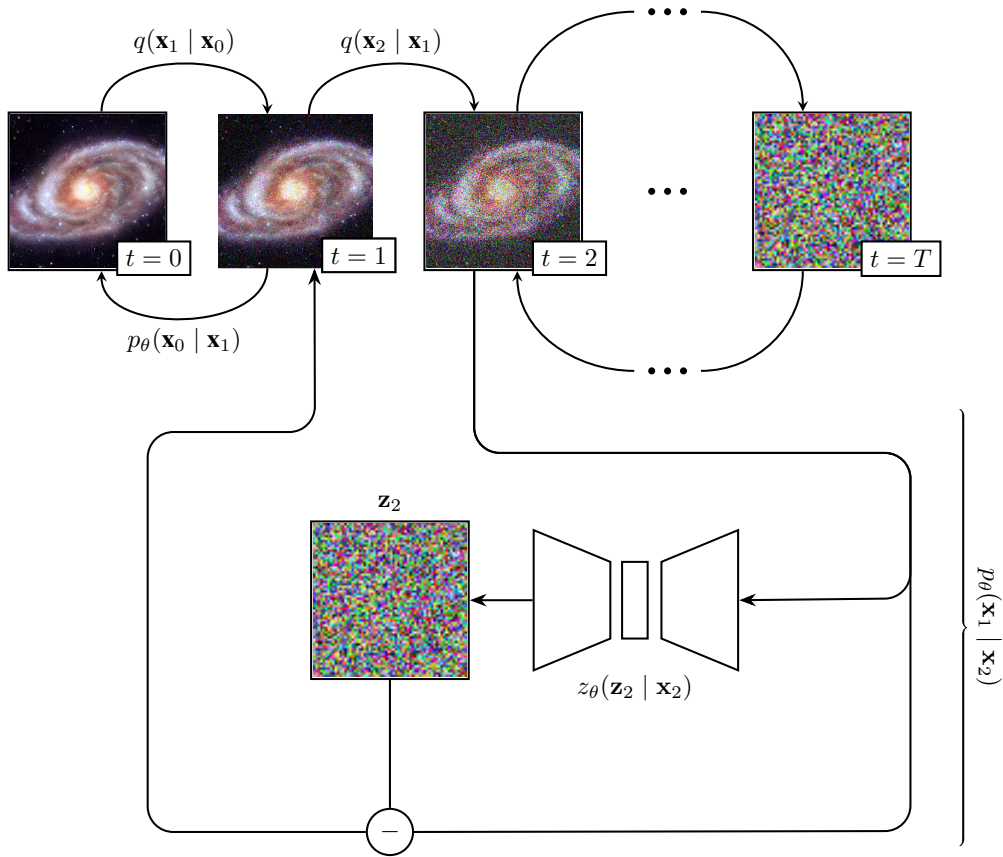


Figure 19: It is easy (and achievable without learnt parameters) to add noise to an image, but more difficult to remove it. Diffusion models attempt to learn an iterative removal process via training an appropriate neural network, $p_\theta(\mathbf{x}_{t-1} | \mathbf{x}_t)$.

This process is applied incrementally to the input image. Since we can define the above equation such that it only depends on \mathbf{x}_0 we can immediately calculate an image representation \mathbf{x}_t for any t [164]. If we define $\alpha_t = 1 - \beta_t$ and $\bar{\alpha}_t = \prod_{i=1}^t \alpha_i$:

$$\begin{aligned}
 \mathbf{x}_t &= \sqrt{\alpha_t} \mathbf{x}_{t-1} + \sqrt{1 - \alpha_t} \mathbf{z}_{t-1} \\
 &= \sqrt{\alpha_t \alpha_{t-1}} \mathbf{x}_{t-2} + \sqrt{(1 - \alpha_t) + \alpha_t (1 - \alpha_{t-1})} \bar{\mathbf{z}}_{t-2} \\
 &= \sqrt{\alpha_t \alpha_{t-1} \alpha_{t-2}} \mathbf{x}_{t-3} + \sqrt{(1 - \alpha_t \alpha_{t-1}) + \alpha_t \alpha_{t-1} (1 - \alpha_{t-2})} \bar{\mathbf{z}}_{t-3} \\
 &= \dots \\
 &= \sqrt{\bar{\alpha}_t} \mathbf{x}_0 + \sqrt{1 - \bar{\alpha}_t} \mathbf{z},
 \end{aligned} \tag{6.4}$$

where $\mathbf{z}_t \sim \mathcal{N}(\mathbf{0}, \mathbf{1})$ and $\bar{\mathbf{z}}$ is a combination of Gaussians. Plugging the above expression into Eq. 6.3 removes the \mathbf{x}_{t-1} dependency and yields

$$q(\mathbf{x}_t | \mathbf{x}_0) = \mathcal{N}(\mathbf{x}_t; \sqrt{\bar{\alpha}_t} \mathbf{x}_0, (1 - \bar{\alpha}_t) \mathbf{1}).$$

6(c.ii) Reverse process

Diffusion models attempt to reverse the forward process by applying a Markov chain with learnt Gaussian transitions. These transitions can be learnt via an appropriate neural network, p_θ :

$$p_\theta(\mathbf{x}_{0:T}) = p(\mathbf{x}_T) \prod_{t=1}^T p_\theta(\mathbf{x}_{t-1} | \mathbf{x}_t),$$

$$p_\theta(\mathbf{x}_{t-1} | \mathbf{x}_t) = \mathcal{N}(\mathbf{x}_{t-1}; \boldsymbol{\mu}_\theta(\mathbf{x}_t, t), \boldsymbol{\Sigma}_\theta(\mathbf{x}_t, t)).$$

While $\boldsymbol{\Sigma}_\theta(\mathbf{x}_t, t)$ can be learnt²⁸, the Ho et al. [164] formulation fixes $\boldsymbol{\Sigma}_\theta$ to an iteration-dependent constant $\sigma_t^2 \mathbb{1}$, where $\sigma_t^2 = 1 - \alpha_t$.

By recognising that diffusion models are a restricted class of hierarchical VAE²⁹, we see that we can train p_θ by optimising the evidence lower bound [ELBO, introduced in 160] that can be written as a summation over the Kullback-Leibler divergences at each iteration step³⁰:

$$\mathcal{L}_{\text{ELBO}} = \mathbb{E}_q \left[D_{\text{KL}}(q(\mathbf{x}_T | \mathbf{x}_0) \| p(\mathbf{x}_T)) + \sum_{t>1} D_{\text{KL}}(q(\mathbf{x}_{t-1} | \mathbf{x}_t, \mathbf{x}_0) \| p_\theta(\mathbf{x}_{t-1} | \mathbf{x}_t)) + \log p_\theta(\mathbf{x}_0 | \mathbf{x}_1) \right]. \quad (6.5)$$

In the Ho et al. [164] formulation, the first term in Eq. 6.5 is a constant during training and the final term is modelled as an independent discrete decoder. This leaves the middle summation. Each summand can be written as

$$\mathcal{L}(\boldsymbol{\mu}_t, \boldsymbol{\mu}_\theta) = \frac{1}{2\sigma_t^2} \|\boldsymbol{\mu}_t(\mathbf{x}_t, \mathbf{x}_0) - \boldsymbol{\mu}_\theta(\mathbf{x}_t, t)\|^2, \quad (6.6)$$

where $\boldsymbol{\mu}_\theta$ is the neural network's estimation of the forward process posterior mean $\boldsymbol{\mu}_t$. In practice it would be preferable to predict the noise addition in each iteration step (\mathbf{z}_t), as \mathbf{z}_t has a distribution that by definition is centred about zero, with a well defined variance. To this end we can define $\boldsymbol{\mu}_\theta$ as

$$\boldsymbol{\mu}_\theta(\mathbf{x}_t, t) = \frac{1}{\sqrt{\alpha_t}} \left(\mathbf{x}_t - \frac{1 - \alpha_t}{\sqrt{1 - \bar{\alpha}_t}} \mathbf{z}_\theta(\mathbf{x}_t, t) \right), \quad (6.7)$$

and by combining Eqs. 6.6 and 6.7 we get

$$\begin{aligned} \mathcal{L}(\mathbf{z}_t, \mathbf{z}_\theta) &= \frac{1}{2\sigma_t^2} \left\| \frac{1}{\sqrt{\alpha_t}} \left(\mathbf{x}_t - \frac{1 - \alpha_t}{\sqrt{1 - \bar{\alpha}_t}} \mathbf{z}_t \right) - \frac{1}{\sqrt{\alpha_t}} \left(\mathbf{x}_t - \frac{1 - \alpha_t}{\sqrt{1 - \bar{\alpha}_t}} \mathbf{z}_\theta(\mathbf{x}_t, t) \right) \right\|^2 \\ &= \frac{(1 - \alpha_t)^2}{2\sigma_t^2 \alpha_t (1 - \bar{\alpha}_t)} \|\mathbf{z}_t - \mathbf{z}_\theta(\mathbf{x}_t, t)\|^2. \end{aligned} \quad (6.8)$$

Ho et al. [164] empirically found that a simplified version of the loss described in Eq. 6.8 results in better sample quality. They use a simplified version of Eq. 6.8 as their loss, and optimise to predict the noise required to reverse a forward process iteration step:

$$\mathcal{L}(\mathbf{z}_t, \mathbf{z}_\theta) = \|\mathbf{z}_t - \mathbf{z}_\theta(\mathbf{x}_t, t)\|^2, \quad \text{where } \mathbf{x}_t = \sqrt{\bar{\alpha}_t} \mathbf{x}_0 + \sqrt{1 - \bar{\alpha}_t} \mathbf{z}_t. \quad (6.9)$$

By recognising that $\mathbf{z}_t = \sigma_t^2 \nabla_{\mathbf{x}_t} \log q(\mathbf{x}_t | \mathbf{x}_{t-1})$, we see that Eq. 6.9 is equivalent to denoising score matching over t noise levels [166]. This connection establishes a link between diffusion models and other SBGMs [such as 167,168,180].

²⁸See for example Nichol and Dhariwal [171].

²⁹Denoising autoencoders (§6(a)) have an interesting relationship with score-based generative (or diffusion) models. As a taster, Turner [178] reframe diffusion models as a class of hierarchical denoising VAE, and Dieleman [179] show through a brief derivation that diffusion models optimise the same loss as a denoising autoencoder.

³⁰See Appendix B in Sohl-Dickstein et al. [163] and Appendix A in Ho et al. [164] for the full derivation.

To run inference for the reverse process, one progressively removes the predicted noise \mathbf{z}_θ from an image. The predicted noise is weighted according to a variance schedule:

$$\mathbf{x}_{t-1} = \frac{1}{\sqrt{\bar{\alpha}_t}} \left(\mathbf{x}_t - \frac{1 - \alpha_t}{\sqrt{1 - \bar{\alpha}_t}} \mathbf{z}_\theta(\mathbf{x}_t, t) \right) + \sigma_t \mathbf{z}.$$

If we take $p(\mathbf{x}_T) \sim \mathcal{N}(\mathbf{x}_T; \mathbf{0}, \mathbf{1})$, we can use p_θ to generate entirely novel data that are similar, but not identical to, those found in the training set.

6(c.iii) Denoising diffusion implicit models

Ho et al.'s diffusion model performs inference at a rate orders of magnitude slower than single shot generative models like the VAE (§6(a)) or the GAN (§6(b)). This is because diffusion models need to sequentially reverse every step in the forward process Markov Chain. Reducing the inference time for diffusion models is an active area of research [169,181,182], and here we will review one proposed solution to the problem; the denoising diffusion implicit model [DDIM; 183].

Song et al. [183] propose the following decomposition of Eq. 6.4:

$$\begin{aligned} \mathbf{x}_{t-1} &= \sqrt{\bar{\alpha}_{t-1}} \mathbf{x}_0 + \sqrt{1 - \bar{\alpha}_{t-1}} \mathbf{z}_\theta(\mathbf{x}_t, t) \\ &= \sqrt{\bar{\alpha}_{t-1}} \mathbf{x}_0 + \sqrt{1 - \bar{\alpha}_{t-1} - \sigma_t^2} \mathbf{z}_\theta + \sigma_t \mathbf{z}_t \\ &= \sqrt{\bar{\alpha}_{t-1}} \underbrace{\left(\frac{\mathbf{x}_t - \sqrt{1 - \bar{\alpha}_t} \mathbf{z}_\theta}{\sqrt{\bar{\alpha}_t}} \right)}_{\mathbf{x}_0 \text{ prediction}} + \underbrace{\sqrt{1 - \bar{\alpha}_{t-1} - \sigma_t^2} \mathbf{z}_\theta}_{\text{vector towards } \mathbf{x}_t} + \underbrace{\sigma_t \mathbf{z}_t}_{\text{noise}}. \end{aligned}$$

Intuitively, the first term can be thought of as the prediction of the input image \mathbf{x}_0 , given an iteration step t . The second term can be thought of as a vector from \mathbf{x}_{t-1} towards the current iteration step image \mathbf{x}_t . The third term is random noise. If we substitute in \mathbf{x}_t from Eq. 6.9 we make this intuition explicit:

$$\mathbf{x}_{t-1} = \sqrt{\bar{\alpha}_{t-1}} \mathbf{x}_0 + \sqrt{1 - \bar{\alpha}_{t-1} - \sigma_t^2} \frac{\mathbf{x}_t - \sqrt{\bar{\alpha}_t} \mathbf{x}_0}{\sqrt{1 - \bar{\alpha}_t}} + \sigma_t \mathbf{z}_t.$$

If we then set $\sigma_t = 0$, we remove the noise dependency and the forward process becomes deterministic:

$$q_{\text{DDIM}}(\mathbf{x}_{t-1} | \mathbf{x}_t, \mathbf{x}_0) = \sqrt{\bar{\alpha}_{t-1}} \mathbf{x}_0 + \sqrt{1 - \bar{\alpha}_{t-1}} \frac{\mathbf{x}_t - \sqrt{\bar{\alpha}_t} \mathbf{x}_0}{\sqrt{1 - \bar{\alpha}_t}}. \quad (6.10)$$

This means that DDIMs can deterministically map to and from the latent space, and so inherit all the benefits of this property. For example, two objects sampled from similar latent vectors share high level properties, latent space arithmetic is possible, and we can perform meaningful interpolation within this space. We demonstrate DDIM latent space interpolation in Fig. 20.

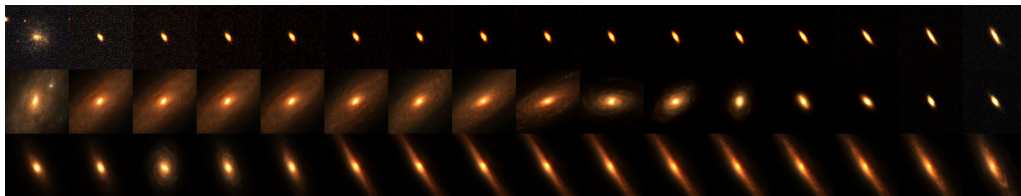


Figure 20: Meaningful latent space interpolation via a DDIM model [183,184]. This property comes ‘for free’ with most other generative models, however the Denoising Diffusion Probabilistic Model [164] requires a tweak to its sampling scheme (Eq. 6.10).

We can also subsample every τ number of steps at inference time, where τ is a set of evenly spaced steps between 0 and T , the maximum number of steps in the forward process:

$$q_{\text{DDIM}}(\mathbf{x}_{\tau_{i-1}} | \mathbf{x}_{\tau_i}, \mathbf{x}_0) = \sqrt{\bar{\alpha}_{t-1}} \mathbf{x}_0 + \sqrt{1 - \bar{\alpha}_{t-1}} \frac{\mathbf{x}_{\tau_i} - \sqrt{\bar{\alpha}_t} \mathbf{x}_0}{\sqrt{1 - \bar{\alpha}_t}}. \quad (6.11)$$

As shown in Song et al. [183] this results in acceptable generations with a T/τ inference speed up.

7. Representation learning

Self-supervised representation learning has recently exploded in popularity, with a slew of models being developed in rapid succession [e.g. 185–189]. At its core, representation learning attempts to produce semantically meaningful compressed representations (or embeddings) of complex highly dimensional data. Aside from simply being a compression device, these embeddings can also be taken and used in downstream tasks, like clustering, anomaly detection, or classification.

In this section we will describe two approaches to representation learning that are popular within astronomy. The first approach uses contrastive learning as defined by the SimCLR model [185,186]. The second approach defines and uses a ‘surrogate task’ (such as autoencoding or next value prediction) to train a deep learning model, and extracts semantically meaningful representations from the subsequent trained network.

7(a) Contrastive learning

Fig. 21 describes a simple contrastive learning model similar to SimCLR [185]. This model takes as input a sample \mathbf{x} from the training set, and augments it to produce $\mathcal{A}(\mathbf{x})$. This augmentation is performed in such a way that $\mathcal{A}(\mathbf{x})$ shares enough semantically meaningful data with \mathbf{x} to belong to the same class. In the contrastive learning literature $(\mathbf{x}, \mathcal{A}(\mathbf{x}))$ is known as a positive pair. This positive pair is passed to a Siamese neural network Φ , which projects the high dimensional input data onto a lower dimensional ‘embedding space’. All other training set samples are assumed to belong to a different class to \mathbf{x} , and so can be combined with \mathbf{x} to produce ‘negative pairs’. Once we produce some embeddings we need to define a loss that clusters similar samples together, while simultaneously pushing away dissimilar samples. Hadsell et al. [190] propose such a loss—the maximum margin contrastive loss:

$$\mathcal{L}(\mathbf{z}_i, \mathbf{z}_j) = \delta_{ij} \mathbf{z}_i^T \mathbf{z}_j + (1 - \delta_{ij}) \max(0, m - \mathbf{z}_i^T \mathbf{z}_j),$$

where δ is the Kronecker delta, \mathbf{z}_i and \mathbf{z}_j are embedding vectors³¹, and m is the margin. If \mathbf{z}_i and \mathbf{z}_j are a positive pair, the loss pulls the embeddings closer, and if they are a negative pair the loss pushes the embeddings away from each other. The margin imposes an upper distance bound on dissimilar embeddings.

While useful, the maximum margin contrastive loss does not take into account the embedding space beyond the pair it is attending to in each training step. This limitation ultimately results in a less expressive embedding space. The triplet loss [191] solves this issue by taking into account the broader embedding space and simultaneously attracting a positive pair while repulsing a negative pair with each training step:

$$\mathcal{L}(\mathbf{z}_i, \mathbf{z}_j, \mathbf{z}_k) = \max(0, \mathbf{z}_i^T \mathbf{z}_j - \mathbf{z}_i^T \mathbf{z}_k + m) \quad (7.1)$$

where \mathbf{z}_k is a sampled from a different class to \mathbf{z}_i , and \mathbf{z}_j is sampled from the same class as \mathbf{z}_i .

If we study Eq. 7.1 we see that it is possible to generalise our loss even further, taking into account an arbitrary number of negative samples. The normalized temperature-scaled cross

³¹All embeddings in this subsection are normalised.

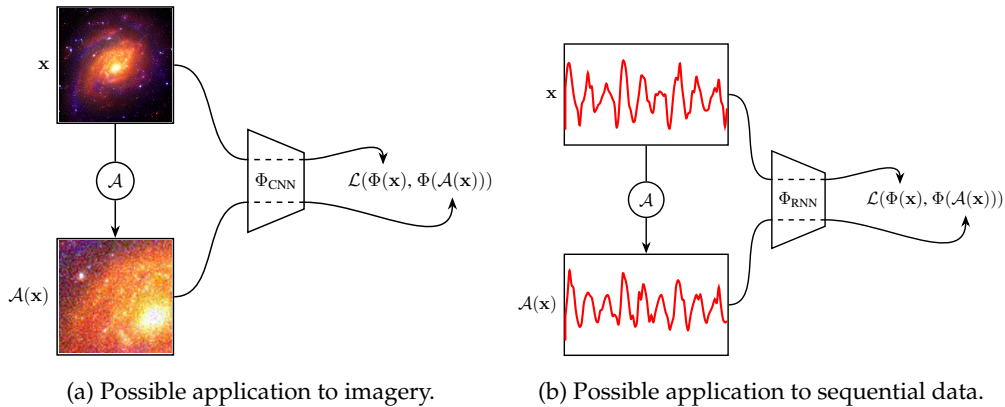


Figure 21: A simple contrastive learning model is applied to both imagery and sequential data. \mathcal{A} is an augmentation pipeline. For imagery, \mathcal{A} could consist of random crops, noise addition, and colour jitter. For sequential data, \mathcal{A} could consist of noise addition, stochastic temporal shifting, and random data deletion. Φ is a function approximator that projects inputs onto an embedding space. Φ is typically a neural network: when processing imagery, Φ could take the form of a CNN, and when processing sequential data Φ could be an RNN. The loss \mathcal{L} measures the distance between the embeddings $\Phi(\mathbf{x}) = \mathbf{z}_i$ and $\Phi(\mathcal{A}(\mathbf{x})) = \mathbf{z}_j$, and we train by attempting to minimise this distance while maximising the distance between dissimilar samples.

entropy loss [NT-Xent; 192] does precisely this:

$$\mathcal{L}(\mathbf{z}_i, \mathbf{z}_j) = -\log \left(\frac{\exp(\mathbf{z}_i^T \mathbf{z}_j / \mathcal{T})}{\sum_{k=1}^{2N} (1 - \delta_{ki}) \exp(\mathbf{z}_i^T \mathbf{z}_k / \mathcal{T})} \right), \quad (7.2)$$

where \mathbf{z}_i and \mathbf{z}_j are a positive embedding pair, and \mathbf{z}_i and \mathbf{z}_k are a negative pair. \mathcal{T} is a ‘temperature’ hyperparameter introduced in Chen et al. [185] to help the model learn from hard negatives (negatives closer to the anchor than the comparison positive, see Fig. 22b).

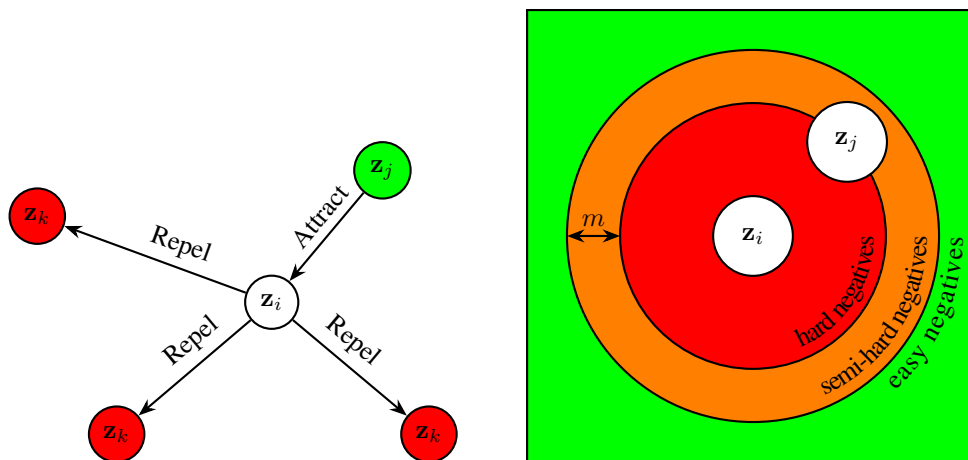
7(b) Learning representations via a surrogate task

One can also learn representations via a surrogate task. A surrogate task is any task that is unrelated to the network’s final use. However, in the process of learning to perform the surrogate task, the network learns what is important, and what is unimportant about data within the training set. This information can then be extracted in the form of learnt representations. If the surrogate task is general enough, these representations will contain useful semantic information about the items in the dataset, and can then be used for downstream applications (i.e. clustering, classification, anomaly detection).

Let us concretise this process by revisiting an example that we previously discussed in §4(b). Let us imagine we have a large set of galaxy rotation curves that we want to extract embeddings from. We could train an LSTM model (Fig. 23) on the task of predicting the next item in the rotation curve, with the model only having access to the previous items in the profile. Once the LSTM model is trained on this task, we can feed in a full, new rotation curve, and repurpose the final hidden state as a representative embedding. Note that this set up does not rely on any external labels, only on the rotation curve itself³².

We can generate embeddings via an autoencoding task. Again, let us use an astronomical example to specify this, and say that we want to extract embeddings from a set of galaxy

³²This self-supervised training set up is similar to that used to train autoregressive foundation models. These models will be explored in detail in §9(a).



(a) The triplet (Eq. 7.1) and NT-Xent (Eq. 7.2) losses simultaneously incentivise attraction between embeddings sampled from the same class (z_i and z_j), and repulsion between embeddings sampled from different classes (z_i and z_k).

(b) Types of negative embeddings. z_i and z_j form a positive embedding pair. If a negative is closer than the current positive it is considered a hard negative, if it lies within the margin it is considered a semi-hard negative, and if it is beyond the margin it is considered an easy negative.

Figure 22: More information on self-supervised embeddings. Fig. 22a depicts the inner workings of the triplet and NT-Xent losses, and Fig. 22b shows the three possible negative embedding types as described in the literature.

observations. We could repurpose a variational autoencoder for this, training it as normal as described in §6(a). However, once the model is trained we would discard the decoding part of the network, and only consider the encoder. To generate embeddings we would then simply pass in our galaxy images to the trained encoder. The same process can be carried out by a GAN (§6(b)). In the GAN case, we would discard the generator after training, and use the discriminator’s penultimate layer outputs as our embeddings.

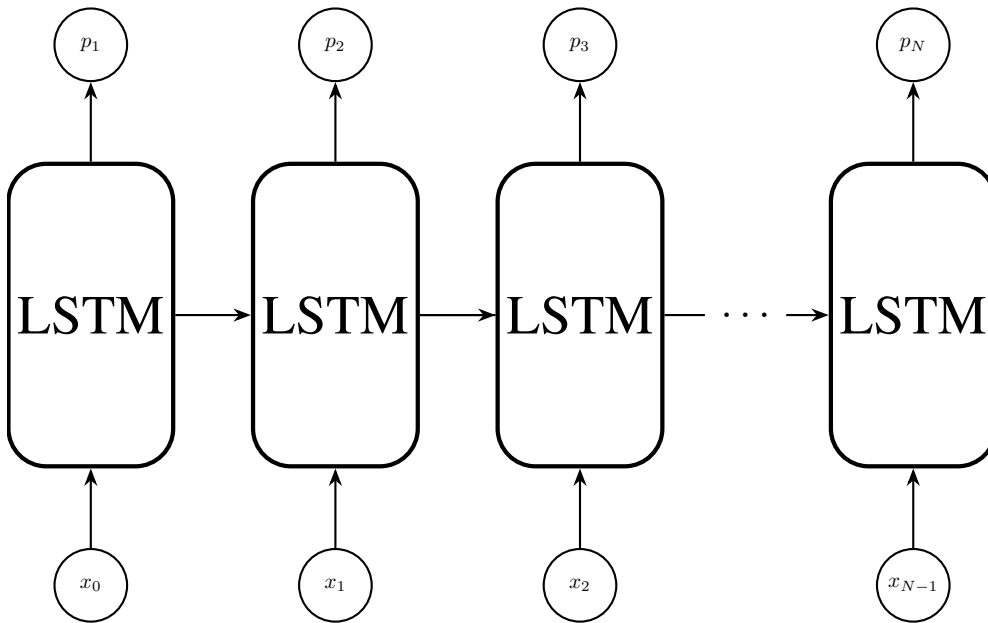
Supervised networks can also be used to generate embeddings. If a network has been trained in a supervised manner to classify or regress data, it will have learnt some properties about that data that helps it to carry out its task. We can access these learnt representations by taking the outputs from a trained network’s penultimate layer as an embedding³³.

8. Astronomy’s third wave of connectionism

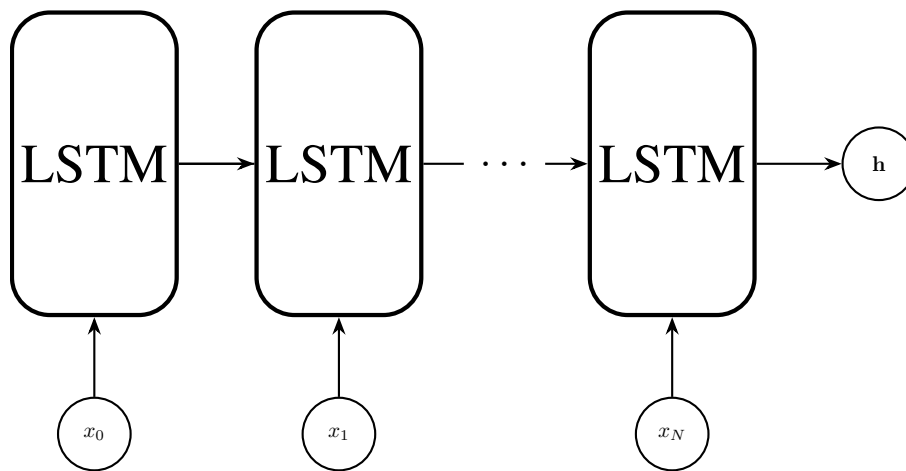
Since its astronomical debut in the mid-2010s [196]³⁴, deep generative modelling has become a popular subfield within astronomical connectionism. This popularity is driven by its inherent scalability; the lack of a need for labelled data allows the methods to be repurposed for any dataset that might be at hand. Self-supervised connectionism has been around for longer [i.e. 198], but again has recently exploded in popularity due to its usefulness in wrangling enormous unlabelled datasets. This section is split into two major parts. We will first outline the history of deep astronomical generative modelling in §8(a), and the history of astronomical representation learning will be discussed in §8(b). Although representation learning is the explicit goal for only

³³Interestingly, this process is used in the calculation for the Fréchet Inception Distance (FID) [193,194]. The FID acts as a measurement of the visual similarity between two datasets. The FID works by taking the penultimate layer representations from a trained Inception-v3 model [195] for each dataset and calculating the distance between them.

³⁴Also compare its companion paper [197].



(a) While training we feed in the galaxy rotation curve, and predict the next observation in its sequence.



(b) While inferring we feed in the full galaxy rotation curve, and extract the LSTM hidden state as a compressed representation embedding of the curve. Otherwise, we ignore whatever output (i.e. $\{p_1, \dots, p_N\}$) the LSTM generates.

Figure 23: A hypothetical surrogate task for extracting rotation curve representations is shown. $\{x_0, \dots, x_N\}$ is a set of observations from a galaxy rotation curve, in order of radial distance from the galactic centre. $\{p_1, \dots, p_N\}$ is the LSTM's corresponding set of predictions for $\{x_1, \dots, x_N\}$. h is the LSTM hidden state vector. See Fig. 11 for more about the internal workings of the LSTM.

the studies described in §8(b), it must be stressed that representations *can also be extracted from all the deep generative models described in §8(a).*

8(a) Deep astronomical generative modelling

Seminally, Regier et al. [196] proposed the use of a VAE to model galaxy observations. They trained their network on downscaled 69×69 crops of galaxies from a SDSS-sampled dataset containing 43 444 galaxies. They trained their network in the same way as described in §6(a), and find that the network is capable of generating galaxies similar to those found in the training set. They also find that their network produces semantically meaningful embeddings, noting that their galaxies are clustered by orientation and morphological type. This same line of enquiry was followed by Ravanbakhsh et al. [199], who showed that VAEs could be used to generate galaxies conditionally. Ravanbakhsh et al. [199] also pioneered the use of GANs to generate galaxy imagery. Spindler et al. [200] used a VAE combined with a Gaussian mixture model prior (see Eq. 6.2 and accompanying text) to generate and cluster galaxy images into morphological types. While the previous studies in this paragraph used images with relatively small pixel dimensions in their training set, Fussell and Moews [201] and Holzschuh et al. [202] demonstrated that GANs are capable of generating large high fidelity galaxy observations. Fussell and Moews [201] achieved this with a stacked GAN architecture [203], and Holzschuh et al. [202] use the related StyleGAN architecture [204] to the same end. Bretonnière et al. [205] use a flow-based model³⁵ [207,208] to conditionally simulate galaxy observations. They found that their approach could produce more accurate simulations than the previous analytical approach, at the cost of inference time. Relatedly, Smith et al. [184] use a diffusion model to generate large high fidelity galaxies. They trained their network on two datasets comprised of galaxies as observed by the Dark Energy Spectroscopic Instrument [DESI; 209]. One, a set of 306 006 galaxies catalogued in the SDSS Data Release 7 [74,210,211], and the other a set of 1962 late-type galaxies, as catalogued in the Photometry and Rotation curve OBservations from Extragalactic Surveys [PROBES; 212] dataset. PROBES contains well resolved galaxies that exhibit spiral arms, bars, and other features characteristic of late-type galaxies. They found that their model produces galaxies that are both qualitatively and statistically indistinguishable from those in the training set, proving that diffusion models are a competitive alternative to the more established GAN and VAE models for astronomical simulation. From all of these studies we can conclude that deep generative models can internalise a model capable of physically and morphologically describing galaxies.

Generative models have also been used to simulate astronomical data on larger scales. In a use-case tangential to galaxy generation, Smith and Geach [213] show that a Spatial-GAN [214] can simulate arbitrarily wide field surveys. They train on the Hubble eXtreme Deep Field, and find that galaxies ‘detected’ within their model’s synthetic deep fields are statistically indistinguishable from the real thing. Cosmological simulations have also been explored, with Rodriguez et al. [215] using a GAN to generate cosmic web simulations at pace, and Mustafa et al. [216] generating weak lensing convergence maps at a pace faster than classic simulations. Beyond GANs, Remy et al. [217]³⁶ trained a SBGM on simulated maps from MassiveNus [219], and found that their model was capable of replicating these maps. They also demonstrated that their model was capable of producing a likely spread in the posterior predictions. Finally, they demonstrate that a SBGM is capable of predicting the mass map of the real Hubble Cosmic Evolution Survey (COSMOS) field [220].

The image domain translation abilities of GANs in a Pix2Pix-like formulation [162, also see Fig. 18b.] is particularly useful in astronomy. Schawinski et al. [221] demonstrated this use first by training a Pix2Pix-like model to denoise astronomical data. They trained their network on 4550 galaxies sampled from SDSS. The galaxies were convolved to increase the seeing, and speckle noise was added. The GAN was tasked with reversing this process. They found that

³⁵Flow-based models have not been discussed in detail in this review, but see Weng [206] for a magisterial introduction to the subject.

³⁶This preliminary work has been subsequently extended in Remy et al. [218].

their method outperformed both blind deconvolution, and Lucy-Richardson deconvolution. Generative models are also capable of separating sources, as Stark et al. [222] demonstrate by using a Pix2Pix model to deblend a quasar's point source emission from the extended light of its host galaxy. Reiman and Göhre [223] use a similar model to Stark et al. [222] to deblend overlapping galaxies.

At the time of writing there are only three examples of score-based (or diffusion) modelling in the astronomy literature [184,217,218]. It is surprising that these studies are the only examples of score-based modelling in astronomy, as SBGMs produce generations that rival that of state-of-the-art GAN models, without drawbacks present in other models (like blurring in the case of VAEs, or mode collapse and training instability in the case of GANs). SBGMs also have some natural uses in astronomical data pipelines. For example, an implementation similar to Sasaki et al. [176] could be used for survey-to-survey photometry translation similarly to Buncher et al. [224]. The source image separation model described in Jayaram and Thickstun [177] has the obvious application as an astronomical object deblender [i.e. 222,223,225]. To summarise, SBGMs are ripe for exploitation by the astronomical community and we hope to see much interest in this area in the coming years.

8(b) Self-supervised astronomical representation learning

In 1993, Serra-Ricart et al. [198] proposed using an autoencoder to learn embeddings for stars as observed by the Two Micron Galactic Survey [226]. They first proved that their autoencoder model worked better than principle component analysis (PCA) on the toy problem of separating Gaussian distributions, and they then showed that their model also outperformed the classic PCA method on real data. More than twenty years later, Graff et al. [227]³⁷ showed that autoencoders are also capable of capturing the properties of galaxies as described in the Mapping Dark Matter Challenge [228] by demonstrating that embeddings extracted from their autoencoder were beneficial for computing the ellipticities of their galaxies as a downstream task. We are not limited to imagery; Yang and Li [229] show that an autoencoder can learn representations that can then be used to train a neural network for the downstream task of estimating stars' atmospheric parameters, and Tsang and Schultz [230] demonstrate that an autoencoder can generate embeddings that can then be used to classify variable star light curves. From these studies we must conclude that neural networks trained via a surrogate task are capable of learning semantically meaningful embeddings across astronomical domains.

Very recently there has been work applying self-supervised contrastive learning models to galaxy image clustering. Hayat et al. [231] trained SimCLR [185] on multi-band galaxy photometry from the SDSS [74]. They show that the resulting embeddings capture useful information by directly using them in a training set for a galaxy morphology classification model, and a redshift estimation model. Similarly, Sarmiento et al. [232] trained SimCLR on integral field spectroscopy data captured from galaxies in the Mapping Nearby Galaxies at Apache Point Observatory survey [MaNGA; 233]. Again, they find that SimCLR produces semantically meaningful embeddings. Slijepcevic et al. [234] demonstrate that the 'Bootstrap Your Own Latent' [BYOL; 187]³⁸ contrastive learning model is capable of learning semantically meaningful representations of radio galaxies. Their model is trained on 100 000 Radio Galaxy Zoo galaxies, and inference is run on the 1256 galaxy strong Mirabest dataset [235]. They find that embeddings derived from their model are semantically meaningful, suggesting that self-supervised methods are transferable between disparate surveys. These studies show that contrastive learning is applicable to imagery, further study will be required to demonstrate its effectiveness with other types of astronomical data, such as time series and volumetric data.

³⁷See Footnote 43 for commentary of this study in the context of astronomical foundation models.

³⁸A contrastive learning framework that unlike SimCLR does not use negative samples to learn an embedding space.

9. Foundation models: a fourth astroconnectionist wave?

This review has shown thus far that deep learning has found wide use in astronomy, a use predicated on the availability of enormous amounts of computational power and data. This section looks to the future and predicts an outcome if astronomy continues to follow in the footsteps of other applied deep learning fields. In short, we predict and argue that astronomical connectionism will likely see the removal of expertly crafted deep learning models, to be replaced with an all encompassing ‘foundation’ model. In §9(a) we explore what foundation models are, and their context within deep learning. §9(b) then contextualises these models within astronomy, and suggests actions we can take as a community to realise an astronomical foundation model. Finally, §9(c) demonstrates as a thought experiment a state-of-the-art use-case for an astronomical foundation model.

9(a) Foundation models

Since its inception, connectionism has followed a path of greater compute and greater generality [84,85]. In that time, human crafted biases have fallen by the wayside, to be replaced with models and techniques that learn directly from data. Sutton [84] exemplifies this process via the field of speech recognition:

In speech recognition, there was an early competition, sponsored by DARPA [Defense Advanced Research Projects Agency], in the 1970s. Entrants included a host of special methods that took advantage of human knowledge—knowledge of words, of phonemes, of the human vocal tract, etc. On the other side were newer methods that were more statistical in nature and did much more computation, based on hidden Markov models (HMMs). Again, the statistical methods won out over the human-knowledge-based methods. This led to a major change in all of natural language processing, gradually over decades, where statistics and computation came to dominate the field. The recent rise of deep learning in speech recognition is the most recent step in this consistent direction. Deep learning methods rely even less on human knowledge, and use even more computation, together with learning on huge training sets, to produce dramatically better speech recognition systems. As in [computer Go and computer chess], researchers always tried to make systems that worked the way the researchers thought their own minds worked—they tried to put that knowledge in their systems—but it proved ultimately counterproductive, and a colossal waste of researcher’s time, when, through Moore’s law, massive computation became available and a means was found to put it to good use.

We are seeing this principal play out once again through a new paradigm shift in deep learning, where even the underlying neural network architecture does not matter. Previously, neural networks were adapted for a specific domain via inductive biases injected by researchers, such as convolutions for computer vision, and recurrence for language processing. Now we are seeing transformer networks [see §4(d) and 110] competing³⁹ in all deep learning domains applied or otherwise: from language processing [12,116]⁴⁰ to computer vision [13,153] to graph learning [238] to protein folding [11] to astronomy [154,155,157]. The transformer’s versatility allows us to take a model trained on one task and apply it to a similar yet different task, a process known as transfer learning. For example, we could train a model on the ‘surrogate’ task of predicting the next word in a sequence, and then apply that model to a similar yet different task of predicting the answer to a geography question. In this example the first model is known as a ‘foundation’ model, and the downstream model is derived from it. This set up brings with it some useful advantages. For example, if the foundation model is improved, all downstream tasks also see

³⁹For now! It may be that network architecture does not matter all that much at scale, and that any sufficiently large neural network is adequate. If this is true, we will see the simplest (and most scalable) architectures win out. Although this theory has not yet been rigorously tested, we are currently seeing rumblings that suggest that this is the case [e.g. the section ‘Transformers are not special’ in 236]. Bo [237] stands as a particularly notable example of this hypothesis, showing that an attention-free RNN is capable of matching the performance of a similarly-scaled transformer network. Also see Footnote 13 for commentary on the performance capabilities of MLPs and transformers.

⁴⁰These models are collectively known in the literature as large language models, or LLMs.

improvement. Therefore, the need for only one model allows researchers to pool their efforts in a way not possible when resources are split between many projects.

To train a foundation model, we first need to define a surrogate task. As labelled datasets are expensive, and raw data is relatively cheap, the easiest and most scalable way to do this is via self-supervised learning⁴¹. Self-supervised learning does not require a human to provide a labelled dataset for training. Instead, the supervisory signal is generated automatically from the raw data. For example, in the context of astronomy this task could be predicting a masked value in a variable star’s light curve [154]. Another task could be using an autoencoder (§6(a)) to replicate a galaxy observation [200]. A further task could be training within a self-supervised framework, like contrastive learning (§7(a)). The important thing about self-supervised learning is that it does not require annotated data. This means that we can leverage vast reserves of raw data (such as textbooks, scraped Internet text, raw imagery, etc.).

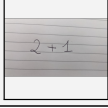
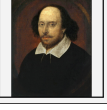
Input prompt				Completion	
 This is a chinchilla. They are mainly found in Chile.	 This is a shiba. They are very popular in Japan.	 This is		a flamingo. They are found in the Caribbean and South America.	
 What is the title of this painting? Answer: The Hallucinogenic Toreador.	 Where is this painting displayed? Answer: Louvres Museum, Paris.	 What is the name of the city where this was painted? Answer:		Arles.	
 Output: 'Underground'	 Output: 'Congress'	 Output:		'Soulomes'	
 2+1	2+1=3	 5+6	5+6=11	 3x6	3x6=18
 pandas: 3	 dogs: 2			giraffes: 4	
I like reading	 , my favourite play is Hamlet. I also like	 , my favorite book is		Dreams from my Father.	

Figure 24: Flamingo is a foundation model that is capable of understanding images within the context of natural language. Here we see some examples of Flamingo’s emergent abilities. This figure is adapted from Fig. 1 in Alayrac et al. [239].

Very large models trained on vast amounts of data demonstrate surprising emergent behaviour. For instance, GPT-3 [12] is a 175B parameter model that can be ‘prompted’ to perform a novel task (see Fig. 24 for more on prompting foundation models). This ability was not shown at all in GPT-3’s older, smaller 1.5B parameter sibling [115]. Furthermore, a meta-study described in Wei et al. [240] found that larger models suddenly ‘unlock’ abilities such as arithmetic, translation, and understanding of figures of speech once they reach a certain scale. These findings suggest that architectural changes are not required beyond scaling to perform many tasks in natural language processing [85,241]. In Fig. 24 we see some results from Alayrac et al. [239], a model comprising of

⁴¹For more on self-supervised learning see §7.

an LLM, and an image encoder. In this figure we can see that the model is capable of arithmetic, reading, counting, and has a broad knowledge (albeit not ‘understanding’) of art, geography and zoology⁴², and literature. This model is comprised of a ResNet variant [112,243] to encode imagery, and the Chinchilla LLM [244] to encode and generate text. Chinchilla (and therefore Flamingo) was trained with the surrogate task of predicting the next word in a text sequence, and so none of the emergent properties stated above were explicitly optimised for.

In the next subsection, we will state and explain the need for an astronomical foundation model⁴³, not only for astronomy’s sake, but also for the sake of openness in deep learning research.

9(b) Scaling laws and data moats

Hoffmann et al. [244] suggested an update to the foundation model scaling law first proposed in Kaplan et al. [246]. Their scaling law equation relates the size of a neural network model and the training dataset size to the minimum achievable loss. Mathematically, the equation is

$$\mathcal{L}_{\min}(N, D) = \underbrace{\frac{A}{N^\alpha}}_{\text{parameter term}} + \underbrace{\frac{B}{D^\beta}}_{\text{data term}} + \underbrace{E}_{\text{dataset entropy}}, \tag{9.1}$$

where E is a constant that represents the lowest possible loss, given a particular training dataset. N is the number of trainable parameters within the neural network, and D is the size of the dataset in tokens (see §4(d) for more about tokenisation). We can see that when we have an infinitely large model trained on an infinitely large dataset (i.e. $N = D = \infty$), the only term remaining is the ‘dataset entropy’ constant, E . We can therefore only reduce the loss by increasing the size of our model, or the size of our training set.

After fitting Eq. 9.1, Hoffmann et al. [244] find

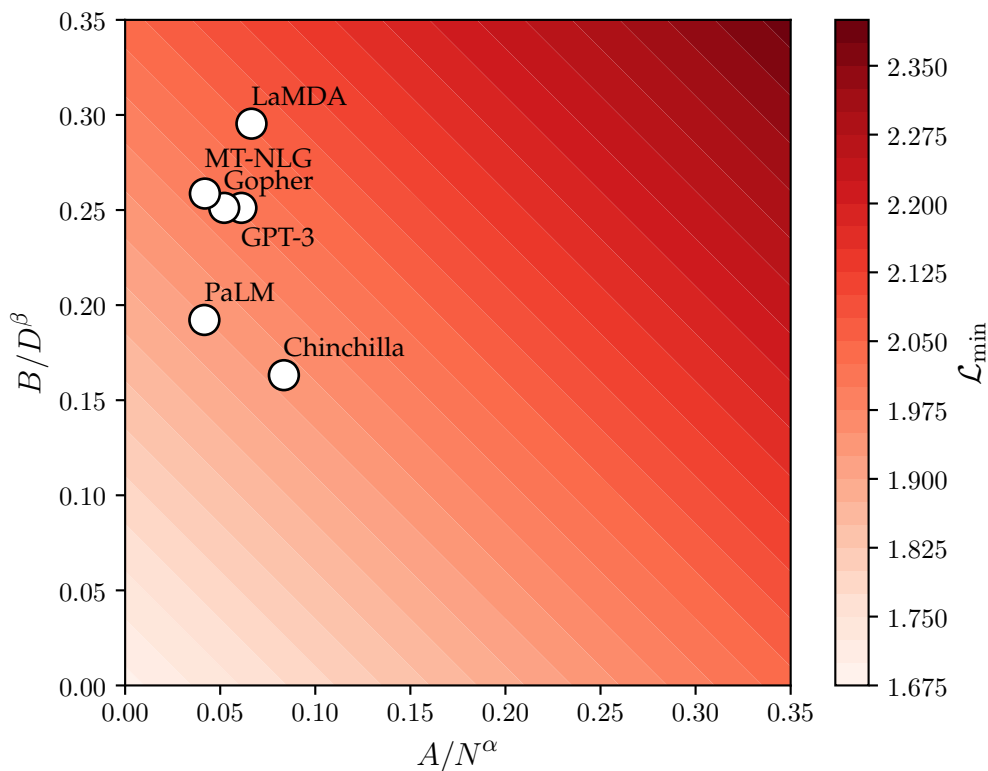
$$\mathcal{L}_{\min}(N, D) = \frac{406.4}{N^{0.34}} + \frac{410.7}{D^{0.28}} + 1.69.$$

If we then plug in N and D for a selection of real foundation models we arrive at Fig. 25. We can see in Fig. 25 that the model size term for real foundation models is far lower than the dataset size term. This means that an increase in dataset size has the potential to reduce the minimum loss by a far larger amount than a larger model would. Therefore, an obvious next step to improve these foundation models further is by increasing their dataset size.

The largest dataset [MassiveText-English; 244] in the comparison shown in Fig. 25 amounts to 1.4T tokens. However, this dataset is proprietary, being only available to researchers employed by Google. The largest public text dataset available at the time of writing is The Pile [250], with a total size of ~260B tokens. We could increase the size of these datasets by indefinitely scraping text data from the surface web, but this data tends to be of low quality. Also, we have already exhausted some important high quality data reserves, like fundamental research papers, and open source code [251]. We also have to ask ourselves: what happens when generative models start to create data *en masse*, and dump it indiscriminately onto the Internet? If a significant proportion of text in a dataset scraped from the Internet is generated via an LLM, training on it will cause unforeseen

⁴²Interestingly, the authors of Flamingo first assumed that Flamingo’s prediction of the species range of its eponymous bird was incorrect: flamingos are found in the Caribbean, South America, Africa, Europe, and South Asia. However, they later realised that the picture in Fig. 24 is of an *American* flamingo, which is specifically found in the Caribbean and South America, so the network was right after all! See the reddit thread for the full context [242].

⁴³Walmsley et al. [245] explore in a preliminary study a ‘galaxy foundation model’ trained on Galaxy Zoo labels, and corresponding paired galaxy observations. They find that their pretraining is beneficial for training a network that performs a downstream task. However, the idea has been around for far longer than that; possibly the first demonstration of an astronomical foundation model was described eight years earlier in Graff et al. [227]. Graff et al. [227] demonstrated that embeddings learnt with their autoencoding SkyNet network can be used for downstream tasks, but they do not use the moniker ‘foundation model’ to describe SkyNet as the term had not yet been invented! Notably, neither study trains a model of the scale required to exhibit emergent properties or task generalisability. These ‘blessings of scale’ require data and compute at a level that has not yet been seen within astronomical connectionism.



Model	N	D	A/N^α	B/D^β	\mathcal{L}_{\min}
LaMDA [247]	137B	168B	0.066	0.295	2.051
GPT-3 [12]	175B	300B	0.061	0.251	2.002
Gopher [248]	280B	300B	0.052	0.251	1.993
MT-NLG [249]	530B	270B	0.041	0.259	1.990
Chinchilla [244]	70B	1.4T	0.083	0.163	1.936
PaLM [241]	540B	780B	0.042	0.192	1.924

Figure 25: A comparison between the minimum losses of a selection of foundation models. The table above shows the number of parameters in a model (N), the number of tokens within that model’s training set (D), and their corresponding calculated emergent terms from Eq. 9.1. Here we use Hoffmann et al. [244] to source values for A , α , B , and β . The minimum loss for each model according to Hoffmann et al. [244] is shown as \mathcal{L}_{\min} . The contour plot shows the emergent parameters B/D^β and A/N^α plotted against each other for our models. The closer the models’ scatterpoints are to the bottom left, the lower their minimum loss value.

issues and may ultimately result in a model with worse performance. We must therefore ensure that the data is not generated by a deep generative model. In addition to all this, the academy and the public at large will never have access to the vast reserves of data contained in the deep web administered by ByteDance, Google, Meta, Microsoft, and other tech giants. For all these reasons, we will need to think outside the box if we want to mine new high quality data.

Enter the multimodal foundation model. Reed et al. [117]⁴⁴ demonstrated that a large transformer neural network is capable of learning many tasks, from playing Atari, to captioning

⁴⁴Earlier work from Kaiser et al. [252] also demonstrated a deep learning model that could learn from disparate tasks, however Gato is the first model that achieves this while staying within a single deep learning paradigm.

images, to chatting, to operating a real robot arm. The model shares weights across all tasks, and decides at inference time from context which task to predict. Importantly, Reed et al. [117] find that their model follows the same scaling laws as other foundation models, and so multimodal foundation models have the same hunger for data that we see in Fig. 25. We can therefore augment (or replace) our text datasets with high quality, publicly available astronomical data.

The Vera Rubin Observatory's 189 16 megapixel CCDs will observe 1000 science frames per night while conducting LSST [253]. This amounts to 3×10^{12} pixels per night, or approximately 12B tokens a night if we use the same tokenising scheme as Dosovitskiy et al.'s vision transformer [13]. After only one year of observing, the LSST will have produced 4.4T tokens of raw data, larger than even the MassiveText-English dataset⁴⁵. This data, and other astronomical data like it, could be compiled into a very large open dataset similar to EleutherAI's Pile [250]. This dataset would provide a way for academics employed outside of Big Tech to train and research very large foundation models. Compiling a dataset like this would be difficult for a single relatively underresourced research group, but it could be accomplished via bazaar style open development [254]. We have already seen this development model succeed in large open source projects, the most famous of which is the Linux kernel. This development model has also been shown to work within the field of deep learning by EleutherAI [e.g. 250,255,256], and with HuggingFace's BigScience initiative⁴⁶. Once compiled, we must ensure that progress is kept in the open, and that the data is not simply absorbed into proprietary datasets—to do this we must give our dataset a strong (viral) copyleft style licence.

Once the dataset is compiled all we need are some self-supervised surrogate tasks for our 'astrofoundation' model to attempt. These tasks could include predicting the next observation in a variable star's time sequence, predicting the low surface brightness profile of a galaxy, predicting a galaxy's morphological parameters, or simply generating the next crop in a sequence of observations⁴⁷. Our astrofoundation model will inherit all the interesting properties that LLMs enjoy, such as few to zero-shot generation and other emergent behaviours. We could also finetune astrofoundation to downstream tasks, saving much time and compute. In the next section we will outline one possible downstream task that would be useful in astronomy; a conditional generative model for galaxy simulation.

9(c) A new class of simulation

If we train an unconditional generative model, we cannot control its output at inference time. This is an issue if we want to generate specific classes of observations to train models for downstream tasks, such as redshift estimation, or galaxy type classification. To achieve a model capable of generating specific classes, one could simply train a conditional generative model of the form

$$G_{\phi}(\hat{\mathbf{x}} | \mathbf{z}, \mathbf{y}), \quad (9.2)$$

where $\hat{\mathbf{x}}$ is a generated image, \mathbf{z} is some noise that acts to capture all detail not encoded in \mathbf{y} , and \mathbf{y} is a conditioning vector. As an example, \mathbf{y} could contain a galaxy's redshift or morphological type. However, this means that we must be very specific when choosing \mathbf{y} . Multimodal modelling provides us the means to sidestep this fundamental issue, and lets us play with fuzzy inputs.

As a thought experiment let us consider Google's recent 'Imagen' model⁴⁸, and imagine how it could be repurposed for an astronomical use case [Figs. 26 and 27; 259]. Imagen is a combination

⁴⁵Of course, the reduced, useful data will be far smaller than our raw estimate here. The motivation behind this calculation is to show that even a single astronomical survey rivals the largest text dataset in size. A compilation of all useful astronomical data would certainly dwarf any contemporary text dataset, whether public or proprietary.

⁴⁶<https://bigscience.huggingface.co>

⁴⁷This is essentially training the model to act as a physics simulator. Viewing foundation models as world simulators is not unprecedented. This perspective has already been explored in the simulation of thousands of 'social simulacra' within a model online community [257], and with the simulation of participants in classic (i.e. Milgram's shock experiment, the Ultimatum Game) and novel psychological studies [258].

⁴⁸Naturally, no implementation is provided by Google. However, there is already a fantastic MIT licenced implementation of Imagen provided by Phil Wang and others (<https://github.com/lucidrains/imagen-pytorch>). All we are missing now is the data and the means to train with it!



A wall in a royal castle. There are two paintings on the wall. The one on the left a detailed oil painting of the royal raccoon king. The one on the right a detailed oil painting of the royal raccoon queen.



A group of teddy bears in suit in a corporate office celebrating the birthday of their friend. There is a pizza cake on the desk.



An angry duck doing heavy weightlifting at the gym.



A cloud in the shape of two bunnies playing with a ball. The ball is made of clouds too.



A photo of a person with the head of a cow, wearing a tuxedo and black bowtie. Beach wallpaper in the background.



A chrome-plated duck with a golden beak arguing with an angry turtle in a forest.

Figure 26: Select 1024×1024 Imagen samples generated from text inputs. Below each image is its corresponding conditioning text. Figure adapted from Fig. A.2 in [259].

of a frozen LLM [specifically T5-XXL; 260] and a cascaded diffusion model [261, also see §6(c)]. The LLM acts as a language encoder, and then passes its generated latent space representations onto the diffusion model as a conditioning vector. If we were to replace the frozen LLM with an ‘astrofoundation’ model (see §9(a) and §9(b)), we could leverage astronomy’s fundamentally multimodal nature. For example, if our astrofoundation model were trained to understand the Galaxy Zoo 2 (GZ2) morphological classifications [262], we could take the GZ2 descriptors as y and their corresponding galaxy pair as x and train on those.

Once trained, our astronomical Imagen model could generate synthetic galaxies that resemble the real galaxy observations that it was trained on. However, unlike an unconditional astronomical simulator, this model would be capable of generating galaxies that specifically resemble a real galaxy that shares the conditioning set of GZ2 parameters!

Unlike the conditional model described by Eq. 9.2, an astrofoundation type model allows us to be creative with the conditioning vector. For example, we could run the model in reverse to generate representations that refer to a very specific astronomical object, and then generate many more objects of that ‘class’ with injected features like satellite occlusion, a specific instrument response function, a specific redshift, etc. [see work on ‘textual inversion’ by 263]. We could even create a ‘Galaxy Zoo’ type dataset that asks citizen scientists to describe galaxy morphology via natural language. This is possible since the encoding foundation model does not fundamentally

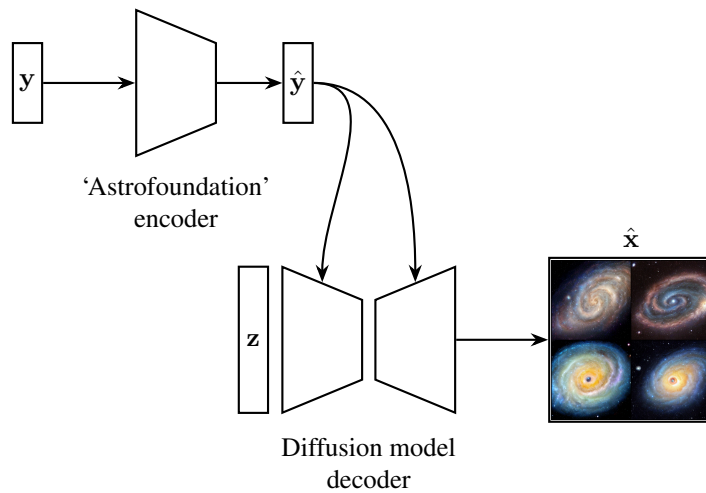


Figure 27: An Imagen-like model uses a frozen foundation model to encode text, and then uses that encoding to condition a cascaded diffusion model of the form $G_\phi(\hat{x} | z, \hat{y})$ [259,261]. Here we see one possible realisation of this type of model in astronomy. y is some kind of descriptive vector that can be paired with a ground truth image. For example, y could be the surface brightness profile of a galaxy, or the summary statistics of a variable star light curve, or some cosmological parameters. In general, y could be any vector that the astrofoundation model understands. \hat{y} is y 's projected latent space equivalent. Since we do not need to train the foundation model here, training cost is far lower than for an equivalent end-to-end trained model.

care about which form the caption takes. This approach would cut down on citizen scientist training cost due to natural language's inherent intuitiveness.

10. A word about the carbon footprint of deep learning

The training of deep learning models in general requires a considerable amount of energy, and it is only natural that the training of ultra-large foundation models significantly ups the ante. In this section we illustrate connectionism's hunger for energy by estimating the total carbon footprint created in the training of the GPT-3 and PaLM foundation models [12,241].

Let us start with the eminent GPT-3 model. Unfortunately, the total energy cost is not stated in Brown et al. [12] but we can make a ballpark estimate using information from that work. GPT-3 was trained on a high performance computing cluster containing $N = 10\,000$ NVIDIA V100 chips, and required a total $\Sigma = 3.14 \times 10^{23}$ FLOPs to train to completion [12]. A single V100 has a throughput of $C = 2.8 \times 10^{13}$ FLOPS for half precision floats and so we can estimate GPT-3's total training time in datacentre-seconds as

$$\frac{\Sigma}{C \cdot N} = \frac{3.14 \times 10^{23}}{2.8 \times 10^{12} \cdot 10^4} = 1.12 \times 10^6 \text{ s,}$$

which is approximately 311 hours. We know the thermal design power of a single V100 chip is 300 W and so we can safely assume a lower bound on the datacentre power usage as 3000 kW. Therefore, we estimate the total power consumed while training GPT-3 as

$$3000 \cdot 311 = 933\,000 \text{ kWh.}$$

The emissions per kWh of the datacentre where GPT-3 was trained is 0.429 kg CO₂e kWh⁻¹ [264], leaving us with a total emission of around 400 000 kg CO₂e⁴⁹.

However, GPT-3 is already two years old; so we will also estimate the energy used when training Google’s state-of-the-art ‘PaLM’ foundation model. Chowdhery et al. [241] state: ‘We trained PaLM-540B on 6144 TPU v4 chips for 1200 hours and 3072 TPU v4 chips for 336 hours including some downtime and repeated steps. . . [We found a] 378.5 W measured system power per TPU v4 chip. . .’ We can therefore calculate PaLM’s total energy usage as

$$378.5 \cdot (6144 \cdot 1200 + 3072 \cdot 336) \approx 3\,180\,000 \text{ kWh.}$$

If PaLM was trained on the same datacentre as GPT-3 (i.e. at an emissivity of 0.429 kg CO₂e kWh⁻¹) it would have emitted a staggering 1 400 000 kg CO₂e – quadruple the average person’s lifetime carbon footprint [265] and approaching the annual emission of some small countries. Luckily, the datacentre that PaLM was trained on was far greener than that used by OpenAI, and PaLM actually produced ~270 000 kg CO₂e [241], although this is still rather large. We contextualise our calculated footprints visually in Fig. 28.

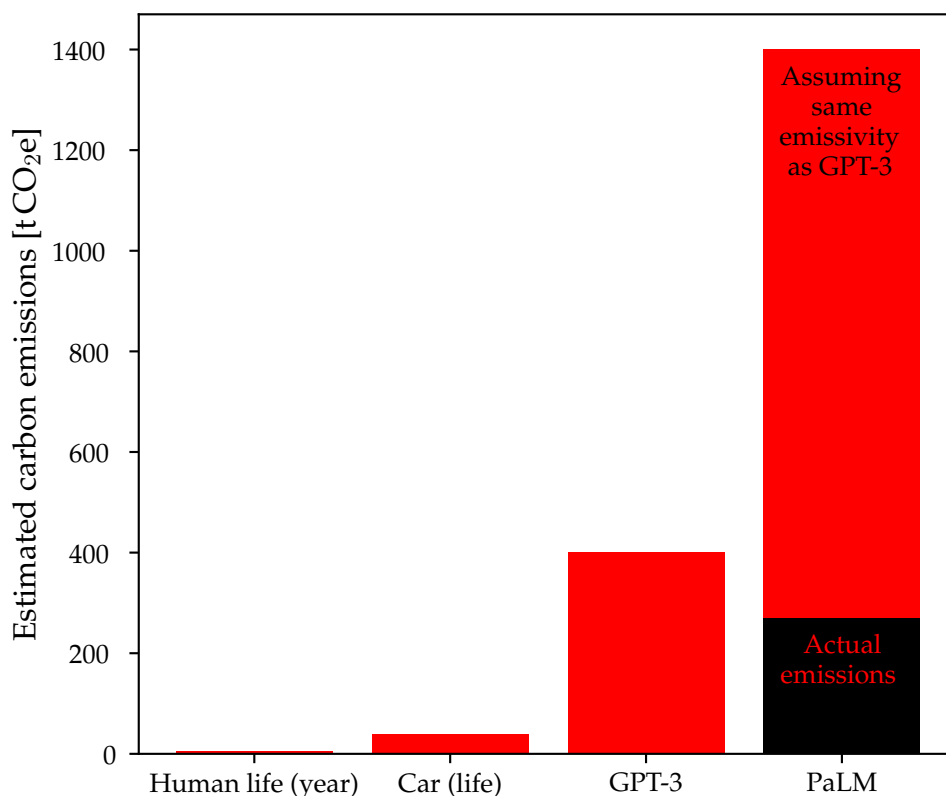


Figure 28: Here we contextualise the huge carbon footprints generated when training foundation models. The average person’s yearly carbon footprint is estimated as 4750 kg CO₂e using data from Friedlingstein et al. [265], and the car lifetime emissions is 38 504 kg CO₂e assuming a Mercedes-Benz C 300 d model [266].

PaLM’s contribution to Fig. 28 demonstrates the importance of choosing and using datacentres that run on clean energy sources when training deep learning models, and make efficient use

⁴⁹We must keep in mind that this estimate is a lower limit. We do not include CPU power, cooling, or any other overheads in our calculation, never mind the cost to do a full hyperparameter sweep!

of heat output (e.g. through recovery systems). Besides this, researchers can also take care when optimising their neural network models to reduce their carbon footprint. For instance by choosing hyperparameters through a more efficient manual or randomised search, instead of via a brute force method [267]. As stated in Strubell et al. [268] researchers can also combat redundant retraining of models (and thus unnecessary energy usage) by ensuring that fully trained models, data, and code are released under an open licence. The publishing of a fully trained model’s energy usage, computation requirements, and carbon footprint also allows downstream researchers to determine whether replication of a work is economically and environmentally viable. Calculating one’s energy usage in the spirit of openness does not have to be difficult: we have been using the excellent and user-friendly ‘Machine Learning CO₂ Impact Calculator’ in our own work to calculate and publish the carbon footprint of our models [269]. A recommendation of this review is that an environmental impact statement should become standard practice in journal articles, conference presentations and proceedings when deep learning models (or any HPC-heavy research for that matter) is used.

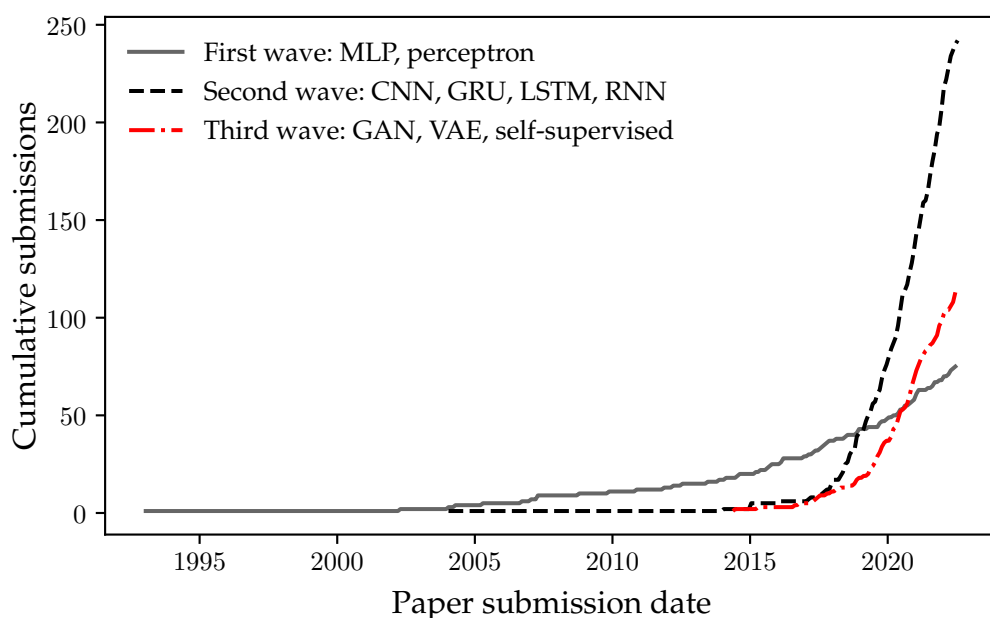


Figure 29: Here we see the number of arXiv:astro-ph submissions whose titles or abstracts match the terms given in the legend. We can see three distinct ‘waves’. The first corresponds to studies that use MLPs (§2(a)-§3), the second corresponds to studies that use ‘deep learning’ methods that ingest raw data (§4(a)-§5) and the third corresponds to studies that use generative or self-supervised models (§6-§8). The raw data is in the public domain, and is available at <https://www.kaggle.com/Cornell-University/arxiv>.

11. Final comments, or how we learnt to stop worrying and love astronomy’s Big Data Era

To repeat our introductory statement: in every field that deep learning has infiltrated we have seen a reduction in the use of specialist knowledge, to be replaced with knowledge automatically derived from data. We have already seen this process play out in many disparate fields from computer Go [10], to protein folding [11], to natural language processing [12], to computer vision

[13]. This process is already well known within the deep learning community as ‘*The Bitter Lesson*,’ a precept that is summarised by the quote:

The biggest lesson that can be read from 70 years of AI research is that general methods that leverage computation are ultimately the most effective, and by a large margin. [84]

There is no reason to believe that astronomy is fundamentally different. Indeed, within this review we have seen a narrative pointing to this conclusion (Fig. 29). Initial work on MLPs within astronomy required manually selected emergent properties as input [e.g. 44,66]. With the advent of CNNs and RNNs, these manually selected inputs gave way to raw data ingestion [e.g. 124,139]. Now we are seeing the removal of human supervision altogether with deep learning methods inferring labels and knowledge directly from the data [e.g. 155,200]. Ultimately, if astronomy follows in the footsteps of other applied deep learning fields, we will see the removal of expertly crafted deep learning models, to be replaced with finetuned versions of an all-encompassing ‘foundation’ model [158]. This process is by no means a bad thing; the removal of human bias in the astronomical discovery process allows us to find ‘unknown unknowns’ through serendipity [154,232]. Likewise, the ability to leverage data allows us to directly generate and interrogate realistic yet synthetic observations, sidestepping the need for an expensive and fragile classical simulation [184,213].

Astronomy’s relative data wealth gives us the opportunity to form a symbiotic relationship with the cutting edge of deep learning research, an increasingly data hungry field [85,251]. Many ultra-large datasets in machine learning are proprietary, and so the astronomical community has the opportunity to step in and provide a high quality multimodal public dataset. In turn, this dataset could be used to train an astronomical ‘foundation’ model that can be used for state-of-the-art downstream tasks (such as astronomical simulation, see §9(c)). Finally, following recent developments in connectionism [12,244] most astronomers lack the resources to train models on the cutting edge of the field. If astronomy is to have any chance of keeping up with the Big Tech goliaths, we must follow the examples of EleutherAI and HuggingFace and pool our resources in a grassroots-style open source fashion (§9(b)). We leave this as a challenge for the community.

Ethics. This article is a review and so no ethical approval is required.

Data Accessibility. This article has no additional data.

Competing Interests. There are no competing interests.

Funding. MJS acknowledges support from the Alan Turing Institute by way of the Turing Enrichment Scheme. JEG acknowledges funding from the Royal Society and the Science and Technology Facilities Council.

Acknowledgements. The authors would like to thank Hans-Martin Adorf for providing access to his manuscripts. The galaxy icon shown in Fig. 15 is by Agata Kuczmńska and is reproduced here under the CC-BY-4.0 licence.

Disclaimer. This study is an adaptation of work presented in Chapters 1 and 5 of MJS’s PhD thesis [19]. GPT-3 wrote the abstract.

References

1. Leibniz GW. Dissertation on the Art of Combinations. In: Philosophical Papers and Letters. Dordrecht, The Netherlands: Springer; 1989. p. 73–84.
2. Fidora A, C S. Ramon Llull: From the Ars Magna to Artificial Intelligence. Spain: Artificial Intelligence Research Inst.; 2011. Available from: https://books.google.co.uk/books/about/Ramon_Llull_From_the_Ars_Magna_to_Artifi.html?id=RLkVtwAACAAJ&redir_esc=y.
3. Gray J. 'Let us Calculate!' Leibniz, Llull, and the Computational Imagination; 2016. Available from: <https://publicdomainreview.org/essay/let-us-calculate-leibniz-llull-and-the-computational-imagination>.
4. Turing AM. I.—COMPUTING MACHINERY AND INTELLIGENCE. *Mind*. 1950 10;LIX(236):433–460.
5. Moor J. The Dartmouth College Artificial Intelligence Conference: The Next Fifty Years. *AI Magazine*. 2006 12;27(4):87.
6. Bostrom N. Superintelligence: Paths, Dangers, Strategies. Oxford, England, UK: Oxford University Press; 2014. Available from: https://books.google.co.uk/books/about/Superintelligence.html?id=7_H8AwAAQBAJ&redir_esc=y.
7. Mitchell M. Artificial Intelligence: A Guide for Thinking Humans. London, England, UK: Penguin Books, Limited; 2019. Available from: https://books.google.co.uk/books?id=uOUIwQEACAAJ&source=gbs_book_other_versions.
8. Lahav O. Artificial neural networks as non-linear extensions of statistical methods in astronomy. *Vistas in Astronomy*. 1994 1;38:251–IN2.
9. LeCun Y. My take on Ali Rahimi's 'Test of Time' award talk at NIPS; 2017. Available from: <https://www.facebook.com/yann.lecun/posts/10154938130592143>.
10. Silver D, Huang A, Maddison CJ, Guez A, Sifre L, van den Driessche G, et al. Mastering the game of Go with deep neural networks and tree search. *Nature*. 2016 Jan;529:484–489.
11. Jumper J, Evans R, Pritzel A, Green T, Figurnov M, Ronneberger O, et al. Highly accurate protein structure prediction with AlphaFold. *Nature*. 2021;596(7873):583–589.
12. Brown T, Mann B, Ryder N, Subbiah M, Kaplan JD, Dhariwal P, et al. Language Models are Few-Shot Learners. In: Larochelle H, Ranzato M, Hadsell R, Balcan MF, Lin H, editors. *Advances in Neural Information Processing Systems*. vol. 33. Curran Associates, Inc.; 2020. p. 1877–1901. Available from: <https://proceedings.neurips.cc/paper/2020/file/1457c0d6bfc4967418bfb8ac142f64a-Paper.pdf>.
13. Dosovitskiy A, Beyer L, Kolesnikov A, Weissenborn D, Zhai X, Unterthiner T, et al. An Image is Worth 16x16 Words: Transformers for Image Recognition at Scale. *CoRR*. 2020;abs/2010.11929. Available from: <https://arxiv.org/abs/2010.11929>.
14. Zhang Y, Zhao Y. Astronomy in the Big Data Era. *Data Science Journal*. 2015;14:11.
15. Springel V, Pakmor R, Pillepich A, Weinberger R, Nelson D, Hernquist L, et al. First results from the IllustrisTNG simulations: matter and galaxy clustering. *Monthly Notices of the Royal Astronomical Society*. 2018 3;475(1):676–698.
16. Miller AS. A review of neural network applications in Astronomy. *Vistas in Astronomy*. 1993 1;36:141–161.
17. Ball NM, Brunner RJ. DATA MINING AND MACHINE LEARNING IN ASTRONOMY. *International Journal of Modern Physics D*. 2010 7;19(07):1049–1106.
18. Huertas-Company M, Lanusse F. The DAWES review 10: The impact of deep learning for the analysis of galaxy surveys. *arXiv e-prints*. 2022 10;p. arXiv:2210.01813. Available from: <https://ui.adsabs.harvard.edu/abs/2022arXiv221001813H/exportcitation>.
19. Smith M. Using Deep Learning to Explore Ultra-Large Scale Astronomical Datasets. University of Hertfordshire; 2022.
20. McCulloch W, Pitts W. A Logical Calculus of Ideas Immanent in Nervous Activity. *Bulletin of Mathematical Biophysics*. 1943;5:127–147.
21. Rosenblatt F. The Perceptron: A Probabilistic Model for Information Storage and Organization in The Brain. *Psychological Review*. 1958;p. 65–386.

22. Hebb DO. The organization of behavior: A neuropsychological theory. Wiley; 1949.
23. Minsky M, Papert S. Perceptrons: An Introduction to Computational Geometry. Cambridge, MA, USA: MIT Press; 1969.
24. Metz C. Genius Makers: The Mavericks Who Brought AI to Google, Facebook, and the World. Penguin Random House; 2021.
25. Ivakhnenko A, Lapa V. Cybernetic Predicting Devices. CCM Information Corporation; 1965. English translation available as of 2022-06-08 at <https://www.gwern.net/docs/ai/1966-ivakhnenko.pdf>.
26. Ivakhnenko A. Polynomial Theory of Complex Systems. IEEE Transactions on Systems, Man, and Cybernetics. 1971;SMC-1(4):364–378.
27. Rosenblatt F. Principles of Neurodynamics: Perceptrons and the Theory of Brain Mechanisms. Cornell Aeronautical Laboratory. Report no. VG-1196-G-8. Spartan Books; 1962. Available from: <https://apps.dtic.mil/sti/pdfs/AD0256582.pdf>.
28. Cybenko G. Approximation by superpositions of a sigmoidal function. Mathematics of Control, Signals, and Systems (MCSS). 1989;2(4):303–314. Available from: <http://dx.doi.org/10.1007/BF02551274>.
29. Hornik K, Tinchcombe M, White H. Approximation capabilities of multilayer feedforward networks. Neural Networks. 1991;4(2):251–257. Available from: <http://www.sciencedirect.com/science/article/pii/089360809190009T>.
30. Lu Z, Pu H, Wang F, Hu Z, Wang L. The Expressive Power of Neural Networks: A View from the Width. In: Guyon I, Luxburg UV, Bengio S, Wallach H, Fergus R, Vishwanathan S, et al., editors. Advances in Neural Information Processing Systems. vol. 30. Curran Associates, Inc.; 2017. p. 6232–6240. Available from: <https://proceedings.neurips.cc/paper/2017/file/32cbf687880eb1674a07bf717761dd3a-Paper.pdf>.
31. Fukushima K. Neocognitron: A self-organizing neural network model for a mechanism of pattern recognition unaffected by shift in position. Biological Cybernetics. 1980;36(4):193–202. Available from: <https://doi.org/10.1007/bf00344251>.
32. Nair V, Hinton GE. Rectified Linear Units Improve Restricted Boltzmann Machines. In: Proceedings of the 27th International Conference on International Conference on Machine Learning. ICML'10. Madison, WI, USA: Omnipress; 2010. p. 807–814.
33. Clevert D, Unterthiner T, Hochreiter S. Fast and Accurate Deep Network Learning by Exponential Linear Units (ELUs). In: 4th International Conference on Learning Representations, ICLR 2016, San Juan, Puerto Rico, May 2-4, 2016, Conference Track Proceedings, abs/1511.07289; 2016. .
34. Ramachandran P, Zoph B, Le QV. Searching for Activation Functions. arXiv e-prints. 2017;p. arXiv:1710.05941.
35. Misra D. Mish: A Self Regularized Non-Monotonic Neural Activation Function. CoRR. 2019;abs/1908.08681. Available from: <http://arxiv.org/abs/1908.08681>.
36. Linnainmaa S. Taylor expansion of the accumulated rounding error. BIT. 1976;16(2):146–160. Available from: <https://doi.org/10.1007/bf01931367>.
37. Werbos PJ. Applications of Advances in Nonlinear Sensitivity Analysis. In: Proceedings of the 10th IFIP Conference, 31.8 - 4.9, NYC; 1981. p. 762–770.
38. Rumelhart DE, Hinton GE, Williams RJ. Learning representations by back-propagating errors. Nature. 1986;323(6088):533–536. Available from: <https://doi.org/10.1038/2F323533a0>.
39. Linnainmaa S. The representation of the cumulative rounding error of an algorithm as a Taylor expansion of the local rounding errors. The University of Helsinki; 1970. In Finnish.
40. Schmidhuber J. Deep Learning in Neural Networks: An Overview. arXiv e-prints. 2014;p. arXiv:1404.7828.
41. Baydin AG, Pearlmutter BA, Radul AA, Siskind JM. Automatic Differentiation in Machine Learning: a Survey. Journal of Machine Learning Research. 2018;18(153):1–43. Available from: <http://jmlr.org/papers/v18/17-468.html>.
42. Rappaport B, Anderson K. Automated galaxy recognition. In: European Southern Observatory Conference and Workshop Proceedings. vol. 28 of European Southern Observatory Conference and Workshop Proceedings; 1988. p. 233–238.

43. Adorf HM, Johnston MD. Artificial neural nets in astronomy. In: Arbeitspapier der Gesellschaft für Mathematik und Datenverarbeitung. vol. 329 of Arbeitspapier der Gesellschaft für Mathematik und Datenverarbeitung; 1988. .
44. Odewahn SC, Stockwell EB, Pennington RL, Humphreys RM, Zumach WA. Automated Star/Galaxy Discrimination With Neural Networks. *The Astronomical Journal*. 1992;103:318.
45. Pennington RL, Humphreys RM, Odewahn SC, Zumach W, Thurmes PM. The Automated Plate Scanner Catalog of the Palomar Sky Survey. I. Scanning Parameters and Procedures on JSTOR. *Publications of the Astronomical Society of the Pacific*. 1993 5;105(687):521–526. Available from: <https://www.jstor.org/stable/40680062>.
46. Odewahn SC, Humphreys RM, Aldering G, Thurmes P. Star-Galaxy Separation with a Neural Network. II. Multiple Schmidt Plate Fields. *Publications of the Astronomical Society of the Pacific*. 1993;105:1354.
47. Bazell D, Peng Y. A Comparison of Neural Network Algorithms and Preprocessing Methods for Star-Galaxy Discrimination. *Astrophysical Journal Supplement Series*. 1998 5;116(1):47–55.
48. Bertin E, Arnouts S. SExtractor: Software for source extraction. *Astronomy and Astrophysics Supplement Series*. 1996;117:393–404.
49. Andreon S, Gargiulo G, Longo G, Tagliaferri R, Capuano N. Wide field imaging — I. Applications of neural networks to object detection and star/galaxy classification. *Monthly Notices of the Royal Astronomical Society*. 2000 12;319(3):700–716.
50. Storrie-Lombardi MC, Lahav O, Sodre J L, Storrie-Lombardi LJ. Morphological Classification of Galaxies by Artificial Neural Networks. *Monthly Notices of the Royal Astronomical Society*. 1992;259:8P.
51. Lahav O, Naim A, Buta RJ, Corwin HG, de Vaucouleurs G, Dressler A, et al. Galaxies, Human Eyes, and Artificial Neural Networks. *Science*. 1995;267(5199):859–862.
52. Lahav O, Naim A, Sodré L Jr, Storrie-Lombardi MC. Neural computation as a tool for galaxy classification: methods and examples. *Monthly Notices of the Royal Astronomical Society*. 1996 10;283(1):207–221.
53. Naim A, Lahav O, Sodré L Jr, Storrie-Lombardi MC. Automated morphological classification of APM galaxies by supervised artificial neural networks. *Monthly Notices of the Royal Astronomical Society*. 1995 8;275(3):567–590.
54. Naim A, Lahav O, Buta RJ, Corwin HG Jr, de Vaucouleurs G, Dressler A, et al. A comparative study of morphological classifications of APM galaxies. *Monthly Notices of the Royal Astronomical Society*. 1995 6;274(4):1107–1125.
55. Odewahn SC, Windhorst RA, Driver SP, Keel WC. ADS. *Astrophysical Journal Letters* v472, pL13. 1996 11;472:L13.
56. Ball NM, Loveday J, Fukugita M, Nakamura O, Okamura S, Brinkmann J, et al. Galaxy types in the Sloan Digital Sky Survey using supervised artificial neural networks. *Monthly Notices of the Royal Astronomical Society*. 2004;348(3):1038–1046.
57. von Hippel T, Storrie-Lombardi LJ, Storrie-Lombardi MC, Irwin MJ. Automated classification of stellar spectra – I. Initial results with artificial neural networks. *Monthly Notices of the Royal Astronomical Society*. 1994 7;269(1):97–104.
58. Klusch M, Napiwotzki R. HNS : a hybrid neural system and its use for the classification of stars. *Astronomy and Astrophysics*. 1993 9;276:309–319. Available from: <https://ui.adsabs.harvard.edu/abs/1993A%26A...276..309K/abstract>.
59. Chon MC. Muon physics and neural network event classifier for the Sudbury Neutrino Observatory; 1998. Available from: <https://ui.adsabs.harvard.edu/abs/1998PhDT.....227C/abstract>.
60. Carballo R, Cofiño AS, González-Serrano JI. Selection of quasar candidates from combined radio and optical surveys using neural networks. *Monthly Notices of the Royal Astronomical Society*. 2004 9;353(1):211–220.
61. Claeskens JF, Smette A, Vandenbulcke L, Surdej J. Identification and redshift determination of quasi-stellar objects with medium-band photometry: application to Gaia. *Monthly Notices of the Royal Astronomical Society*. 2006 4;367(3):879–904.

62. Carballo R, González-Serrano JI, Benn CR, Jiménez-Luján F. Use of neural networks for the identification of new $z \geq 3.6$ QSOs from FIRST-SDSS DR5. *Monthly Notices of the Royal Astronomical Society*. 2008 11;391(1):369–382.
63. White RL, Becker RH, Gregg MD, Laurent-Muehleisen SA, Brotherton MS, Impey CD, et al. The FIRST Bright Quasar Survey. II. 60 Nights and 1200. *Astrophysical Journal Supplement Series*. 2000 2;126(2):133–207.
64. Kessler R, Bassett B, Belov P, Bhatnagar V, Campbell H, Conley A, et al. Results from the Supernova Photometric Classification Challenge. *Publications of the Astronomical Society of the Pacific*. 2010 11;122(898):1415–1431.
65. Karpenka NV, Feroz F, Hobson MP. A simple and robust method for automated photometric classification of supernovae using neural networks. *Monthly Notices of the Royal Astronomical Society*. 2013;429(2):1278–1285.
66. Angel J, Wizinowich P, Lloyd-Hart M, Sandler D. Adaptive optics for array telescopes using neural-network techniques. *Nature*. 1990;348(6298):221–224.
67. Sandler DG, Barrett TK, Palmer DA, Fugate RQ, Wild WJ. Use of a neural network to control an adaptive optics system for an astronomical telescope. *Nature*. 1991 5;351(6324):300–302.
68. Lloyd-Hart M, Wizinowich P, McLeod B, Wittman D, Colucci D, Dekany R, et al. First Results of an On-Line Adaptive Optics System with Atmospheric Wavefront Sensing by an Artificial Neural Network. *The Astrophysical Journal Letters*. 1992;390:L41.
69. Firth AE, Lahav O, Somerville RS. Estimating photometric redshifts with artificial neural networks. *Monthly Notices of the Royal Astronomical Society*. 2003 3;339(4):1195–1202.
70. Tagliaferri R, Longo G, Andreon S, Capozziello S, Donalek C, Giordano G. Neural Networks for Photometric Redshifts Evaluation. In: *Neural Nets*. Berlin, Germany: Springer; 2003. p. 226–234.
71. Vanzella E, Cristiani S, Fontana A, Nonino M, Arnouts S, Giallongo E, et al. Photometric redshifts with the Multilayer Perceptron Neural Network: Application to the HDF-S and SDSS. *Astronomy & Astrophysics*. 2004 8;423(2):761–776.
72. Collister AA, Lahav O. ANNz: Estimating Photometric Redshifts Using Artificial Neural Networks. *The Publications of the Astronomical Society of the Pacific*. 2004;116(818):345–351.
73. Stoughton C, Lupton RH, Bernardi M, Blanton MR, Burles S, Castander FJ, et al. Sloan Digital Sky Survey: Early Data Release. *Astronomical Journal*. 2002 1;123(1):485–548.
74. York DG, Adelman J, Anderson J J E, Anderson SF, Annis J, Bahcall NA, et al. The Sloan Digital Sky Survey: Technical Summary. *Astronomical Journal*. 2000;120(3):1579–1587.
75. Koons HC, Gorney DJ. A sunspot maximum prediction using a neural network. *Eos, Transactions American Geophysical Union*. 1990 5;71(18):677–688.
76. Bailer-Jones CAL, Irwin M, Gilmore G, von Hippel T. Physical parametrization of stellar spectra: the neural network approach. *Monthly Notices of the Royal Astronomical Society*. 1997 11;292(1):157–166.
77. Auld T, Bridges M, Hobson MP, Gull SF. Fast cosmological parameter estimation using neural networks. *Monthly Notices of the Royal Astronomical Society: Letters*. 2007 3;376(1):L11–L15.
78. Auld T, Bridges M, Hobson MP. cosmonet: fast cosmological parameter estimation in non-flat models using neural networks. *Monthly Notices of the Royal Astronomical Society*. 2008 7;387(4):1575–1582.
79. Nørgaard-Nielsen HU, Jørgensen HE. Foreground removal from CMB temperature maps using an MLP neural network. *Astrophysics and Space Science*. 2008;318(3-4):195–206.
80. Tolstikhin IO, Hounsby N, Kolesnikov A, Beyer L, Zhai X, Unterthiner T, et al. MLP-Mixer: An all-MLP Architecture for Vision. In: Ranzato M, Beygelzimer A, Dauphin Y, Liang PS, Vaughan JW, editors. *Advances in Neural Information Processing Systems*. vol. 34. Curran Associates, Inc.; 2021. p. 24261–24272. Available from: <https://proceedings.neurips.cc/paper/2021/file/cba0a4ee5ccd02fda0fe3f9a3e7b89fe-Paper.pdf>.
81. Touvron H, Bojanowski P, Caron M, Cord M, El-Nouby A, Grave E, et al. ResMLP: Feedforward networks for image classification with data-efficient training. *arXiv e-prints*. 2021;p. arXiv:2105.03404.

82. Liu H, Dai Z, So DR, Le QV. Pay Attention to MLPs. arXiv e-prints. 2021;p. arXiv:2105.08050.
83. Melas-Kyriazi L. Do You Even Need Attention? A Stack of Feed-Forward Layers Does Surprisingly Well on ImageNet. arXiv e-prints. 2021;p. arXiv:2105.02723.
84. Sutton R. The Bitter Lesson; 2019. Available from: <http://incompleteideas.net/IncIdeas/BitterLesson.html>.
85. Branwen G. The Scaling Hypothesis; 2022. Available from: <https://www.gwern.net/Scaling-hypothesis>.
86. LeCun Y, Boser B, Denker JS, Henderson D, Howard RE, Hubbard W, et al. Backpropagation Applied to Handwritten Zip Code Recognition. *Neural Computation*. 1989;1(4):541–551. Available from: <https://doi.org/10.1162/neco.1989.1.4.541>.
87. Rombach R, Blattmann A, Lorenz D, Esser P, Ommer B. High-Resolution Image Synthesis with Latent Diffusion Models. arXiv e-prints. 2021;p. arXiv:2112.10752.
88. Lin M, Chen Q, Yan S. Network In Network. arXiv e-prints. 2013;p. arXiv:1312.4400.
89. Crawford K. Bright Spiral Galaxy M81; 2015. [Online; accessed 2020-07-16]. Available from: <https://apod.nasa.gov/apod/ap151017.html>.
90. Werbos PJ. Backpropagation through time: what it does and how to do it. *Proceedings of the IEEE*. 1990;78:1550–1560.
91. Hochreiter S. Untersuchungen zu dynamischen neuronalen Netzen (investigations on dynamic neural networks). The Technical University of Munich; 1991. In German. Available from: <http://www.bioinf.jku.at/publications/older/3804.pdf>.
92. Bengio Y, Simard P, Frasconi P. Learning long-term dependencies with gradient descent is difficult. *IEEE Transactions on Neural Networks*. 1994;5(2):157–166.
93. Frankle J, Carbin M. The Lottery Ticket Hypothesis: Finding Sparse, Trainable Neural Networks. arXiv e-prints. 2018;p. arXiv:1803.03635.
94. Glorot X, Bordes A, Bengio Y. Deep Sparse Rectifier Neural Networks. In: Gordon G, Dunson D, Dudík M, editors. *Proceedings of the Fourteenth International Conference on Artificial Intelligence and Statistics*. vol. 15 of *Proceedings of Machine Learning Research*. Fort Lauderdale, FL, USA: *Proceedings of Machine Learning Research*; 2011. p. 315–323. Available from: <http://proceedings.mlr.press/v15/glorot11a.html>.
95. Oh K, Jung K. GPU implementation of neural networks. *Pattern Recognition*. 2004;37(6):1311–1314. Available from: <https://www.sciencedirect.com/science/article/pii/S0031320304000524>.
96. Steinkrau D, Simard P, Buck I. Using GPUs for Machine Learning Algorithms. In: *Proceedings of the Eighth International Conference on Document Analysis and Recognition*. ICDAR '05. USA: IEEE Computer Society; 2005. p. 1115–1119. Available from: <https://doi.org/10.1109/ICDAR.2005.251>.
97. Chellapilla K, Puri S, Simard P. High Performance Convolutional Neural Networks for Document Processing. In: Lorette G, editor. *Tenth International Workshop on Frontiers in Handwriting Recognition*. Université de Rennes 1. La Baule (France): Suvisoft; 2006. [Http://www.suvisoft.com](http://www.suvisoft.com). Available from: <https://hal.inria.fr/inria-00112631>.
98. Raina R, Madhavan A, Ng AY. Large-Scale Deep Unsupervised Learning Using Graphics Processors. In: *Proceedings of the 26th Annual International Conference on Machine Learning*. ICML '09. New York, NY, USA: Association for Computing Machinery; 2009. p. 873–880. Available from: <https://doi.org/10.1145/1553374.1553486>.
99. Cireşan D, Meier U, Gambardella LM, Schmidhuber J. Deep Big Simple Neural Nets Excel on Handwritten Digit Recognition. arXiv e-prints. 2010;p. arXiv:1003.0358.
100. Cireşan D, Meier U, Masci J, Gambardella LM, Schmidhuber J. Flexible, High Performance Convolutional Neural Networks for Image Classification. In: Walsh T, editor. *IJCAI 2011, Proceedings of the 22nd International Joint Conference on Artificial Intelligence, Barcelona, Catalonia, Spain, July 16-22, 2011*. IJCAI/AAAI; 2011. p. 1237–1242. Available from: <https://doi.org/10.5591/978-1-57735-516-8/IJCAI11-210>.
101. Krizhevsky A, Sutskever I, Hinton GE. ImageNet Classification with Deep Convolutional Neural Networks. In: Bartlett PL, Pereira FCN, Burges CJC, Bottou

- L, Weinberger KQ, editors. *Advances in Neural Information Processing Systems 25: 26th Annual Conference on Neural Information Processing Systems 2012. Proceedings of a meeting held December 3-6, 2012, Lake Tahoe, Nevada, United States; 2012.* p. 1106-1114. Available from: <http://papers.nips.cc/paper/4824-imagenet-classification-with-deep-convolutional-neural-networks>.
102. Russakovsky O, Deng J, Su H, Krause J, Satheesh S, Ma S, et al. ImageNet Large Scale Visual Recognition Challenge. *International Journal of Computer Vision (IJCV)*. 2015;115(3):211-252.
 103. Srivastava N, Hinton GE, Krizhevsky A, Sutskever I, Salakhutdinov R. Dropout: A Simple Way to Prevent Neural Networks from Overfitting. *Journal of Machine Learning Research*. 2014;15(56):1929-1958. Available from: <http://jmlr.org/papers/v15/srivastava14a.html>.
 104. Sevilla J, Heim L, Ho A, Besiroglu T, Hobbhahn M, Villalobos P. Compute Trends Across Three Eras of Machine Learning. arXiv e-prints. 2022;p. arXiv:2202.05924.
 105. Hochreiter S, Schmidhuber J. Long Short-Term Memory. *Neural Computation*. 1997;9(8):1735-1780. Available from: <https://doi.org/10.1162/neco.1997.9.8.1735>.
 106. Gers F, Schmidhuber J, Cummins F. Learning to Forget: Continual Prediction with LSTM. *Neural Computation*. 2000;12(10):2451-2471.
 107. Cho K, van Merriënboer B, Gulcehre C, Bahdanau D, Bougares F, Schwenk H, et al. Learning Phrase Representations using RNN Encoder-Decoder for Statistical Machine Translation. ArXiv e-prints. 2014; Available from: <https://arxiv.org/abs/1406.1078>.
 108. Bayer J. Learning Sequence Representations. Technical University Munich; 2015. Available from: <https://nbn-resolving.org/urn:nbn:de:bvb:91-diss-20151102-1256381-1-9>.
 109. Sutskever I, Vinyals O, Le QV. Sequence to Sequence Learning with Neural Networks. arXiv e-prints. 2014;p. arXiv:1409.3215.
 110. Vaswani A, Shazeer N, Parmar N, Uszkoreit J, Jones L, Gomez AN, et al. Attention Is All You Need. arXiv e-prints. 2017;p. arXiv:1706.03762.
 111. Srivastava RK, Greff K, Schmidhuber J. Highway Networks. arXiv e-prints. 2015;p. arXiv:1505.00387.
 112. He K, Zhang X, Ren S, Sun J. Deep Residual Learning for Image Recognition. arXiv e-prints. 2015;p. arXiv:1512.03385.
 113. Ronneberger O, Fischer P, Brox T. U-Net: Convolutional Networks for Biomedical Image Segmentation. In: *Medical Image Computing and Computer-Assisted Intervention - MICCAI 2015 - 18th International Conference Munich, Germany, October 5 - 9, 2015, Proceedings, Part III*. vol. 9351 of *Lecture Notes in Computer Science*. Springer; 2015. p. 234-241.
 114. Bahdanau D, Cho K, Bengio Y. Neural Machine Translation by Jointly Learning to Align and Translate. CoRR. 2014;abs/1409.0473.
 115. Radford A, Wu J, Child R, Luan D, A D, Sutskever I. Language Models are Unsupervised Multitask Learners. OpenAI Whitepaper. 2019; Available from: https://cdn.openai.com/better-language-models/language_models_are_unsupervised_multitask_learners.pdf.
 116. Devlin J, Chang M, Lee K, Toutanova K. BERT: Pre-training of Deep Bidirectional Transformers for Language Understanding. In: *Proceedings of the 2019 Conference of the North American Chapter of the Association for Computational Linguistics: Human Language Technologies, Volume 1 (Long and Short Papers)*. Minneapolis, Minnesota: Association for Computational Linguistics; 2019. p. 4171-4186. Available from: <https://aclanthology.org/N19-1423>.
 117. Reed S, Zolna K, Parisotto E, Gomez Colmenarejo S, Novikov A, Barth-Maron G, et al. A Generalist Agent. arXiv e-prints. 2022;p. arXiv:2205.06175.
 118. Aussem A, Murtagh F, Sarazin M. Dynamical recurrent neural networks and pattern recognition methods for time series prediction: Application to seeing and temperature

- forecasting in the context of ESO's VLT astronomical weather station. *Vistas in Astronomy*. 1994 1;38:357–374.
119. Wu JG, Lundstedt H. Prediction of geomagnetic storms from solar wind data using Elman Recurrent Neural Networks. *Geophysical Research Letters*. 1996 2;23(4):319–322.
 120. Lundstedt H, Gleisner H, Wintoft P. Operational forecasts of the geomagnetic Dst index. *Geophysical Research Letters*. 2002 12;29(24):34–1–34–4.
 121. Vassiliadis D, Klimas AJ, Valdivia JA, Baker DN. The nonlinear dynamics of space weather. *Advances in Space Research*. 2000 1;26(1):197–207.
 122. Brodrick D, Taylor D, Diederich J. Recurrent Neural Networks for Narrowband Signal Detection in the Time-Frequency Domain. *Symposium - International Astronomical Union*. 2004;213:483–486.
 123. Elman JL. Finding structure in time. *Cognitive Science*. 1990;14(2):179–211. Available from: <https://www.sciencedirect.com/science/article/pii/036402139090002E>.
 124. Charnock T, Moss A. Deep Recurrent Neural Networks for Supernovae Classification. *The Astrophysical Journal Letters*. 2017;837(2):L28.
 125. Naul B, Bloom JS, Pérez F, van der Walt S. A recurrent neural network for classification of unevenly sampled variable stars. *Nature Astronomy*. 2018;2(2):151–155.
 126. Gonzalez CAG, Absil O, Van Droogenbroeck M. Supervised detection of exoplanets in high-contrast imaging sequences. *Astronomy & Astrophysics*. 2018 5;613:A71.
 127. Carrasco-Davis R, Cabrera-Vives G, Förster F, Estévez PA, Huijse P, Protopapas P, et al. Deep Learning for Image Sequence Classification of Astronomical Events. *Publications of the Astronomical Society of the Pacific*. 2019;131(1004):108006.
 128. Finke T, Krämer M, Manconi S. Classification of Fermi-LAT sources with deep learning using energy and time spectra. *Monthly Notices of the Royal Astronomical Society*. 2021 11;507(3):4061–4073.
 129. Weddell SJ, Webb RY. Reservoir Computing for Prediction of the Spatially-Variant Point Spread Function. *IEEE Journal of Selected Topics in Signal Processing*. 2008 10;2(5):624–634.
 130. Jaeger H, Haas H. Harnessing Nonlinearity: Predicting Chaotic Systems and Saving Energy in Wireless Communication. *Science*. 2004 4;304(5667):78–80.
 131. Capizzi G, Napoli C, Paternò L. An Innovative Hybrid Neuro-wavelet Method for Reconstruction of Missing Data in Astronomical Photometric Surveys. In: *Artificial Intelligence and Soft Computing*. Berlin, Germany: Springer; 2012. p. 21–29.
 132. Shen H, George D, Huerta EA, Zhao Z. Denoising Gravitational Waves using Deep Learning with Recurrent Denoising Autoencoders. *arXiv e-prints*. 2017;p. arXiv:1711.09919.
 133. Morningstar WR, Levasseur LP, Hezaveh YD, Blandford R, Marshall P, Putzky P, et al. Data-driven Reconstruction of Gravitationally Lensed Galaxies Using Recurrent Inference Machines. *Astrophysical Journal*. 2019 9;883(1):14.
 134. Liu H, Liu C, Wang JTL, Wang H. Predicting Solar Flares Using a Long Short-term Memory Network. *The Astrophysical Journal*. 2019;877(2):121.
 135. Kügler SD, Gianniotis N, Polsterer KL. An explorative approach for inspecting Kepler data. *Monthly Notices of the Royal Astronomical Society*. 2016 2;455(4):4399–4405.
 136. Smith MJ, Arora N, Stone C, Courteau S, Geach JE. Pix2Prof: fast extraction of sequential information from galaxy imagery via a deep natural language 'captioning' model. *Monthly Notices of the Royal Astronomical Society*. 2021;503(1):96–105.
 137. Zhu WW, Berndsen A, Madsen EC, Tan M, Stairs IH, Brazier A, et al. Searching for pulsars using image pattern recognition. *Astrophysical Journal*. 2014 1;781(2):117.
 138. Hála P. Spectral classification using convolutional neural networks. *arXiv e-prints*. 2014;p. arXiv:1412.8341.
 139. Dieleman S, Willett KW, Dambre J. Rotation-invariant convolutional neural networks for galaxy morphology prediction. *Monthly Notices of the Royal Astronomical Society*. 2015;450(2):1441–1459.
 140. Raddick MJ, Bracey G, Gay PL, Lintott CJ, Murray P, Schawinski K, et al. Galaxy Zoo: Exploring the Motivations of Citizen Science Volunteers. *Astronomy Education Review*. 2010;9(1):010103.

141. Huertas-Company M, Gravet R, Cabrera-Vives G, Pérez-González PG, Kartaltepe JS, Barro G, et al. A CATALOG OF VISUAL-LIKE MORPHOLOGIES IN THE 5 CANDELS FIELDS USING DEEP LEARNING. *Astrophysical Journal Supplement Series*. 2015 10;221(1):8.
142. Koekemoer AM, Faber SM, Ferguson HC, Grogin NA, Kocevski DD, Koo DC, et al. CANDELS: THE COSMIC ASSEMBLY NEAR-INFRARED DEEP EXTRAGALACTIC LEGACY SURVEY—THE HUBBLE SPACE TELESCOPE OBSERVATIONS, IMAGING DATA PRODUCTS, AND MOSAICS. *Astrophysical Journal Supplement Series*. 2011 12;197(2):36.
143. Aniyani AK, Thorat K. Classifying Radio Galaxies with the Convolutional Neural Network. *Astrophysical Journal Supplement Series*. 2017 6;230(2):20.
144. Wilde J, Serjeant S, Bromley JM, Dickinson H, Koopmans LVE, Metcalf RB. Detecting gravitational lenses using machine learning: exploring interpretability and sensitivity to rare lensing configurations. *Monthly Notices of the Royal Astronomical Society*. 2022 5;512(3):3464–3479.
145. Zeiler MD, Fergus R. Visualizing and Understanding Convolutional Networks. In: *Computer Vision – ECCV 2014*. Cham, Switzerland: Springer; 2014. p. 818–833.
146. Selvaraju RR, Das A, Vedantam R, Cogswell M, Parikh D, Batra D. Grad-CAM: Why did you say that? Visual Explanations from Deep Networks via Gradient-based Localization. *CoRR*. 2016;abs/1610.02391. Available from: <http://arxiv.org/abs/1610.02391>.
147. Akeret J, Chang C, Lucchi A, Refregier A. Radio frequency interference mitigation using deep convolutional neural networks. *Astronomy and Computing*. 2017;18:35–39.
148. Berger P, Stein G. A volumetric deep Convolutional Neural Network for simulation of mock dark matter halo catalogues. *Monthly Notices of the Royal Astronomical Society*. 2019 1;482(3):2861–2871.
149. Milletari F, Navab N, Ahmadi S. V-Net: Fully Convolutional Neural Networks for Volumetric Medical Image Segmentation. *CoRR*. 2016;abs/1606.04797. Available from: <http://arxiv.org/abs/1606.04797>.
150. Aragon-Calvo MA. Classifying the large-scale structure of the universe with deep neural networks. *Monthly Notices of the Royal Astronomical Society*. 2019 4;484(4):5771–5784.
151. Hausen R, Robertson BE. Morpheus: A Deep Learning Framework for the Pixel-level Analysis of Astronomical Image Data. *Astrophysical Journal Supplement Series*. 2020 5;248(1):20.
152. Lauritsen L, Dickinson H, Bromley J, Serjeant S, Lim CF, Gao ZK, et al. Superresolving Herschel imaging: a proof of concept using Deep Neural Networks. *Monthly Notices of the Royal Astronomical Society*. 2021 10;507(1):1546–1556.
153. Parmar N, Vaswani A, Uszkoreit J, Kaiser L, Shazeer N, Ku A, et al. Image Transformer. In: Dy J, Krause A, editors. *Proceedings of the 35th International Conference on Machine Learning*. vol. 80 of *Proceedings of Machine Learning Research*. PMLR; 2018. p. 4055–4064. Available from: <https://proceedings.mlr.press/v80/parmar18a.html>.
154. Donoso-Oliva C, Becker I, Protopapas P, Cabrera-Vives G, Vishnu M, Vardhan H. ASTROMER: A transformer-based embedding for the representation of light curves. *arXiv e-prints*. 2022;p. arXiv:2205.01677.
155. Morvan M, Nikolaou N, Hou Yip K, Waldmann I. Don't Pay Attention to the Noise: Learning Self-supervised Representations of Light Curves with a Denoising Time Series Transformer. *arXiv e-prints*. 2022;p. arXiv:2207.02777.
156. Ricker GR, Winn JN, Vanderspek R, Latham DW, Bakos GÁ, Bean JL, et al. Transiting Exoplanet Survey Satellite (TESS). *Journal of Astronomical Telescopes, Instruments, and Systems*. 2015 Jan;1:014003.
157. Pan J, Ting Y, Yu J. Astroconformer: Inferring Surface Gravity of Stars from Stellar Light Curves with Transformer. *arXiv e-prints*. 2022;p. arXiv:2207.02787.
158. Bommasani R, Hudson DA, Adeli E, Altman R, Arora S, von Arx S, et al. On the Opportunities and Risks of Foundation Models. *arXiv e-prints*. 2021 Aug;p. arXiv:2108.07258.
159. Rumelhart DE, Hinton GE, Williams RJ. 4. In: *Learning Internal Representations by Error Propagation*. Cambridge, MA, USA: MIT Press; 1986. p. 318–362.

160. Kingma DP, Welling M. Auto-Encoding Variational Bayes. arXiv e-prints. 2013;p. arXiv:1312.6114.
161. Goodfellow I, Pouget-Abadie J, Mirza M, Xu B, Warde-Farley D, Ozair S, et al. Generative Adversarial Nets. In: Ghahramani Z, Welling M, Cortes C, Lawrence ND, Weinberger KQ, editors. Advances in Neural Information Processing Systems 27. Curran Associates, Inc.; 2014. p. 2672–2680. Available from: <http://papers.nips.cc/paper/5423-generative-adversarial-nets.pdf>.
162. Isola P, Zhu J, Zhou T, Efros AA. Image-to-Image Translation with Conditional Adversarial Networks. arXiv e-prints. 2016;p. arXiv:1611.07004.
163. Sohl-Dickstein J, Weiss E, Maheswaranathan N, Ganguli S. Deep Unsupervised Learning using Nonequilibrium Thermodynamics. In: Bach F, Blei D, editors. Proceedings of the 32nd International Conference on Machine Learning. vol. 37 of Proceedings of Machine Learning Research. Lille, France: PMLR; 2015. p. 2256–2265. Available from: <http://proceedings.mlr.press/v37/sohl-dickstein15.html>.
164. Ho J, Jain A, Abbeel P. Denoising Diffusion Probabilistic Models. In: Larochelle H, Ranzato M, Hadsell R, Balcan MF, Lin H, editors. Advances in Neural Information Processing Systems. vol. 33. Curran Associates, Inc.; 2020. p. 6840–6851.
165. Hyvärinen A. Estimation of Non-Normalized Statistical Models by Score Matching. Journal of Machine Learning Research. 2005;6(24):695–709. Available from: <http://jmlr.org/papers/v6/hyvarinen05a.html>.
166. Vincent P. A Connection between Score Matching and Denoising Autoencoders. Neural Computation. 2011;23(7):1661–1674. Available from: https://doi.org/10.1162/NECO_a_00142.
167. Song Y, Ermon S. Improved Techniques for Training Score-Based Generative Models. In: Larochelle H, Ranzato M, Hadsell R, Balcan MF, Lin H, editors. Advances in Neural Information Processing Systems. vol. 33. Curran Associates, Inc.; 2020. p. 12438–12448. Available from: <https://proceedings.neurips.cc/paper/2020/file/92c3b916311a5517d9290576e3ea37ad-Paper.pdf>.
168. Jolicœur-Martineau A, Piché-Taillefer R, des Combes RT, Mitliagkas I. Adversarial score matching and improved sampling for image generation. CoRR. 2020;abs/2009.05475. Available from: <https://arxiv.org/abs/2009.05475>.
169. Jolicœur-Martineau A, Li K, Piché-Taillefer R, Kachman T, Mitliagkas I. Gotta Go Fast When Generating Data with Score-Based Models. CoRR. 2021;abs/2105.14080. Available from: <https://arxiv.org/abs/2105.14080>.
170. Song Y, Sohl-Dickstein J, Kingma DP, Kumar A, Ermon S, Poole B. Score-Based Generative Modeling through Stochastic Differential Equations. In: International Conference on Learning Representations; 2021. Available from: <https://openreview.net/forum?id=PXTIG12RRHS>.
171. Nichol A, Dhariwal P. Improved Denoising Diffusion Probabilistic Models. CoRR. 2021;abs/2102.09672. Available from: <https://arxiv.org/abs/2102.09672>.
172. Dhariwal P, Nichol A. Diffusion Models Beat GANs on Image Synthesis. CoRR. 2021;abs/2105.05233. Available from: <https://arxiv.org/abs/2105.05233>.
173. Ramesh A, Dhariwal P, Nichol A, Chu C, Chen M. Hierarchical Text-Conditional Image Generation with CLIP Latents. ArXiv e-prints. 2022 4;
174. Kadkhodaie Z, Simoncelli EP. Solving Linear Inverse Problems Using the Prior Implicit in a Denoiser. CoRR. 2020;abs/2007.13640. Available from: <https://arxiv.org/abs/2007.13640>.
175. Saharia C, Ho J, Chan W, Salimans T, Fleet DJ, Norouzi M. Image Super-Resolution via Iterative Refinement. CoRR. 2021;abs/2104.07636. Available from: <https://arxiv.org/abs/2104.07636>.
176. Sasaki H, Willcocks CG, Breckon TP. UNIT-DDPM: UNpaired Image Translation with Denoising Diffusion Probabilistic Models. CoRR. 2021;abs/2104.05358. Available from: <https://arxiv.org/abs/2104.05358>.
177. Jayaram V, Thickstun J. Source Separation with Deep Generative Priors. CoRR. 2020;abs/2002.07942. Available from: <https://arxiv.org/abs/2002.07942>.

178. Turner A. Diffusion Models as a kind of VAE; 2021. Available from: https://angusturner.github.io/generative_models/2021/06/29/diffusion-probabilistic-models-I.html.
179. Dieleman S. Diffusion models are autoencoders; 2022. Available from: <https://benanne.github.io/2022/01/31/diffusion.html>.
180. Song Y, Ermon S. Generative Modeling by Estimating Gradients of the Data Distribution. In: Wallach H, Larochelle H, Beygelzimer A, d'Alché-Buc F, Fox E, Garnett R, editors. Advances in Neural Information Processing Systems. vol. 32. Curran Associates, Inc.; 2019. Available from: <https://proceedings.neurips.cc/paper/2019/file/3001ef257407d5a371a96dcd947c7d93-Paper.pdf>.
181. Luhman E, Luhman T. Knowledge Distillation in Iterative Generative Models for Improved Sampling Speed. arXiv e-prints. 2021;p. arXiv:2101.02388.
182. Watson D, Chan W, Ho J, Norouzi M. Learning Fast Samplers for Diffusion Models by Differentiating Through Sample Quality. arXiv e-prints. 2022;p. arXiv:2202.05830.
183. Song J, Meng C, Ermon S. Denoising Diffusion Implicit Models. CoRR. 2020;abs/2010.02502. Available from: <https://arxiv.org/abs/2010.02502>.
184. Smith MJ, Geach JE, Jackson RA, Arora N, Stone C, Courteau S. Realistic galaxy image simulation via score-based generative models. Monthly Notices of the Royal Astronomical Society. 2022;511(2):1808–1818.
185. Chen T, Kornblith S, Norouzi M, Hinton GE. A Simple Framework for Contrastive Learning of Visual Representations. CoRR. 2020;abs/2002.05709. Available from: <https://arxiv.org/abs/2002.05709>.
186. Chen T, Kornblith S, Swersky K, Norouzi M, Hinton GE. Big Self-Supervised Models are Strong Semi-Supervised Learners. CoRR. 2020;abs/2006.10029. Available from: <https://arxiv.org/abs/2006.10029>.
187. Grill J, Strub F, Altché F, Tallec C, Richemond PH, Buchatskaya E, et al. Bootstrap Your Own Latent: A New Approach to Self-Supervised Learning. CoRR. 2020;abs/2006.07733. Available from: <https://arxiv.org/abs/2006.07733>.
188. He K, Fan H, Wu Y, Xie S, Girshick RB. Momentum Contrast for Unsupervised Visual Representation Learning. CoRR. 2019;abs/1911.05722. Available from: <http://arxiv.org/abs/1911.05722>.
189. Chen X, Fan H, Girshick RB, He K. Improved Baselines with Momentum Contrastive Learning. CoRR. 2020;abs/2003.04297. Available from: <https://arxiv.org/abs/2003.04297>.
190. Hadsell R, Chopra S, LeCun Y. Dimensionality Reduction by Learning an Invariant Mapping. In: 2006 IEEE Computer Society Conference on Computer Vision and Pattern Recognition (CVPR'06). vol. 2; 2006. p. 1735–1742.
191. Chechik G, Sharma V, Shalit U, Bengio S. Large Scale Online Learning of Image Similarity Through Ranking. Journal of Machine Learning Research. 2010;11(36):1109–1135. Available from: <http://jmlr.org/papers/v11/chechik10a.html>.
192. Sohn K. Improved Deep Metric Learning with Multi-class N-pair Loss Objective. In: Lee D, Sugiyama M, Luxburg U, Guyon I, Garnett R, editors. Advances in Neural Information Processing Systems. vol. 29. Curran Associates, Inc.; 2016. Available from: <https://proceedings.neurips.cc/paper/2016/file/6b180037abbebea991d8b1232f8a8ca9-Paper.pdf>.
193. Heusel M, Ramsauer H, Unterthiner T, Nessler B, Hochreiter S. GANs Trained by a Two Time-Scale Update Rule Converge to a Local Nash Equilibrium. In: Guyon I, Luxburg UV, Bengio S, Wallach H, Fergus R, Vishwanathan S, et al., editors. Advances in Neural Information Processing Systems. vol. 30. Curran Associates, Inc.; 2017. .
194. Seitzer M. pytorch-fid: FID Score for PyTorch; 2020. Version 0.1.1. <https://github.com/mseitzer/pytorch-fid>.
195. Szegedy C, Vanhoucke V, Ioffe S, Shlens J, Wojna Z. Rethinking the Inception Architecture for Computer Vision. In: Proceedings of the IEEE Conference on Computer Vision and Pattern Recognition (CVPR); 2016. .

196. Regier J, McAuliffe J, Prabhat. A deep generative model for astronomical images of galaxies. In: NIPS Workshop on Advances in Approximate Bayesian Inference; 2015. .
197. Regier J, Miller A, McAuliffe J, Adams R, Hoffman M, Lang D, et al. Celeste: Variational inference for a generative model of astronomical images. In: International Conference on Machine Learning (ICML); 2015. .
198. Serra-Ricart M, Calbet X, Garrido L, Gaitan V. Multidimensional Statistical Analysis Using Artificial Neural Networks: Astronomical Applications. *Astronomical Journal*. 1993 10;106:1685.
199. Ravanbakhsh S, Lanusse F, Mandelbaum R, Schneider J, Poczos B. Enabling Dark Energy Science with Deep Generative Models of Galaxy Images. *arXiv e-prints*. 2016;p. arXiv:1609.05796.
200. Spindler A, Geach JE, Smith MJ. AstroVaDEr: Astronomical Variational Deep Embedder for Unsupervised Morphological Classification of Galaxies and Synthetic Image Generation. *Monthly Notices of the Royal Astronomical Society*. 2020;502:985. Staa3670. Available from: <https://doi.org/10.1093/mnras/staa3670>.
201. Fussell L, Moews B. Forging new worlds: high-resolution synthetic galaxies with chained generative adversarial networks. *Monthly Notices of the Royal Astronomical Society*. 2019;485(3):3203–3214.
202. Holzschuh BJ, O’Riordan CM, Vegetti S, Rodriguez-Gomez V, Thuerey N. Realistic galaxy images and improved robustness in machine learning tasks from generative modelling. *Monthly Notices of the Royal Astronomical Society*. 2022 9;515(1):652–677.
203. Zhou B, Khosla A, Lapedriza A, Oliva A, Torralba A. Learning Deep Features for Discriminative Localization. In: *Computer Vision and Pattern Recognition*; 2016. .
204. Karras T, Laine S, Aila T. A Style-Based Generator Architecture for Generative Adversarial Networks. *CoRR*. 2018;abs/1812.04948. Available from: <http://arxiv.org/abs/1812.04948>.
205. Bretonnière H, Huertas-Company M, Boucaud A, Lanusse F, Jullo E, Merlin E, et al. Euclid preparation: XVI. Forecasts for galaxy morphology with the Euclid Survey using Deep Generative Models. *arXiv e-prints*. 2021;p. arXiv:2105.12149.
206. Weng L. Flow-based Deep Generative Models; 2018. Available from: <https://lilianweng.github.io/posts/2018-10-13-flow-models/>.
207. Germain M, Gregor K, Murray I, Larochelle H. MADE: Masked Autoencoder for Distribution Estimation. In: *International Conference on Machine Learning*. PMLR; 2015. p. 881–889. Available from: <https://proceedings.mlr.press/v37/germain15.html>.
208. Papamakarios G, Pavlakou T, Murray I. Masked autoregressive flow for density estimation. In: *NIPS’17: Proceedings of the 31st International Conference on Neural Information Processing Systems*. Red Hook, NY, USA: Curran Associates Inc.; 2017. p. 2335–2344.
209. Dey A, Schlegel DJ, Lang D, Blum R, Burleigh K, Fan X, et al. Overview of the DESI Legacy Imaging Surveys. *The Astronomical Journal*. 2019;157(5):168.
210. Abazajian KN, Adelman-McCarthy JK, Agüeros MA, Allam SS, Prieto CA, An D, et al. THE SEVENTH DATA RELEASE OF THE SLOAN DIGITAL SKY SURVEY. *The Astrophysical Journal Supplement Series*. 2009;182(2):543–558. Available from: <https://doi.org/10.1088/0067-0049/182/2/543>.
211. Wilman DJ, Zibetti S, Budavári T. A multiscale approach to environment and its influence on the colour distribution of galaxies. *Monthly Notices of the Royal Astronomical Society*. 2010;406(3):1701–1720.
212. Stone C, Courteau S. The Intrinsic Scatter of the Radial Acceleration Relation. *The Astrophysical Journal*. 2019;882(1):6.
213. Smith MJ, Geach JE. Generative deep fields: arbitrarily sized, random synthetic astronomical images through deep learning. "Monthly Notices of the Royal Astronomical Society". 2019;490(4):4985–4990.
214. Jetchev N, Bergmann U, Vollgraf R. Texture Synthesis with Spatial Generative Adversarial Networks. *CoRR*. 2016;abs/1611.08207. Available from: <http://arxiv.org/abs/1611.08207>.

215. Rodriguez AC, Kacprzak T, Lucchi A, Amara A, Sgier R, Fluri J, et al. Fast cosmic web simulations with generative adversarial networks. *Computational Astrophysics and Cosmology*. 2018;5(1):4.
216. Mustafa M, Bard D, Bhimji W, Lukić Z, Al-Rfou R, Kratochvil JM. CosmoGAN: creating high-fidelity weak lensing convergence maps using Generative Adversarial Networks. *Computational Astrophysics and Cosmology*. 2019;6(1):1.
217. Remy B, Lanusse F, Ramzi Z, Liu J, Jeffrey N, Starck J. Probabilistic Mapping of Dark Matter by Neural Score Matching. arXiv e-prints. 2020;p. arXiv:2011.08271.
218. Remy B, Lanusse F, Jeffrey N, Liu J, Starck JL, Osato K, et al. Probabilistic Mass Mapping with Neural Score Estimation. ArXiv e-prints. 2022 1;.
219. Liu J, Bird S, Matilla JMZ, Hill JC, Haiman Z, Madhavacheril MS, et al. MassiveNuS: cosmological massive neutrino simulations. *Journal of Cosmology and Astroparticle Physics*. 2018 3;2018(03):049.
220. Scoville N, Abraham RG, Aussel H, Barnes JE, Benson A, Blain AW, et al. COSMOS: Hubble Space Telescope Observations*. *Astrophysical Journal Supplement Series*. 2007 9;172(1):38–45.
221. Schawinski K, Zhang C, Zhang H, Fowler L, Santhanam GK. Generative adversarial networks recover features in astrophysical images of galaxies beyond the deconvolution limit. *Monthly Notices of the Royal Astronomical Society*. 2017;467:L110–L114.
222. Stark D, Launet B, Schawinski K, Zhang C, Koss M, Turp MD, et al. psfgan: a generative adversarial network system for separating quasar point sources and host galaxy light. *Monthly Notices of the Royal Astronomical Society*. 2018 6;477(2):2513–2527.
223. Reiman DM, Göhre BE. Deblending galaxy superpositions with branched generative adversarial networks. "Monthly Notices of the Royal Astronomical Society". 2019;485(2):2617–2627.
224. Buncher B, Sharma AN, Carrasco Kind M. Survey2Survey: a deep learning generative model approach for cross-survey image mapping. *Monthly Notices of the Royal Astronomical Society*. 2021;503(1):777–796.
225. Arcelin B, Doux C, Aubourg E, Roucelle C, LSST Dark Energy Science Collaboration. Deblending galaxies with variational autoencoders: A joint multiband, multi-instrument approach. *Monthly Notices of the Royal Astronomical Society*. 2021;500(1):531–547.
226. Calbet X, Mahoney T, Hammersley P, Garzon F, Selby M. ADS. Galactic bulges: proceedings of the 153rd Symposium of the International Astronomical Union held in Ghent, Belgium, August 17-22, 1992 Edited by Herwig DeJonghe and Harm Jan Habing International Astronomical Union Symposium no 153, Kluwer Academic Publishers, Dordrecht, p293. 1993;153:293. Available from: <https://ui.adsabs.harvard.edu/abs/1993IAUS..153..293C/abstract>.
227. Graff P, Feroz F, Hobson MP, Lasenby A. ADS. Monthly Notices of the Royal Astronomical Society, Volume 441, Issue 2, p1741-1759. 2014 6;441(2):1741.
228. Kitching TD, Rhodes J, Heymans C, Massey R, Liu Q, Cobzarenco M, et al. Image analysis for cosmology: Shape measurement challenge review & results from the Mapping Dark Matter challenge. *Astronomy and Computing*. 2015 4;10:9–21.
229. Yang T, Li X. An autoencoder of stellar spectra and its application in automatically estimating atmospheric parameters. *Monthly Notices of the Royal Astronomical Society*. 2015 9;452(1):158–168.
230. Tsang BTH, Schultz WC. Deep Neural Network Classifier for Variable Stars with Novelty Detection Capability. *Astrophysical Journal Letters*. 2019 5;877(2):L14.
231. Hayat MA, Stein G, Harrington P, Lukić Z, Mustafa M. Self-supervised Representation Learning for Astronomical Images. *The Astrophysical Journal Letters*. 2021;911(2):L33. Available from: <https://doi.org/10.3847/2041-8213/abf2c7>.
232. Sarmiento R, Huertas-Company M, Knapen JH, Sánchez SF, Domínguez Sánchez H, Drory N, et al. Capturing the physics of MaNGA galaxies with self-supervised Machine Learning. arXiv e-prints. 2021;p. arXiv:2104.08292.

233. Bundy K, Bershady MA, Law DR, Yan R, Drory N, MacDonald N, et al. OVERVIEW OF THE SDSS-IV MaNGA SURVEY: MAPPING NEARBY GALAXIES AT APACHE POINT OBSERVATORY. *The Astrophysical Journal*. 2014;798(1):7. Available from: <https://doi.org/10.1088/0004-637x/798/1/7>.
234. Slijepcevic IV, Scaife AMM, Walmsley M, Bowles M. Learning useful representations for radio astronomy "in the wild" with contrastive learning. *ArXiv e-prints*. 2022 7;.
235. Porter FAM. MiraBest Batched Dataset. *Zenodo*. 2020 11;.
236. Porby. Why I think strong general AI is coming soon; 2022. Available from: <https://www.lesswrong.com/posts/K4urTDkBbtNuLivJx/why-i-think-strong-general-ai-is-coming-soon>.
237. Bo P. BlinkDL/RWKV-LM: 0.01. *Zenodo*; 2021. Available from: <https://doi.org/10.5281/zenodo.5196577>.
238. Kim J, Dat Nguyen T, Min S, Cho S, Lee M, Lee H, et al. Pure Transformers are Powerful Graph Learners. *arXiv e-prints*. 2022 Jul;p. arXiv:2207.02505.
239. Alayrac J, Donahue J, Luc P, Miech A, Barr I, Hasson Y, et al. Flamingo: a Visual Language Model for Few-Shot Learning. *arXiv e-prints*. 2022;p. arXiv:2204.14198.
240. Wei J, Tay Y, Bommasani R, Raffel C, Zoph B, Borgeaud S, et al. Emergent Abilities of Large Language Models. *arXiv e-prints*. 2022 Jun;p. arXiv:2206.07682.
241. Chowdhery A, Narang S, Devlin J, Bosma M, Mishra G, Roberts A, et al. PaLM: Scaling Language Modeling with Pathways. *arXiv e-prints*. 2022;p. arXiv:2204.02311.
242. alumiqu, Agressive-Scheme-99. A reddit argument about flamingos; 2022. Available from: https://old.reddit.com/r/MachineLearning/comments/ue2ptk/r_flamingo_a_visual_language_model_for_fewshot/.
243. Brock A, De S, Smith SL, Simonyan K. High-Performance Large-Scale Image Recognition Without Normalization. *CoRR*. 2021;abs/2102.06171. Available from: <https://arxiv.org/abs/2102.06171>.
244. Hoffmann J, Borgeaud S, Mensch A, Buchatskaya E, Cai T, Rutherford E, et al. Training Compute-Optimal Large Language Models. *arXiv e-prints*. 2022;p. arXiv:2203.15556.
245. Walmsley M, Slijepcevic IV, Bowles M, Scaife AMM. Towards Galaxy Foundation Models with Hybrid Contrastive Learning. *arXiv e-prints*. 2022 Jun;p. arXiv:2206.11927.
246. Kaplan J, McCandlish S, Henighan T, Brown TB, Chess B, Child R, et al. Scaling Laws for Neural Language Models. *CoRR*. 2020;abs/2001.08361. Available from: <https://arxiv.org/abs/2001.08361>.
247. Thoppilan R, Freitas DD, Hall J, Shazeer N, Kulshreshtha A, Cheng H, et al. LaMDA: Language Models for Dialog Applications. *CoRR*. 2022;abs/2201.08239. Available from: <https://arxiv.org/abs/2201.08239>.
248. Rae JW, Borgeaud S, Cai T, Millican K, Hoffmann J, Song HF, et al. Scaling Language Models: Methods, Analysis & Insights from Training Gopher. *CoRR*. 2021;abs/2112.11446. Available from: <https://arxiv.org/abs/2112.11446>.
249. Smith S, Patwary M, Norick B, LeGresley P, Rajbhandari S, Casper J, et al. Using DeepSpeed and Megatron to Train Megatron-Turing NLG 530B, A Large-Scale Generative Language Model. *CoRR*. 2022;abs/2201.11990. Available from: <https://arxiv.org/abs/2201.11990>.
250. Gao L, Biderman S, Black S, Golding L, Hoppe T, Foster C, et al. The Pile: An 800GB Dataset of Diverse Text for Language Modeling. *arXiv e-prints*. 2020;p. arXiv:2101.00027.
251. Friel R. Chinchilla's Wild Implications; 2022. Available from: <https://www.alignmentforum.org/posts/6Fpvch8RR29qLEWNH/chinchilla-s-wild-implications>.
252. Kaiser L, Gomez AN, Shazeer N, Vaswani A, Parmar N, Jones L, et al. One Model To Learn Them All. *arXiv e-prints*. 2017;p. arXiv:1706.05137.
253. Ivezić Ž, Kahn SM, Tyson JA, Abel B, Acosta E, Allsman R, et al. LSST: From Science Drivers to Reference Design and Anticipated Data Products. *The Astrophysical Journal*. 2019;873:111.
254. Raymond ES. *The Cathedral and the Bazaar*. 1st ed. USA: O'Reilly & Associates, Inc.; 1999.

255. Black S, Biderman S, Hallahan E, Anthony Q, Gao L, Golding L, et al. GPT-NeoX-20B: An Open-Source Autoregressive Language Model. arXiv e-prints. 2022 Apr;p. arXiv:2204.06745.
256. Crowson K, Biderman S, Kornis D, Stander D, Hallahan E, Castricato L, et al. VQGAN-CLIP: Open Domain Image Generation and Editing with Natural Language Guidance. arXiv e-prints. 2022 Apr;p. arXiv:2204.08583.
257. Park JS, Popowski L, Cai CJ, Ringel Morris M, Liang P, Bernstein MS. Social Simulacra: Creating Populated Prototypes for Social Computing Systems. arXiv e-prints. 2022 Aug;p. arXiv:2208.04024.
258. Aher G, Arriaga RI, Tauman Kalai A. Using Large Language Models to Simulate Multiple Humans. arXiv e-prints. 2022 Aug;p. arXiv:2208.10264.
259. Saharia C, Chan W, Saxena S, Li L, Whang J, Denton E, et al. Photorealistic Text-to-Image Diffusion Models with Deep Language Understanding. arXiv e-prints. 2022 May;p. arXiv:2205.11487.
260. Tay Y, Dehghani M, Rao J, Fedus W, Abnar S, Chung HW, et al. Scale Efficiently: Insights from Pre-training and Fine-tuning Transformers. CoRR. 2021;abs/2109.10686. Available from: <https://arxiv.org/abs/2109.10686>.
261. Ho J, Saharia C, Chan W, Fleet DJ, Norouzi M, Salimans T. Cascaded Diffusion Models for High Fidelity Image Generation. CoRR. 2021;abs/2106.15282. Available from: <https://arxiv.org/abs/2106.15282>.
262. Willett KW, Lintott CJ, Bamford SP, Masters KL, Simmons BD, Casteels KRV, et al. Galaxy Zoo 2: detailed morphological classifications for 304 122 galaxies from the Sloan Digital Sky Survey. Monthly Notices of the Royal Astronomical Society. 2013 Nov;435(4):2835–2860.
263. Gal R, Alaluf Y, Atzmon Y, Patashnik O, Bermano AH, Chechik G, et al. An Image is Worth One Word: Personalizing Text-to-Image Generation using Textual Inversion. arXiv e-prints. 2022;p. arXiv:2208.01618.
264. Patterson D, Gonzalez J, Le Q, Liang C, Munguia LM, Rothchild D, et al. Carbon Emissions and Large Neural Network Training. ArXiv e-prints. 2021 4;.
265. Friedlingstein P, Jones MW, O'Sullivan M, Andrew RM, Bakker DCE, Hauck J, et al. Global Carbon Budget 2021. Earth System Science Data. 2022 4;14(4):1917–2005.
266. Buberger J, Kersten A, Kuder M, Eckerle R, Weyh T, Thiringer T. Total CO₂-equivalent life-cycle emissions from commercially available passenger cars. Renewable and Sustainable Energy Reviews. 2022 5;159:112158.
267. Bergstra J, Bengio Y. Random Search for Hyper-Parameter Optimization. Journal of Machine Learning Research. 2012;13(10):281–305. Available from: <https://www.jmlr.org/papers/v13/bergstra12a.html>.
268. Strubell E, Ganesh A, McCallum A. Energy and Policy Considerations for Deep Learning in NLP. arXiv e-prints. 2019;p. arXiv:1906.02243.
269. Lacoste A, Luccioni A, Schmidt V, Dandres T. Quantifying the Carbon Emissions of Machine Learning. arXiv e-prints. 2019;p. arXiv:1910.09700.